Doctoral Dissertation (Shinshu University)

Study on fabrication of nanofibers with multifunctions for textile, water filtration, and biomedicine

March 2020

PHAN DUY NAM

Interdisciplinary Graduate School of Science and Technology
Shinshu University

ABSTRACT

Study on Fabrication of Nanofibers with multifunctions for Textile, Water Filtration, and Biomedicine

My research is revolved around the fabrication of composite nanofibers via different methods. Both natural and synthetic polymers have been used with several additional substances for various applications. This dissertation is a part of my work with the aim of advancing nanomaterials to be used for practical purposes such as water treatment and biomedicine.

For the application of water treatment, chitosan and cellulose were opted for electrospinning into hybrid nanofibers. The water pollution caused by industrious waste is a big concern due to the threat to global ecosystem. There are several toxic metals found in waste water that could be harmful to human health. Polymers origin from nature with adsorptive properties such as Chitosan was electrospun into nanofibers for the heavy metal adsorption. Cellulose was also added to the spinning solutions for improving stability of the hybrid nanofibers in aqueous environment. The adsorption results against copper, lead, and arsenic showed promising metal-removable potential for further improvement.

For biotechnology applications, silver, copper, and zinc oxide were incorporated into polyacrylonitrile and cellulose nanofibers. The composite nanofibers were evaluated regarding antibiotic actions against Escherichia coli, Bacillus subtilis, and Staphylococcus aureus. Various characterizations were chosen to demonstrate quantitatively and qualitatively the success of synthesis. The process of preparing these nanofibrous materials was straightforward and simple for scaling up.

We tried to utilize natural substances such as Hinokitiol, known as β-thujaplicin, a powerful antibiotic and insoluble in water. It was integrated into PAN nanofibers

containing ZnO with the aim to hold particles within the nanofibrous membranes. The composite nanofibers exhibited enhanced dye adsorptive efficiency and better antibacterial activities compared to nanofibers containing either ZnO or Hinokitiol.

For characterizations, we have used scanning electron microscopy - energy dispersive X-ray spectroscopy (SEM-EDS, JSM-6010LA by JEOL, Japan) and transmission electron microscopy (TEM, 2010 Fas TEM, JEOL, Tokyo, Japan) to observe the morphology of composite nanofibers. Fourier Transform Infrared (FT-IR) spectrophotometer (Prestige-21, Shimadzu Co., Ltd., Japan) was implemented to verify distinctions between chemical groups. X-ray diffraction instrument (XRD) with CuKα anode (Miniflex 300, Rigaku Co., Ltd., Japan), operating at 30 kV and 500 mA, was performed for detecting diffraction angles. For adsorption tests, UV-Vis spectrophotometer (Shimadzu UV-2600 spectrophotometer, Japan) and inductively coupled plasma-optical emission spectrometry ICP-OES (SPS 3100, Hitachi High-Tech Science Corporation, Tokyo, Japan) were utilized. All antibacterial tests were took placed in Taguchi lab and Tanaka lab with the kind assistance of Ms. Nasanjargal Dorjjugder and Ms. Rina Afiani Rebia.

Keywords: Ag, Cu, ZnO, PAN, Cellulose, Chitosan, Hinokitiol, Dye adsorption, Antibacterial activity, Heavy metal adsorption.

ACKNOWLEDGMENTS

I would like to express my deep gratitude to my supervisor and teacher, **Prof. Kim Ick Soo** for his endless support, constructive advice, kind guidance, and attentive company during 5 years of my study in Japan. Also, I am indebted to Prof. Hiroaki Ishizawa, Prof. Kanji Kajiwara and deceased Prof. Koji Abe for the introduction and the beliefs set upon me on the date we met in Vietnam for the interview. My sincere appreciation is for Prof. Vu Thi Hong Khanh, who was the Dean of The School of Textile, Leather, and Fashion at the time she gave me the recommendation for the Advanced Leading Graduate Program. I would like to thank my Department Head Prof. Phan Thanh Thao for her acceptance to take a 5-year leave so that I could be here and study.

Five years is a long journey for me to achieve the degree of Doctor of Engineering, but it was beautifully worthwhile. My profound gratitude would be to Prof. Makoto Shimosaka - Program Director and Dean of the Faculty of Textile Science and Technology for his contributions to the Leading Program. Without the enlightening guidance from Prof. Mikihiko Miura and Prof. Tsutomu Ishiwatari, I could have not found the appropriate road in my academic career, thus my profound thanks would be for them. I gratefully acknowledge the support from Prof. Masayuki Takatera and Prof. Shigeru Inui, they have been with me for unforgettable foreign excursions, which still imprint deep in my memory.

I would like to express my appreciation for the support and help from all Leading staff, especially for Ms. Akiko Kubota and Ms. Naoko Suguta, they have been with me since the first day I set foot in Japan. I would like to thank all the Gakumu staff for their patience and attention with me, my Japanese speaking sometimes was gibberish and hard to understand.

I would like to say thank you very much to Dr. Hoik Lee, a friend and a teacher of mine, he has guided me to find my footing in the science world. My earnest acknowledgment is to Prof. Yasuhito Mukai (Nagoya University), Prof. Goro Taguchi, Prof. Yasushi Tamada, and Prof. Toshihisa Tanaka for their instruction and acceptance to use lab equipment. My sincere thanks are to Mr. Yusuke Saito, Mr. Davood Kharaghani, Ms. Nasanjargal Dorjjugder, and Ms. Rina Afiani Rebia for their help and assistance with my experiments.

My special thanks to my friends, Mr. Muzamil Khatri, Mr. Nadir Hussain, Mr. Azeem Ullah, Ms. Motahira, Mr. Yuma Inoue, Mr. Hijiri Otani, Mr. Yuko Kaneta, Mr. Sanaullah, Mr. Yohei Hasegawa, Mr. Takayuki Yamamoto, Mr. Takato Matsuhisa, Ms. Wang Qianyu, Ms. Bie Xinyu, Mr. Kosuke Hidaka, Mr. Yasunari Yamauchi, Mr. Sarwar Muhammad Nauman, Mr. Yuji Suzuki, Mr. Yuki Kikuchi, Mr. Takami Yamaguchi, Mr. Kousei Wada, Ms. Wang Feifei, Mr. Sun Lei, Ms. Parastoo Gitigard, Mr. Md. Kaiser Haider.

I would like to show my deep gratitude to my father, mother, my sister, and relatives for their help and support through my ups and downs. Without them, I might have not overcome difficult times. It is more than words to say thanks to my dear wife, the love of my life. Just a short time we have known each other before this dissertation is submitted but her contribution to formulating our future path together is worthwhile.

TABLE OF CONTENTS

LIST OF TABLES

LIST OF FIGURES

LIST OF SCHEMES

CHAPTER 1 Introduction

1.1 Background

When the fiber diameters started to reduce from micrometers to nanometers, new fascinating features were introduced, for instance large surface area to volume ratio, surface functionalities, and superb mechanical properties [1]. There are several methods to prepare fibers at nanoscale including template synthesis, drawing, phase separation, and electrospinning [2, 3]. The latest has potential to be developed at mass-production scale from a wide range of different polymers. The setup utilizes electrostatic force to elongate single or multiple jets of polymer solution onto a collector [4]. The jets become dry on the way travelling by evaporation process. Eventually, nanofibers were gathered in regular sheet form and ready for further applications [5].

In recent years, the electrospinning technique has drawn much attention due to its novelty, straightforwardness, versatility, and peculiarities. One example of the peculiarity is the combination of solution components to acquire desired morphologies [6]. Highly porous nanofibers can be tailored by rapid phase separation phenomena. The resulted nanofibers can be applied for biofunctional materials as scaffolds for promoting the proliferation of different cells [7, 8]. The post-processing and various geometrical modifications have been introduced to achieve new performances on nanofibers and there is still vast space for further improvements. Besides, there are many polymers prove to be difficult for the electrospinning technique, due to poor viscous and elastic properties, short of molecular entanglements, and low solubility. These problems hinder the reproducibility and the scale-up manufacturing [9].

1.2 Nanofibers with adsorptive properties for water filtration

Water and air pollutions are the problems that humankind has to deal with. Harmful aqueous pollutants, including heavy metals or toxic organic compounds, can contaminate water resources; whereas, in the atmosphere, bacteria and viruses can lead to respiratory diseases and degrade human well-being [10, 11].

Conventional treatments for wastewater include three levels of treatment, which are primary, secondary, and tertiary treatments. The primary and secondary treatments remove coarse solids and organic matters. Tertiary treatment or the final treatment stage can remove pathogens and persistent contaminants. Expensive and advanced techniques, such as activated carbon and reverse osmosis, are usually used in this stage. For avoiding aerial pollutants, masks are usually worn. However, for fine particles and viruses smaller than 0.3 μm, regular masks do not remove or effectively protect against those particles and pathogens [12-14].

Some heavy metals, arsenic, cadmium, lead, and mercury, can cause severe illness to humans and need to be removed from ground water before they enter human bodies via food and drink. Modifying membrane surfaces with specific chemical groups can turn these membranes into having adsorption properties towards toxic metals. Another method is by adding natural biomacromolecules which possess adsorptive characteristics, including chitin, collagen, gelatin, chitosan, and DNA [15-17].

1.3 Nanofibers for bio-medical application

Varied materials have been utilized to speed up the healing process of wounds by preventing contamination and proving suitable environments. With the new developments of bioactive materials incorporated into nanofibers, the natural

polymers with biodegradable or biocompatible characteristics, the deposition of healthy tissues is accelerated. Besides, growth factors, vitamins, and natural substances particularly plant-derived compounds were integrated into nanofibers for the production of novel composite nanofibers with enhanced properties. Honey, one of natural substances, has been very appealing material due to its antimicrobial and anti-inflammatory effects.

For centuries, silver and copper have played the roles of antibiotics, due to antibacterial properties. Antibacterial resistance has been one of the major problems needing to be overcome in the field of biomedicine. Silver is a very potent antibacterial agent and has been used in the form of silver sulphadiazine or metallic silver. In recent years, silver finds its applications in silver based wound dressings and medical devices. The mechanistic actions of silver have been suggested by numerous studies which comprise of oxidization, diffusion, and penetration. Whereas, copper promotes cell and tissue regeneration yet exhibits strong toxicity toward bacteria.

1.4 Literature survey

My work aimed at the fabrication of nanofibers with antibacterial activity and adsorptive properties. One of the most emphasizing points of this dissertation is promoting nanofibers as effective carriers of substances for aforementioned purposes. There are published articles, review papers, and books coping with either biomedical or water filtration applications. However, our work targeted engineering composite nanofibers with multifunctional features.

There are a large amount of scientific reports dealing with silver, zinc, and copper integrated in nanofibers for testing against fungi, bacteria, and virus. Adding metals

affects the conductivity of the spinning solution, thus improves the charge density [18]. The elongation force becomes stronger and results in smaller average diameters. The cytotoxicity of metals against microorganism is due to theirs interactions with the cellular membrane and nucleic acids [19]. Silver has been considered as a novel form of antibacterial substance in a quite amount of recently published articles. The most straightforward technique to integrate silver into nanofibers is the suspension of Ag nanoparticles in electrospinning polymer solutions [20-23]. Copper has been used to make cooking and water containing utensils to terminate pathogenic threats [24-27]. In recent years, zinc oxide has risen as a promising antimicrobial agent owing to the bacterial inhibition. The bactericidal action can be attributed to the production of reactive oxygen species [28-31].

On the other hand, in concern to worries about side effects of synthetic substances, there are a growing number of studies focusing on natural compounds, which are extracted from plants or animals and have powerful bio-activities. Chitosan, a natural biopolymer, has applications in wound healing, tissue engineering, food packaging, drug delivery, and filtration. Chitosan has valuable properties such as biocompatibility, antibacterial activities, biodegradability, and non-toxicity [32, 33]. Few articles reported about biochemical and pharmacological activities of chitosan against bacteria, fungi, and yeasts. Hinokitiol has a wide range of antibiotic effects, encompassing antibacterial, antiviral, antifungal, and insecticidal effects [34-36].

1.5 Objectives

The main aim of my research is to promote the development of nanofiber system with multiple functions, applied in antibiotic applications or water filtration. By

adding new substances and compounds into the nanofibrous scaffolds, new composite materials can be introduced with fascinating and unexpected features.

In Chapter 2, we evaluated the adsorption capacity of the hybrid nanofibers of chitosan and cellulose for removing copper, lead, and arsenic in an aqueous environment. The system seemed to improve in mechanical characteristics owing to the tenacious nature of chitosan. The system also exhibited stable nanofibrous structure during adsorption tests.

Chapter 3 discusses about the mechanistic actions of different silver species against gram-negative and gram-positive bacteria. The arguments over the mechanisms of silver against bacteria have been a hot topic, and with multiple theories about the actions, the insights upon the silver exerting bactericidal activities have been more controversially complicated. The chapter 3 dealt with this prominent issue with the hope of contributing a different perspective of silver actions under the influences of chloride ions.

In chapter 4, we tried to bring the antibacterial activities on cellulose nanofibers by adhering silver and copper to the nanofibrous platform. Cellulose is an abundant natural polymer which has attracted more and more interest from academia and industry. The work introduces two different methods to decorate cellulose nanofibers with metal nanoparticles and assesses the antibacterial effects of the resulted composite nanofibers.

Chapter 5 is the combination of natural antibiotic - hinokitiol and synthetic nanoparticles - zinc oxide for the antibacterial application and dye removal. Hinokitiol played the role of a coating substance to secure zinc oxide nanoparticles staying firmly on the surfaces of nanofibers. Furthermore, this chapter presents a novel research upon synergistic actions of hinokitiol and zinc oxide against gram

positive bacteria. The blue and red dyes were removed effectively from the aqueous solutions by the composite membrane.

References

[1] Z.-M. Huang, Y.Z. Zhang, M. Kotaki, S. Ramakrishna, A review on polymer nanofibers by electrospinning and their applications in nanocomposites, Composites Science and Technology 63(15) (2003) 2223-2253.
[2] N.M. Rodriguez, A review of catalytically grown carbon nanofibers, Journal of Materials Research 8(12) (2011) 3233-3250.
[3] M.Z. Elsabee, H.F. Naguib, R.E. Morsi, Chitosan based nanofibers, review, Materials Science and Engineering: C 32(7) (2012) 1711-1726.
[4] M.H. Al-Saleh, U. Sundararaj, A review of vapor grown carbon nanofiber/polymer conductive composites, Carbon 47(1) (2009) 2-22.
[5] I.S. Chronakis, Novel nanocomposites and nanoceramics based on polymer nanofibers using electrospinning process—A review, Journal of Materials Processing Technology 167(2) (2005) 283-293.
[6] J.D. Schiffman, C.L. Schauer, A Review: Electrospinning of Biopolymer Nanofibers and their Applications, Polymer Reviews 48(2) (2008) 317-352.
[7] L. Persano, A. Camposeo, C. Tekmen, D. Pisignano, Industrial Upscaling of Electrospinning and Applications of Polymer Nanofibers: A Review, Macromolecular Materials and Engineering 298(5) (2013) 504-520.
[8] E.P.S. Tan, C.T. Lim, Mechanical characterization of nanofibers – A review, Composites Science and Technology 66(9) (2006) 1102-1111.
[9] G.G. Tibbetts, M.L. Lake, K.L. Strong, B.P. Rice, A review of the fabrication and properties of vapor-grown carbon nanofiber/polymer composites, Composites Science and Technology 67(7) (2007) 1709-1718.
[10] C.C. Ahn, Y. Ye, B.V. Ratnakumar, C. Witham, R.C. Bowman, B. Fultz, Hydrogen desorption and adsorption measurements on graphite nanofibers, Applied Physics Letters 73(23) (1998) 3378-3380.
[11] Z. Ma, M. Kotaki, S. Ramakrishna, Electrospun cellulose nanofiber as affinity membrane, Journal of Membrane Science 265(1) (2005) 115-123.
[12] Q. Wang, J.K. Johnson, Computer Simulations of Hydrogen Adsorption on Graphite Nanofibers, The Journal of Physical Chemistry B 103(2) (1999) 277-281.
[13] P.K. Neghlani, M. Rafizadeh, F.A. Taromi, Preparation of aminated-polyacrylonitrile nanofiber membranes for the adsorption of metal ions: Comparison with microfibers, Journal of Hazardous Materials 186(1) (2011) 182-189.
[14] P. Kampalanonwat, P. Supaphol, Preparation and Adsorption Behavior of Aminated Electrospun Polyacrylonitrile Nanofiber Mats for Heavy Metal Ion Removal, ACS Applied Materials & Interfaces 2(12) (2010) 3619-3627.
[15] Y. Sun, Z.-Y. Wu, X. Wang, C. Ding, W. Cheng, S.-H. Yu, X. Wang, Macroscopic and Microscopic Investigation of U(VI) and Eu(III) Adsorption on Carbonaceous Nanofibers, Environmental Science & Technology 50(8) (2016) 4459-4467.
[16] S. Haider, S.-Y. Park, Preparation of the electrospun chitosan nanofibers and their applications to the adsorption of Cu(II) and Pb(II) ions from an aqueous solution, Journal of Membrane Science 328(1) (2009) 90-96.
[17] K. Yoshimatsu, L. Ye, J. Lindberg, I.S. Chronakis, Selective molecular adsorption using electrospun nanofiber affinity membranes, Biosensors and Bioelectronics 23(7) (2008) 1208-1215.

[18] A. Haider, S. Haider, I.-K. Kang, A comprehensive review summarizing the effect of electrospinning parameters and potential applications of nanofibers in biomedical and biotechnology, Arabian Journal of Chemistry 11(8) (2018) 1165-1188.
[19] T.C. Dakal, A. Kumar, R.S. Majumdar, V. Yadav, Mechanistic Basis of Antimicrobial Actions of Silver Nanoparticles, Front Microbiol 7 (2016) 1831-1831.
[20] W.K. Son, J.H. Youk, W.H. Park, Antimicrobial cellulose acetate nanofibers containing silver nanoparticles, Carbohydrate Polymers 65(4) (2006) 430-434.
[21] H. Kong, J. Jang, Antibacterial Properties of Novel Poly(methyl methacrylate) Nanofiber Containing Silver Nanoparticles, Langmuir 24(5) (2008) 2051-2056.
[22] N.A.M. Barakat, K.-D. Woo, M.A. Kanjwal, K.E. Choi, M.S. Khil, H.Y. Kim, Surface Plasmon Resonances, Optical Properties, and Electrical Conductivity Thermal Hystersis of Silver Nanofibers Produced by the Electrospinning Technique, Langmuir 24(20) (2008) 11982-11987.
[23] A. Melaiye, Z. Sun, K. Hindi, A. Milsted, D. Ely, D.H. Reneker, C.A. Tessier, W.J. Youngs, Silver(I)−Imidazole Cyclophane gem-Diol Complexes Encapsulated by Electrospun Tecophilic Nanofibers: Formation of Nanosilver Particles and Antimicrobial Activity, Journal of the American Chemical Society 127(7) (2005) 2285-2291.
[24] P.-C. Hsu, H. Wu, T.J. Carney, M.T. McDowell, Y. Yang, E.C. Garnett, M. Li, L. Hu, Y. Cui, Passivation Coating on Electrospun Copper Nanofibers for Stable Transparent Electrodes, ACS Nano 6(6) (2012) 5150-5156.
[25] W. Wang, L. Zhang, S. Tong, X. Li, W. Song, Three-dimensional network films of electrospun copper oxide nanofibers for glucose determination, Biosensors and Bioelectronics 25(4) (2009) 708-714.
[26] S. Arai, M. Endo, Carbon nanofiber–copper composite powder prepared by electrodeposition, Electrochemistry Communications 5(9) (2003) 797-799.
[27] D.W. Zhang, C.H. Chen, J. Zhang, F. Ren, Novel Electrochemical Milling Method To Fabricate Copper Nanoparticles and Nanofibers, Chemistry of Materials 17(21) (2005) 5242-5245.
[28] T. Amna, M.S. Hassan, N.A.M. Barakat, D.R. Pandeya, S.T. Hong, M.-S. Khil, H.Y. Kim, Antibacterial activity and interaction mechanism of electrospun zinc-doped titania nanofibers, Applied Microbiology and Biotechnology 93(2) (2012) 743-751.
[29] H. Rodríguez-Tobías, G. Morales, A. Ledezma, J. Romero, D. Grande, Novel antibacterial electrospun mats based on poly(d,l-lactide) nanofibers and zinc oxide nanoparticles, Journal of Materials Science 49(24) (2014) 8373-8385.
[30] K.R. Raghupathi, R.T. Koodali, A.C. Manna, Size-Dependent Bacterial Growth Inhibition and Mechanism of Antibacterial Activity of Zinc Oxide Nanoparticles, Langmuir 27(7) (2011) 4020-4028.
[31] K.T. Shalumon, K.H. Anulekha, S.V. Nair, S.V. Nair, K.P. Chennazhi, R. Jayakumar, Sodium alginate/poly(vinyl alcohol)/nano ZnO composite nanofibers for antibacterial wound dressings, International Journal of Biological Macromolecules 49(3) (2011) 247-254.
[32] X. Fei Liu, Y. Lin Guan, D. Zhi Yang, Z. Li, K. De Yao, Antibacterial action of chitosan and carboxymethylated chitosan, Journal of Applied Polymer Science 79(7) (2001) 1324-1335.
[33] L. Qi, Z. Xu, X. Jiang, C. Hu, X. Zou, Preparation and antibacterial activity of chitosan nanoparticles, Carbohydrate Research 339(16) (2004) 2693-2700.
[34] Y. Inamori, S. Shinohara, H. Tsujibo, T. Okabe, Y. Morita, Y. Sakagami, Y. Kumeda, N. Ishida, Antimicrobial Activity and Metalloprotease Inhibition of Hinokitiol-Related Compounds, the Constituents of Thujopsis dolabrata S. and Z. hondai MAK, Biological & Pharmaceutical Bulletin 22(9) (1999) 990-993.
[35] Y. Morita, E. Matsumura, T. Okabe, T. Fukui, T. Ohe, N. Ishida, Y. Inamori, Biological Activity of β-Dolabrin, γ-Thujaplicin, and 4-Acetyltropolone, Hinokitiol-Related Compounds, Biological and Pharmaceutical Bulletin 27(10) (2004) 1666-1669.
[36] Y. Morita, E. Matsumura, T. Okabe, T. Fukui, M. Shibata, M. Sugiura, T. Ohe, H. Tsujibo, N. Ishida, Y. Inamori, Biological Activity of α-Thujaplicin, the Isomer of Hinokitiol, Biological and Pharmaceutical Bulletin 27(6) (2004) 899-902.

CHAPTER 2 Fabrication of electrospun chitosan/cellulose nanofibers having adsorption property with enhanced mechanical property

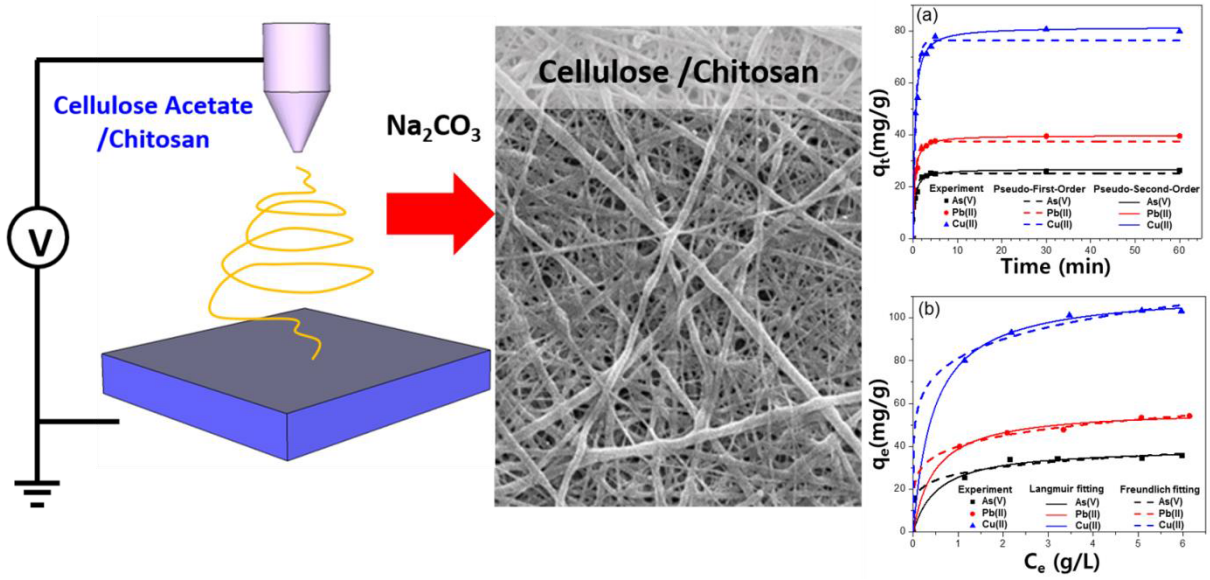

2.1 Introduction

With the rapid growth in industrialization and urbanization, releasing heavy metals into the aquatic ecosystem has become one of the most serious environmental concerns [37, 38]. Heavy metals slowly accumulate in the kidneys, liver, pancreas, bones, central nervous system, and brain after a prolonged exposure; they degrade health and cause severe illnesses, such as cancer, cardiovascular and neurological diseases [39, 40]. Thus, effectively removing undesirable metals from aqueous systems is an urgent yet still challenging task. Conventional techniques commonly applied to remove heavy metals use ion exchange, precipitation, and membrane separation processes [41]. However, these techniques present difficulties in the removal of heavy metals from industrial wastewater due to the high cost or low efficiency [42, 43]. Adsorption is commonly regarded as an effective and economical method for aqueous effluents [44]. Various types of adsorbents have been used for the removal of metal ions from aqueous solutions, such as zeolites, manganese oxides, activated carbons, and ion exchange resins [45]. The adsorption property of those absorbents depends on the functional groups such as thiol, amine, amide, carboxylic acid, hydroxyl groups on their surfaces, which are regarded as adsorption sites [46].

Chitosan, one kind of polysaccharide, has been extensively studied for various applications in separation and biomedical technologies due to its availability in nature and unique properties such as biocompatibility, hydrophilicity, bioactivity, non-antigenicity, and non-toxicity [47, 48]. It can be obtained by partial deacetylation of chitin or by enzymatic hydrolysis in the presence of a chitin deacetylase [49]. In addition, chitosan has been considered a metal adsorbent due to its high adsorption property. Especially, chitosan-based materials for metal

adsorption have been widely investigated [50-52]. It is reported in various literature that capacities (q_{max}) of chitosan for As, Pb and Cu ions calculated by Langmuir equilibrium are in the range of 40-220 mg Cu/g [53], 11.2 - 416.67 mg Pb/g [54], and 22.4 - 71.9 As/g [55].

However, chitosan is difficult to utilize in practical applications owing to its inter- and intra- molecular interactions [56-58], complex chemical structure, polyelectrolyte nature in solution [59], and swelling behavior in an aqueous medium [60]. These drawbacks place limits on fabricating nanofibers through electrospinning, consequently restricting their use in the filtration of aqueous solutions [61]. Cellulose is one of the most naturally abundant biopolymers, and it has excellent thermal stability, chemical resistance, and biodegradability [62, 63]. It has been widely utilized for a variety of potential applications in the form of nanofibers [64-67]. Although it has excellent physicochemical properties, it does not show any adsorption behavior to metal ions; thus, it has not been considered for filtration. Therefore, combining chitosan and cellulose can compensate for the disadvantages of each other, and it can lead to novel materials for filtration membranes. Both materials, chitosan and cellulose, have been widely utilized in different forms such as hydrogel microspheres [68, 69], coated fibers [70], and hollow fiber membranes [71, 72].

Herein, we fabricated a composite of nanofibers consisting of chitosan and cellulose through electrospinning, to create an effective material for removing heavy metal ions. The electrospinning technique is one of the widely utilized methods for fabricating nanofibers due to its simple and well-developed method to produce various polymeric fiber sheets from nanometer to micrometer size in diameter with a large surface area to volume ratio [73-75]. Arsenic(V), lead(II) and copper(II) have been chosen as representatives for heavy metal since they are toxic to the organisms

and are common pollutants found in industrial effluents [76-78]. There are several papers for fabricating nanofibers, using chitosan/cellulose mixture (Salihu et al. 2012; Liu and Bai 2005); however, to our knowledge, this is the first report on the use of electrospun chitosan/cellulose nanofibers for the adsorption of As(V), Pb(II) and Cu(II) ions. In addition, we found a potential use of chitosan/cellulose nanofibers for filtration of wastewater.

2.2 Experimental

2.2.1 Materials

Commercial chitosan (CS, Chitosan 500), trifluoroacetic acid (TFA, 98%) and copper (II) sulfate pentahydrate were purchased from Wako Pure Chemical Industries, Ltd (Osaka, Japan). Cellulose acetate (CA, MW= ~ 30,000 g/mol), acetic acid (99% purity), sodium arsenate dibasic heptahydrate (98% purity), lead (II) nitrate (99% purity) and sodium carbonate (99% purity) were purchased from Sigma Aldrich Chemical Co., Ltd (USA). All chemicals were used as received without further purification.

2.2.2 Nanofiber fabrication via electrospinning

Previous literature on the fabrication methods of CS/CA nanofibers used TFA for dissolving polymer [72]. However, we found that a phase separation phenomenon appears slowly after blending two polymers in TFA. Thus, it is found that TFA alone is not suitable for preparing CS/CA solution for fabricating nanofibers; therefore, we added acetic acid as a co-solvent into TFA. The use of TFA/acetic acid cosolvent prevents the phase separation of CS and CA, resulting in a CS/CA homogeneous solution. This is the first report of the addition of acetic acid into TFA for CS/CA solution preparation, and the successful fabrication CS/CA nanofibers with this co-solvent system.

To fabricate CS/CA nanofibers, CS and CA polymers were blended with 1:1 w/w ratio in TFA/acetic acid solution (7:3 w/w) at different concentrations. Polymeric solutions of single CS or CA were also prepared to fabricate the single-component nanofibers as control samples. All prepared solutions were stirred mildly for 24 h to completely dissolve all components. The resulted solutions were filled in 20 mL plastic syringes fitted with a needle and set up in the electrospinning apparatus. A high-voltage power supply (Har-100*12, Matsusada Co., Tokyo, Japan) was used as a source of the electric field [79]. Electrospinning was set up in horizontal alignment at an applied voltage of 15 kV or 20 kV, at room temperature, and relative humidity approximately 20%. The collector was located 10 cm apart from the tip of the needle. A syringe pump (KDS-100, KD Scientific, Holliston, MA, USA) was used to continuously feed the solution with a certain flow rate. Nanofibers were collected on papers wrapped on the cylinder collector. A summary of blending and electrospinning conditions is listed in **Table 2.1**.

Table 2. 1 - Electrospinning conditions

Polymer	Concentration (wt%)	Voltage (kV)	Flow rate (mL/min)
CS	2	20	0.1
CS	3	20	0.1
CS	4	20	0.2
CS/CA (1:1)	2	20	0.1
CS/CA (1:1)	4	20	0.2
CS/CA (1:1)	6	20	0.3
CA	8	15	0.3
CA	10	15	0.5
CA	12	15	0.8

The resultant electrospun nanofibers, i.e., CS, CS/CA, and CA nanofibers, were further treated in a base solution to obtain stable CS, CS/CL, and CL nanofibrous webs. The fibrous webs should be neutralized because of the strong acid solvent, TFA, used in electrospinning process. In addition, deacetylation of CA is also required to make CL nanofibers. For this purpose, we used Na_2CO_3 solution to neutralize CS and deacetylate CA [80]. The prepared nanofiber webs were immersed in 3M Na_2CO_3 solution for 24 h at room temperature. Subsequently, the resultant nanofibers were washed with distilled water several times until the pH of the wash water was decreased down to 7, and afterward dried at 60 °C for 12 h in a drying chamber (EYELA SLI-220).

2.2.3 Characterization

The morphology of all samples and Energy Dispersive X-ray Spectrometry of As(V), Pb(II), and Cu(II) adsorption testing were observed by scanning electron microscopy (SEM-EDS; JSM-6010LA by JEOL, Japan). The average fiber diameter and distribution in each sample were calculated by means of an image processing program (Image J, version 1.49) based on n = 50 fibers per sample. The prepared nanofiber samples were subjected to Fourier transform infrared spectra (FT-IR, IR Prestige-21, Shimadzu, Japan) to determine the types of functional groups present in the nanofibers. The spectra were recorded from 4,000 to 500 cm^{-1}. The stress-strain curves of electrospun mats were obtained using a universal testing instrument (UTM, RTC-1250A, A&D Co., Ltd., Tokyo, Japan). All nanofiber samples were prepared using a dog-bone shape punch with the size of 15 mm (width) x 60 mm (length). The thicknesses of specimens were 0.12 mm for CS nanofibers, 0.05 mm for neutralized CS nanofibers, 0.11 mm for CS/CA nanofibers, 0.09 mm for neutralized CS/CL nanofibers, 0.19 mm for CA nanofibers, and 0.15 mm for CL nanofibers. For the test

in the wet state, all treated samples were immersed in deionized water for 30 min. Elongation tests were performed under standard conditions with a 10 N load cell at an extension rate of 10 mm/min and a gauge length of 50 mm.

2.2.4 Batch adsorption experiments

The adsorption of heavy metals was studied using batch experiments. 50 mg of nanofiber web was immersed into 10 mL solutions of As(V), Pb(II) or Cu(II) ions with a concentration of 1 g/L. All prepared solutions containing the nanofiber web were shaken at 25 °C for 1 h with 150 rpm. Then the solutions were taken out and sampled at different time intervals from 0.5 min to 1 h to determine As(V), Pb(II), and Cu(II) concentrations in order to obtain the time dependent adsorption isotherm. The concentration dependent adsorption isotherm was also acquired with the initial As(V), Pb(II), or Cu(II) concentrations in the range of 1 to 6 g/L. Ultraviolet-visible (UV-Vis) spectrophotometer (Shimadzu UV-2600 spectrophotometer, Japan) and inductively coupled plasma-optical emission spectrometry ICP-OES (SPS 3100, Hitachi High-Tech Science Corporation, Tokyo, Japan) were used to measure concentrations of solutions before and after the adsorption tests. The amounts of metal ions adsorbed onto nanofiber web specimens were calculated on the basis of the following equation:

$$q = \frac{(C_0 - C_e)V}{M} \qquad (1)$$

Where C_0 and C_e are the initial and the equilibrium concentration of the metal ions in the testing solution (mg/L), respectively, V is the volume of the testing solution (L), and M is the weight of the adsorbent (g).

2.3 Results and discussion

2.3.1 Optimization of nanofiber fabrication and morphology study

The structure and morphology of the CS, CA, and CS/CA electrospun nanofibers are presented in **Figure 2.1.** The top images, **Figure 2.1 (a-c)** represent the CS nanofibers fabricated at concentrations of 2, 3 and 4 wt%, showing well-defined nanofiber structures. The diameter of nanofibers is increased as the concentration increases, from 104 ± 19 nm (2 wt%) to 320 ± 108 nm (4 wt%). It is worth noting that the continuous and fine nanofibers are obtained at 2 wt% concentration as presented in **Figure 2.1 (a)**. However, we could not produce the fibrous structure at 2 wt% with CS/CA blended solution. Only irregular bead particles and a few irregular nanofibers were produced in this concentration, **Figure 2.1 (d)**. For the successful nanofiber fabrication of CS/CA, the concentrations of the solution should be over the 4 wt%. At 4 wt%, the nanofiber structure shows very smooth and randomly orientated nanofibers with 122 ± 35 nm in diameter, and that of the nanofibers is increased up to 349 ± 96 nm at 6 wt%, **Figure 2.1 (e, f).** In case of CA nanofiber fabrication, the nanofiber structure fabricated with 8 wt% contained a lot of beads in the fiber structure, **Figure 2.1 (g)**, while the nanofibers fabricated with 10 and 12 wt% were bead-free and showed well-defined structure with diameters of 331 ± 118 and 546 ± 91 nm, respectively, **Figure 2.1 (h, i)**.

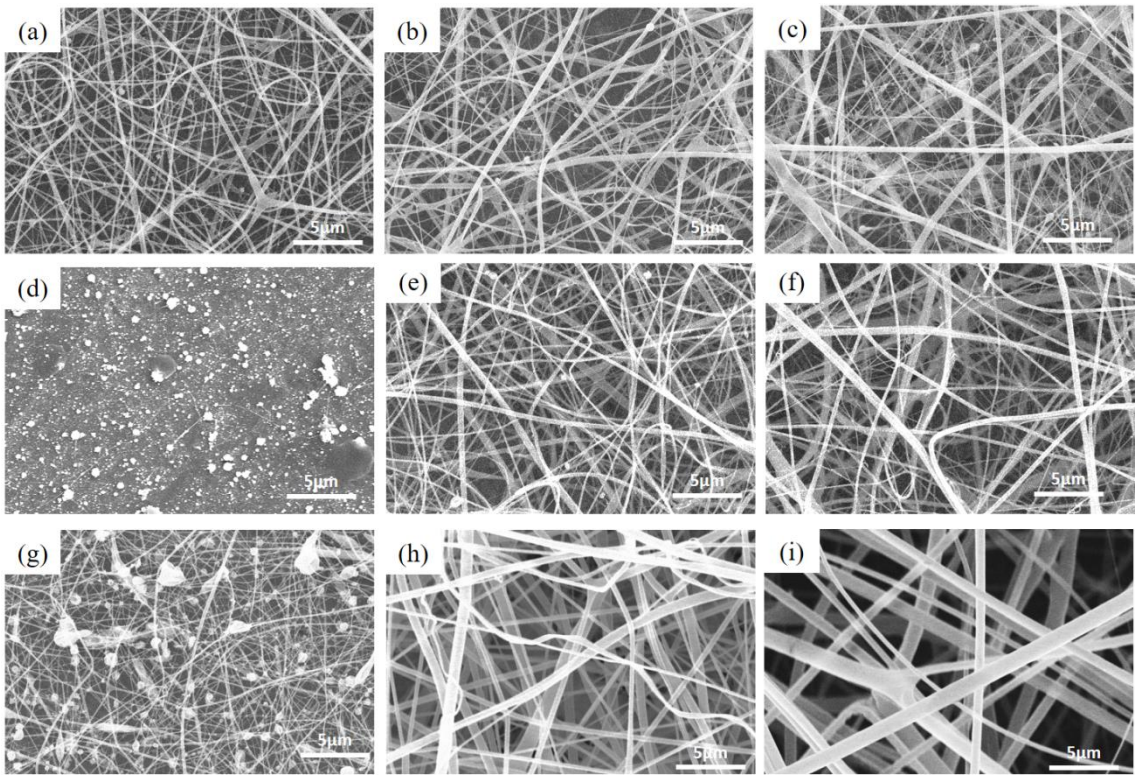

Figure 2. 1 - Morphology of nanofibers prepared with different concentrations; (a) 2, (b) 3, and (c) 4 wt% for CS nanofibers, (d) 2, (e) 4, and (f) 6 wt% for CS/CA nanofibers, and (g) 8, (h) 10, and (i) 12 wt% for CA nanofibers.

Notably, the average diameters of electrospun CS at 4 wt%, CS/CA at 6 wt% and CA at 10 wt% are in the range of 320 to 350 nm. Therefore, we opted for CS, CS/CA and CA nanofiber webs, fabricated with 4, 6 and 10 wt%, respectively, for the further investigation. These nanofiber webs were treated with 3M Na_2CO_3. By this treatment, the CS nanofibers can be neutralized and the CA nanofibers converted to CL nanofibers through deacetylation reaction. The morphologies of the resultant nanofibers are presented in **Figure 2.2 (a, b, c)**. It is worth noting that all nanofibers kept their fiber structure and contained salt impurities on the fiber surface after treatment. To remove the impurities, we washed the nanofibers several times with distilled water, and then observed their morphologies, **Figure 2.2 (d, e, f)**.

Interestingly, only the CS nanofiber web was dissolved and destroyed, while CS/CL and CL nanofibers, after being successfully washed impurities, showed intact nanofibrous structure as shown in **Figure 2.2 (e, f)**. The amino group in chitosan has a pKa value of ~6.5, which leads to a protonation in acidic to a neutral solution, making chitosan water-soluble [81, 82]. In addition, considering the water resistance of CL, owing to strong hydrogen bonding in CL structure, it is acceptable to infer that the water stability of CS/CL nanofibers originates from CL component, which can retain the polymer matrix and prevent the dissolution of chitosan in water.

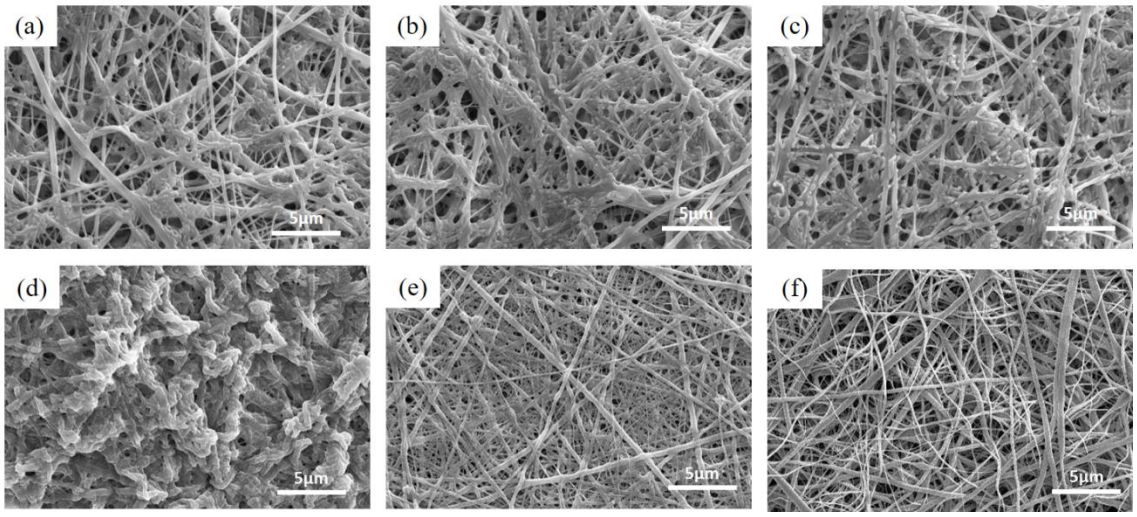

Figure 2. 2 - Morphology of Na_2CO_3 treated nanofibers; (a) CS, (b) CS/CL and (c) CL before washing, and (d) CS, (e) CS/CL and (f) CL after washing.

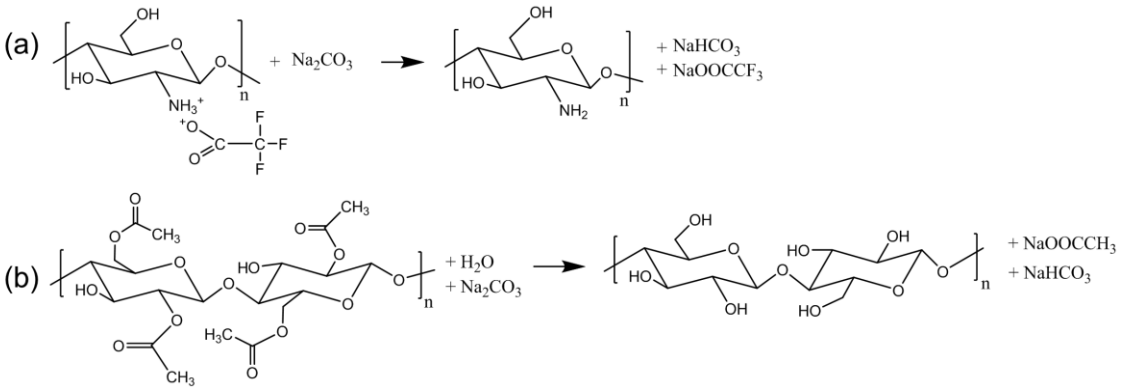

Scheme 2. 1 - (a) chitosan neutralization process and (b) deacetylation of cellulose acetate

2.3.2 Analysis of nanofiber functionality from FT-IR spectroscopy

The functionalities of the prepared nanofibers were confirmed by Fourier-transform infrared spectroscopic analysis (**Figure 2.3**). The FT-IR spectra of the CS nanofibers exhibited absorption peaks corresponding to ammonium ion (1538 cm^{-1}) and C=O stretching of the acetyl groups (1680 cm^{-1}) [83], and those peaks change significantly after neutralization. The peak of ammonium ion largely decreased and the amine peak at 1592 cm^{-1} appeared after neutralization, indicating that the nanofiber webs successfully discarded the remaining amount of TFA solvent and therefore was neutralized. Strong adsorption peaks at 1752 cm^{-1}, 1365 cm^{-1}, and 1236 cm^{-1} are observed in CA nanofibers, which correspond to the carbonyl groups, C-CH_3 and C-O-C stretching, respectively [84]. Disappearance of those three peaks and an emerging of new peak at 3340 cm^{-1} which corresponds to -OH groups imply the successful conversion of CA into CL [85]. The spectrum of CS/CA nanofibers shows absorption peaks at 1732 cm^{-1} and 1682 cm^{-1} which corresponding to carbonyl groups in CA and C=O stretching of the acetyl groups in CS, respectively. This result strongly implies that the polymers are well-blended in nanofibers. In addition, the neutralized and deacetylated CS/CL nanofibers show a similar spectrum as the neutralized CS nanofibers and deacetylated CL nanofibers, which further indicates that the neutralization and deacetylation were successfully conducted on CS/CA nanofibers, resulting in the neutralized and deacetylated CS/CL nanofibers. The absorption peaks at 724, 802 and 842 cm^{-1} in the spectra of CS/CA and CS nanofibers, which are ascribed to the carbon-fluoride stretching vibrations of

trifluoroacetate (–$COCF_3$) groups in TFA and amine ($NH_3^+CF_3COO^-$) salts formed between the TFA solvent and the CS polymer, disappeared after the Na_2CO_3 treatment, indicating that the excessive amounts of solvent on the nanofibers were completely removed.

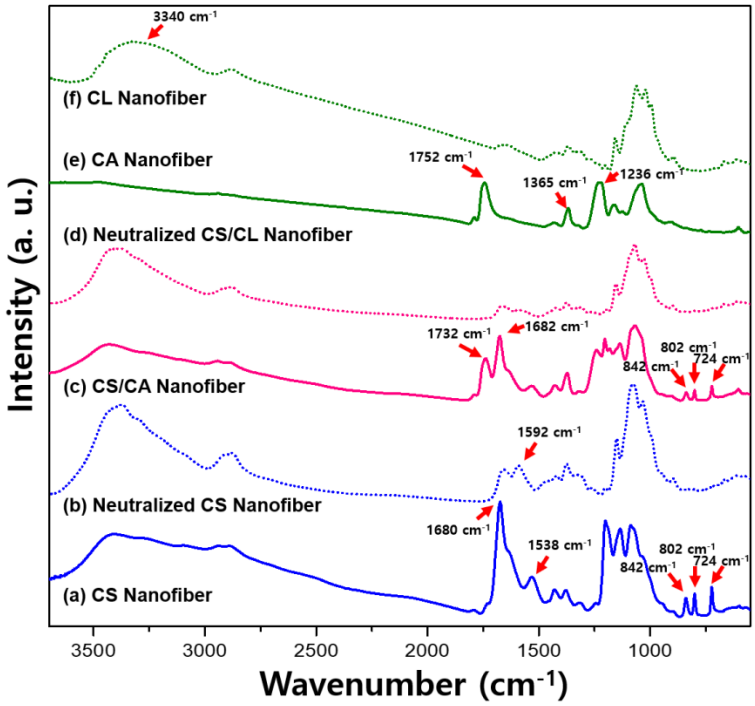

Figure 2. 3 - FT-IR spectra of (a) CS nanofibers, (b) neutralized CS nanofibers, (c) CS/CA nanofibers, (d) neutralized CS/CL nanofibers, (e) CA nanofibers and (f) CL nanofibers.

2.3.3 Mechanical properties of nanofiber mats

Figure 2.4 show representative stress-strain curves of the prepared nanofibers. Deacetylation of CA nanofibers (namely CL nanofibers) result a considerable increase in strength at break compared to CA nanofibers, more than 2.5 times rise from 2.16 ± 0.3 MPa to 5.24 ± 0.3 MPa. It is assumed that the multiple hydroxyl groups of CL form strong hydrogen bonding, holding the chains more firmly together

side-by-side, which gives the CL nanofiber mats higher tensile strength than CA nanofiber mats. In addition, a remarkable change in mechanical properties of CS nanofibers after neutralization is observed. The tensile stress at break increased from 9.76 ± 0.5 MPa to 16.94 ± 2 MPa after neutralization. As shown in **Figure 2.2 (d)**, the CS nanofiber structure is destroyed and welded after the neutralization and washing process, making junction points that restrict the slip of polymer chains [86-88]. As a result, the Na_2CO_3 treatment and washing lead to the enhancement of mechanical properties. The enhancement of tensile strength is also observed in the hybrid nanofiber mats which show the tensile strength at break with of 13.36 ± 1.1 MPa. It is obvious that the combination of CS and CA composite nanofibers attribute to increase of mechanical property, Figure 2.4 (d). This phenomenon might be due to the chemical interaction between CS and CA which induced by ammonium group in chitosan and acetyl group in CA. This interaction makes polymer chains stronger and stiffer than pure CS and pure CA, resulting in the increase of mechanical property of CA/CS nanofibers. The average stress at break of CS/CA nanofibers is higher than that of CS or CA nanofibers. More importantly, the neutralized CS/CL nanofibers demonstrated the highest tensile strength at break with values of 16.30 ± 0.7 MPa among all the samples. Neutralization of CS nanofibers can easily form a hydrogen bond with CL nanofibers which made through deacetylation of CA nanofibers. Therefore, blending of CS/CL can lead to the enhancement of physical properties in nanofibers, broadening the possibility for the filtration properties. At wet state, the tensile strengths of CS, CS/CL and CL samples decreased to 10.74 ± 0.4 MPa, 11.72 ± 0.3 MPa, and 4.7 ± 0.3 MPa, respectively. The reason for the lower strengths of CS and CS/CL nanofibers is that water molecules penetrate and interact with hydroxyl groups of chitosan nanofibers, resulting in the weakening of intermolecular hydrogen

bonds inside molecular network of nanofibers. A similar phenomenon happened to CL nanofibers to a minor extent, the strength at break in the wet state declined slightly from 5.24 to 4.7 MPa as compared to one in the dry state, given that CL nanofibers are intrinsically stable in the aqueous environment.

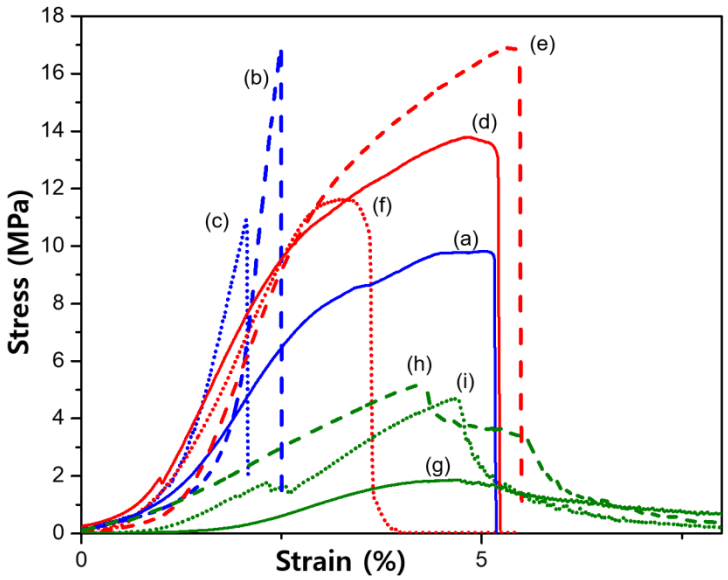

Figure 2. 4 - Stress-strain curves obtained from the samples; (a) CS nanofiber mat, (b) neutralized CS nanofibers mat, (c) wet state of neutralized CS nanofiber mat, (d) CS/CA nanofiber mat, (e) neutralized CS/CL nanofiber mat, (f) wet state of neutralized CS/CL nanofiber mat, (g) CA nanofiber mat, (h) CL nanofiber mat, and (i) wet state of CL nanofiber mat

2.3.4 Adsorption equilibrium isotherm

2.3.4.1 Adsorption kinetics of As, Pb, and Cu metal ions

Figure 2.5 (a) shows the adsorption of As(V), Pb(II) and Cu(II) ions onto the CS/CL nanofiber mats in a 1 g/L solution as a function of time. The adsorption of these ions on CS/CL nanofiber mats was also confirmed by Energy-Dispersive X-ray spectroscopy (EDS) analysis (**Figure 2.6**). The adsorption capacity of As(V), Pb(II) and Cu(II) ions increased as the contact time increased, and the maximum adsorption

capacity of As(V), Pb(II) and Cu(II) ions were 26.1, 39.5, and 80.7 mg/g, respectively. The adsorption of metal ions increased sharply up to 5 min, and then gradually plateaued. The initial increases in metal ion adsorption may be due to the large availability of binding sites such as amines and primary and secondary hydroxyl groups, as well as the high specific surface area of the nanofibers and inter- and intra- pores in the nanofibers. The experimental adsorption equilibrium data of As(V), Pb(II) and Cu(II) ion was analyzed according to the pseudo-first-order and pseudo-second-order kinetic models. The pseudo-first-order equation is generally expressed as follows [89-91];

$$\frac{\mathrm{d}q_t}{\mathrm{dt}} = k_1(q_e - q_t) \quad (2)$$

where q_e is adsorption capacity at equilibrium (mg/g), q_t is adsorption capacity at time (mg/g), and k_1 is the rate constant (1/min). The integrated form of equation (2) from t = 0 to t = t and from $q_t = 0$ to $q_t = q_t$ is:

$$\log(q_e - q_t) = \log(q_e) - \frac{k_1 t}{2.303} \quad (3)$$

The values of q_e and k_1 calculated from the plot in **Figure 2.5 (a)** were 25.13 and 1.54, 37.35 and 1.75, and 76.30 (mg/g) and 1.56 (1/min) for As(V), Pb(II) and Cu(II), respectively. However, these values did not exactly match those from the experiments. On the other hand, it seems that the pseudo-second-order kinetic model is more suitable for fitting the experimental results than the pseudo-second-order kinetic model. The pseudo-second-order equation is [92, 93]:

$$\frac{\mathrm{t}}{q_t} = \frac{1}{k_2 q_e^2} + \frac{t}{q_e} \quad (4)$$

Where q_e is the adsorption capacity at equilibrium (mg/g), q_t the adsorption capacity at time t, and k_2 is the rate constant of the pseudo-second-order adsorption (g/(mg·min)). The experimental adsorption equilibrium data of As(V), Pb(II) and

Cu(II) ions were also analyzed according to the pseudo-second-order equation, and the obtained values of q_e and k_2 were 26.73 mg/g and 0.09 g/(mg·min), 39.73 mg/g and 0.07 g/(mg·min), and 81.51 mg/g and 0.03 g/(mg·min). The fitting model using the pseudo-second-order is closer to experimental data compared to the pseudo-first-order model. Therefore, comparing the results of the two kinetics models reveals that the pseudo-second-order model agrees well with the experimental data.

2.3.4.2 Adsorption equilibrium isotherm of Cu metal ions

Figure 2.5 (b) shows the equilibrium adsorption amounts at 30 min under various concentrations. The experimental equilibrium isotherm data were analyzed according to the Langmuir and Freundlich adsorption equations, which are represented as follows, respectively [13, 94-96].

$$q_e = \frac{q_m K_L C_e}{1 + K_L C_e} \quad (5)$$

$$q_e = K_F C_e^{1/n} \quad (6)$$

where q_e is the equilibrium adsorption capacity (mg/g), q_m is the maximum adsorption capacity (mg/g), C_e is the equilibrium metal ion concentration (mg/L), K_L is Langmuir constant related the adsorption capacity (L/mg), K_F is Freundlich constant related the adsorption capacity (L/mg), and n is Freundlich constant related to the sorbent intensity. The Langmuir model for adsorption is based on the hypothesis that the maximum adsorption capacity consists of a monolayer adsorption. Interactions between adsorbed molecules are ignored and the adsorption energy is homogeneously distributed over the entire surface. On the other hand, the Freundlich model is used to describe the adsorption of molecules on a heterogeneous surface of an adsorbent as well as a multilayer sorption. When applying both models to experimental data, it appears that the experimental data is more suitably fit the

Langmuir model, **Figure 2.5 (b)**. The values of the correlation coefficient (r^2) obtained in case of Langmuir model (r^2 = 0.9889, 0.9980, and 0.9993, processed from adsorption data of As(V), Pb(II) and Cu(II), respectively) were higher than those obtained in case of Freundlich isotherm model (r^2 = 0.9773, 0.9950, and 0.9952). It indicates that the Langmuir model fits well to the ions adsorption data. The values of q_m and K_L calculated from the Langmuir plot are 39.4 mg/g and 1.841 L/mg, 57.4 mg/g and 2.081 L/mg, and 112.6 mg/g and 2.208 L/mg for As(V), Pb(II) and Cu(II), respectively. **Table 2.3** shows the adsorption capacity, q_m, of various chitosan based composite materials and chitosan nanofibers in the previous literature. According to **Table 2.3**, the q_m of CS/CL nanofiber is not the highest value but it is also quite high value among the other similar materials. The values of K_F and n obtained from Freundlich plot are 27.11 mg/g and 5.99, 39.95 mg/g and 5.87, and 81.16 mg/g and 6.68. The values of kinetic and equilibrium isotherm parameters are summarized in **Table 2.2**.

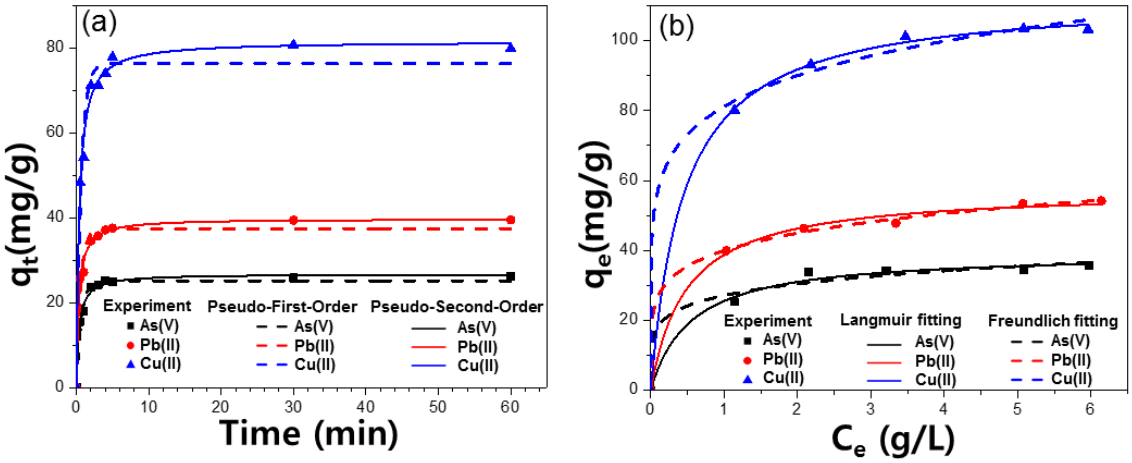

Figure 2. 5 - (a) Adsorption kinetics pseudo-first-order and pseudo-second-order, and (b) Langmuir and Freundlich adsorption isotherm of (■) As(V), (●) Pb(II) and (▲) Cu(II) ions onto the CS/CL nanofiber mat

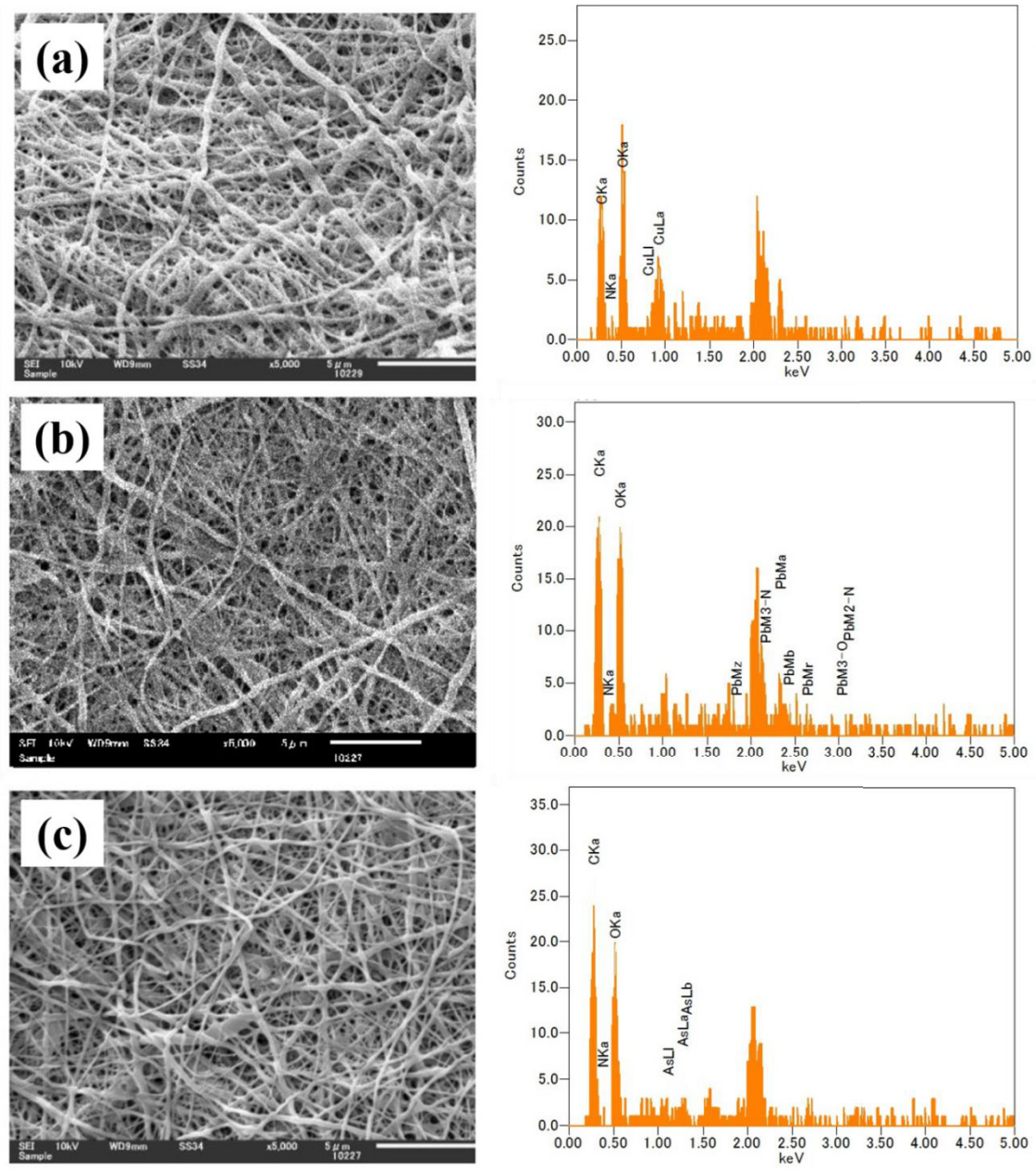

Figure 2. 6 - SEM image and corresponding EDS results of (a) Cu(II), (b) Pb(II), (c) As(V) adsorbed CS/CL nanofibers

Table 2. 2 - Fitted parameters of As, Pb and Cu ion adsorption onto CS/CL nanofiber mat.

		k_1 (min^{-1})	q_e (mg/g)	r^2

Pseudo first order	As	1.54	25.1	0.9813
	Pb	1.75	37.3	0.9613
	Cu	1.56	76.3	0.9684
		k2 ($g.mg^{-1}.min^{-1}$)	**q_e(mg/g)**	**r^2**
Pseudo second order	As	0.09	26.7	0.9899
	Pb	0.07	39.7	0.9901
	Cu	0.03	81.5	0.9911
		q_m (mg/g)	**K_L(L/mg)**	**r^2**
Langmuir model	As	39.4	1.841	0.9889
	Pb	57.4	2.081	0.9980
	Cu	112.6	2.208	0.9993
		n	**K_F(mg/g)**	**r^2**
Freundlich model	As	5.99	27.11	0.9773
	Pb	5.87	39.95	0.9950
	Cu	6.68	81.16	0.9952

Table 2. 3 - Comparison of As(V), Pb(II) and Cu(II) ion adsorption onto a variety of CS based adsorbents, qm is the adsorption capacity of the metals ions adsorbed onto the adsorbents

Metal ions	**Type of adsorbent**	**q_m (mg g^{-1})**
As	Iron–chitosan composites [97]	22.47
	Iron–chitosan composite granules [98]	8.47
	Chitosan [99]	58.0
	Nano-alumina dispersed in chitosan-grafted polyacrylamide [100]	6.56
Pb	Chitosan–MAA nanoparticles [101]	11.3
	Xanthate-modified magnetic chitosan [102]	76.9
	Chitosan-coated sand [103]	12.32

	Chitosan nanofibers [16]	263.15
Cu(II)	Cross-linking chitosan/rectorite nano-hybrid composite microspheres [50]	20.49
	chitosan saturated montmorillonite [51]	34.9
	Nitrogen-doped chitosan-Fe(III) composite [52]	165.8
	Cross-linked Magnetic Chitosan Beads [104]	78.13
	Chitosan nanofibers [16]	485.44

2.4 Conclusion

In this study, we provide an effective way to fabricate CS/CL nanofibers through electrospinning. The hybrid system can overcome the drawbacks of each component; dissolution of CS and metal non-adsorption of CL. The prepared CS/CL nanofibers compensate the disadvantages of each other, showing stability in aqueous solution and reasonable metal adsorption property. Structure and morphology studies showed that the CS/CL nanofibers have very smooth and well-defined structure, and also high-water stability. Moreover, it was found that the CS/CL nanofiber mats have the highest mechanical strength, which originates from the combination of CS. The combination of CS/CL showed an adsorption property against As(V), Pb(II), and Cu(II) ions, which cannot be achieved using single component CS or CL nanofibers, because CS nanofibers are easily dissolved in aqueous solution and CL nanofibers do not have adsorption property. The adsorption capacity of CS/CL nanofibers as a function of contact time was analyzed using the pseudo-first-order and pseudo-

second-order kinetic models. The pseudo-second-order model is more in agreement with the experimental data, showing an equilibrium adsorption capacity of 26.7, 39.7, and 81.51 mg/g toward As, Pb, and Cu ions, respectively. Equilibrium adsorption capacity was also plotted as a function of initial concentration of As(V), Pb(II), and Cu(II) ions. The experimental data are fitted with Langmuir and the Freundlich isotherm models, and the adsorption is more accurately fitted to the Langmuir isotherm model. The calculated maximum adsorption capacity was 39.4, 57.4, and 112.6 mg/g for As(V), Pb(II), and Cu(II), respectively, indicating the CS/CL nanofibers possess great potential for the use as an adsorbent for metal ions in wastewater effluents.

References

[1] R. Yu, X. Yuan, Y. Zhao, G. Hu, X. Tu, Heavy metal pollution in intertidal sediments from Quanzhou Bay, China, Journal of Environmental Sciences 20(6) (2008) 664-669.
[2] Y. Hu, X. Liu, J. Bai, K. Shih, E.Y. Zeng, H. Cheng, Assessing heavy metal pollution in the surface soils of a region that had undergone three decades of intense industrialization and urbanization, Environmental Science and Pollution Research 20(9) (2013) 6150-6159.
[3] J.W. Lee, C.K. Lee, C.S. Moon, I.J. Choi, K.J. Lee, S.-M. Yi, B.-K. Jang, B.j. Yoon, D.S. Kim, D. Peak, D. Sul, E. Oh, H. Im, H.S. Kang, J. Kim, J.-T. Lee, K. Kim, K.L. Park, R. Ahn, S.H. Park, S.C. Kim, C.-H. Park, J.H. Lee, Korea National Survey for Environmental Pollutants in the Human Body 2008: Heavy metals in the blood or urine of the Korean population, International Journal of Hygiene and Environmental Health 215(4) (2012) 449-457.
[4] K.S. Mohammed Abdul, S.S. Jayasinghe, E.P.S. Chandana, C. Jayasumana, P.M.C.S. De Silva, Arsenic and human health effects: A review, Environmental Toxicology and Pharmacology 40(3) (2015) 828-846.
[5] A. Bhatnagar, M. Sillanpää, Removal of natural organic matter (NOM) and its constituents from water by adsorption – A review, Chemosphere 166 (2017) 497-510.
[6] A. Dąbrowski, Z. Hubicki, P. Podkościelny, E. Robens, Selective removal of the heavy metal ions from waters and industrial wastewaters by ion-exchange method, Chemosphere 56(2) (2004) 91-106.
[7] F. Fu, Q. Wang, Removal of heavy metal ions from wastewaters: A review, Journal of Environmental Management 92(3) (2011) 407-418.
[8] G. Crini, Recent developments in polysaccharide-based materials used as adsorbents in wastewater treatment, Progress in Polymer Science 30(1) (2005) 38-70.
[9] D. Mohan, C.U. Pittman, Activated carbons and low cost adsorbents for remediation of tri- and hexavalent chromium from water, Journal of Hazardous Materials 137(2) (2006) 762-811.
[10] W.S. Wan Ngah, M.A.K.M. Hanafiah, Removal of heavy metal ions from wastewater by chemically modified plant wastes as adsorbents: A review, Bioresource Technology 99(10) (2008) 3935-3948.

[11] R. Jayakumar, M. Prabaharan, S.V. Nair, H. Tamura, Novel chitin and chitosan nanofibers in biomedical applications, Biotechnology Advances 28(1) (2010) 142-150.
[12] M. Zhang, X.H. Li, Y.D. Gong, N.M. Zhao, X.F. Zhang, Properties and biocompatibility of chitosan films modified by blending with PEG, Biomaterials 23(13) (2002) 2641-2648.
[13] B.-M. Min, S.W. Lee, J.N. Lim, Y. You, T.S. Lee, P.H. Kang, W.H. Park, Chitin and chitosan nanofibers: electrospinning of chitin and deacetylation of chitin nanofibers, Polymer 45(21) (2004) 7137-7142.
[14] L. Zeng, Y. Chen, Q. Zhang, X. Guo, Y. Peng, H. Xiao, X. Chen, J. Luo, Adsorption of Cd(II), Cu(II) and Ni(II) ions by cross-linking chitosan/rectorite nano-hybrid composite microspheres, Carbohydrate Polymers 130 (2015) 333-343.
[15] C. Hu, P. Zhu, M. Cai, H. Hu, Q. Fu, Comparative adsorption of Pb(II), Cu(II) and Cd(II) on chitosan saturated montmorillonite: Kinetic, thermodynamic and equilibrium studies, Applied Clay Science 143 (2017) 320-326.
[16] C. Zhu, F. Liu, Y. Zhang, M. Wei, X. Zhang, C. Ling, A. Li, Nitrogen-doped chitosan-Fe(III) composite as a dual-functional material for synergistically enhanced co-removal of Cu(II) and Cr(VI) based on adsorption and redox, Chemical Engineering Journal 306 (2016) 579-587.
[17] J. Wang, C. Chen, Chitosan-based biosorbents: Modification and application for biosorption of heavy metals and radionuclides, Bioresource Technology 160 (2014) 129-141.
[18] R. Karthik, S. Meenakshi, Removal of Pb(II) and Cd(II) ions from aqueous solution using polyaniline grafted chitosan, Chemical Engineering Journal 263 (2015) 168-177.
[19] A.S.K. Kumar, S.-J. Jiang, Chitosan-functionalized graphene oxide: A novel adsorbent an efficient adsorption of arsenic from aqueous solution, Journal of Environmental Chemical Engineering 4(2) (2016) 1698-1713.
[20] M.Z. Elsabee, R.E. Morsi, A.M. Al-Sabagh, Surface active properties of chitosan and its derivatives, Colloids and Surfaces B: Biointerfaces 74(1) (2009) 1-16.
[21] H.J. Lee, Y.H. Park, W.-G. Koh, Fabrication of Nanofiber Microarchitectures Localized within Hydrogel Microparticles and Their Application to Protein Delivery and Cell Encapsulation, Adv. Funct. Mater. 23(5) (2013) 591-597.
[22] C. Lim, D.W. Lee, J.N. Israelachvili, Y. Jho, D.S. Hwang, Contact time- and pH-dependent adhesion and cohesion of low molecular weight chitosan coated surfaces, Carbohydrate Polymers 117 (2015) 887-894.
[23] F.-L. Mi, S.-S. Shyu, C.-Y. Kuan, S.-T. Lee, K.-T. Lu, S.-F. Jang, Chitosan–Polyelectrolyte complexation for the preparation of gel beads and controlled release of anticancer drug. I. Effect of phosphorous polyelectrolyte complex and enzymatic hydrolysis of polymer, Journal of Applied Polymer Science 74(7) (1999) 1868-1879.
[24] X. Qu, A. Wirsén, A.C. Albertsson, Novel pH-sensitive chitosan hydrogels: swelling behavior and states of water, Polymer 41(12) (2000) 4589-4598.
[25] N. Bhattarai, D. Edmondson, O. Veiseh, F.A. Matsen, M. Zhang, Electrospun chitosan-based nanofibers and their cellular compatibility, Biomaterials 26(31) (2005) 6176-6184.
[26] H. Lee, M. Nishino, D. Sohn, J.S. Lee, I.S. Kim, Control of the morphology of cellulose acetate nanofibers via electrospinning, Cellulose 25(5) (2018) 2829-2837.
[27] Z. Khatri, F. Ahmed, A. Khatri, M. Khatri, U.A. Qureshi, I.-S. Kim, Screen-printed electrospun cellulose nanofibers using reactive dyes, Cellulose 24(10) (2017) 4561-4568.
[28] R. Konwarh, N. Karak, M. Misra, Electrospun cellulose acetate nanofibers: The present status and gamut of biotechnological applications, Biotechnology Advances 31(4) (2013) 421-437.
[29] L. Zhang, T.J. Menkhaus, H. Fong, Fabrication and bioseparation studies of adsorptive membranes/felts made from electrospun cellulose acetate nanofibers, Journal of Membrane Science 319(1) (2008) 176-184.
[30] D.-G. Yu, J.-H. Yu, L. Chen, G.R. Williams, X. Wang, Modified coaxial electrospinning for the preparation of high-quality ketoprofen-loaded cellulose acetate nanofibers, Carbohydrate Polymers 90(2) (2012) 1016-1023.

[31] Z. Khatri, F. Ahmed, A.K. Jhatial, M.I. Abro, G. Mayakrishnan, I.-S. Kim, Cold pad-batch dyeing of cellulose nanofibers with reactive dyes, Cellulose 21(4) (2014) 3089-3095.
[32] N. Li, R. Bai, Copper adsorption on chitosan–cellulose hydrogel beads: behaviors and mechanisms, Separation and Purification Technology 42(3) (2005) 237-247.
[33] X. Luo, J. Zeng, S. Liu, L. Zhang, An effective and recyclable adsorbent for the removal of heavy metal ions from aqueous system: Magnetic chitosan/cellulose microspheres, Bioresource Technology 194 (2015) 403-406.
[34] X.D. Liu, N. Nishi, S. Tokura, N. Sakairi, Chitosan coated cotton fiber: preparation and physical properties, Carbohydrate Polymers 44(3) (2001) 233-238.
[35] C. Liu, R. Bai, Preparation of chitosan/cellulose acetate blend hollow fibers for adsorptive performance, Journal of Membrane Science 267(1) (2005) 68-77.
[36] G. Salihu, P. Goswami, S. Russell, Hybrid electrospun nonwovens from chitosan/cellulose acetate, Cellulose 19(3) (2012) 739-749.
[37] H. Lee, J.M. Koo, D. Sohn, I.-S. Kim, S.S. Im, High thermal stability and high tensile strength terpolyester nanofibers containing biobased monomer: fabrication and characterization, RSC Advances 6(46) (2016) 40383-40388.
[38] C. Yin, A.W. Jatoi, H. Bang, M. Gopiraman, I.S. Kim, Fabrication of silk fibroin based three dimensional scaffolds for tissue engineering, Fibers and Polymers 17(8) (2016) 1140-1145.
[39] J.A. Wahab, G. Xu, H. Lee, P.D. Nam, K. Wei, S.H. Kim, I.S. Kim, Fabrication of silk fibroin/eggshell nanofiber membranes for facemasks, Fibers and Polymers 17(11) (2016) 1776-1781.
[40] J. Griffitt Robert, J. Luo, J. Gao, J.-C. Bonzongo, S. Barber David, Effects of particle composition and species on toxicity of metallic nanomaterials in aquatic organisms, Environmental Toxicology and Chemistry 27(9) (2009) 1972-1978.
[41] O. Bondarenko, K. Juganson, A. Ivask, K. Kasemets, M. Mortimer, A. Kahru, Toxicity of Ag, CuO and ZnO nanoparticles to selected environmentally relevant test organisms and mammalian cells in vitro: a critical review, Archives of Toxicology 87(7) (2013) 1181-1200.
[42] B.C. Suedel, E. Deaver, J.H. Rodgers, Experimental factors that may affect toxicity of aqueous and sediment-bound copper to freshwater organisms, Archives of Environmental Contamination and Toxicology 30(1) (1996) 40-46.
[43] H. Lee, K. Watanabe, M. Kim, M. Gopiraman, K.-H. Song, J.S. Lee, I.S. Kim, Handspinning Enabled Highly Concentrated Carbon Nanotubes with Controlled Orientation in Nanofibers, Scientific Reports 6 (2016) 37590.
[44] C.M. Buchanan, K.J. Edgar, A.K. Wilson, Preparation and characterization of cellulose monoacetates: the relationship between structure and water solubility, Macromolecules 24(11) (1991) 3060-3064.
[45] J. Srbová, M. Slováková, Z. Křípalová, M. Žárská, M. Špačková, D. Stránská, Z. Bílková, Covalent biofunctionalization of chitosan nanofibers with trypsin for high enzyme stability, Reactive and Functional Polymers 104 (2016) 38-44.
[46] B. Krajewska, Application of chitin- and chitosan-based materials for enzyme immobilizations: a review, Enzyme and Microbial Technology 35(2) (2004) 126-139.
[47] S.A.A.N. Nasreen, S. Sundarrajan, S.A. Syed Nizar, R. Balamurugan, S. Ramakrishna, In situ polymerization of PVDF-HEMA polymers: electrospun membranes with improved flux and antifouling properties for water filtration, Polymer Journal 46 (2013) 167.
[48] Z. Khatri, K. Wei, B.-S. Kim, I.-S. Kim, Effect of deacetylation on wicking behavior of co-electrospun cellulose acetate/polyvinyl alcohol nanofibers blend, Carbohydrate Polymers 87(3) (2012) 2183-2188.
[49] Z. Khatri, G. Mayakrishnan, Y. Hirata, K. Wei, I.-S. Kim, Cationic-cellulose nanofibers: Preparation and dyeability with anionic reactive dyes for apparel application, Carbohydrate Polymers 91(1) (2013) 434-443.
[50] H. Li, C. Zhu, J. Xue, Q. Ke, Y. Xia, Enhancing the Mechanical Properties of Electrospun Nanofiber Mats through Controllable Welding at the Cross Points, Macromolecular Rapid Communications 38(9) (2017) 1600723.

[51] L.A. Goetz, B. Jalvo, R. Rosal, A.P. Mathew, Superhydrophilic anti-fouling electrospun cellulose acetate membranes coated with chitin nanocrystals for water filtration, Journal of Membrane Science 510 (2016) 238-248.
[52] Y. Yao, K.K. Fu, S. Zhu, J. Dai, Y. Wang, G. Pastel, Y. Chen, T. Li, C. Wang, T. Li, L. Hu, Carbon Welding by Ultrafast Joule Heating, Nano Letters 16(11) (2016) 7282-7289.
[53] Y.S. Ho, G. McKay, A Comparison of Chemisorption Kinetic Models Applied to Pollutant Removal on Various Sorbents, Process Safety and Environmental Protection 76(4) (1998) 332-340.
[54] E. Demirbas, M. Kobya, E. Senturk, T. Ozkan, Adsorption kinetics for the removal of chromium (VI) from aqueous solutions on the activated carbons prepared from agricultural wastes, Water SA 30(4) (2004) 533-539.
[55] S. Vasudevan, J. Lakshmi, G. Sozhan, Studies on the Removal of Iron from Drinking Water by Electrocoagulation – A Clean Process, CLEAN – Soil, Air, Water 37(1) (2009) 45-51.
[56] Y.-S. Ho, Using of "pseudo-second-order model" in adsorption, Environmental Science and Pollution Research 21(11) (2014) 7234-7235.
[57] Y.-S. Ho, Second-order kinetic model for the sorption of cadmium onto tree fern: A comparison of linear and non-linear methods, Water Research 40(1) (2006) 119-125.
[58] B.-Y. Yang, Y. Cao, F.-F. Qi, X.-Q. Li, Q. Xu, Atrazine adsorption removal with nylon6/polypyrrole core-shell nanofibers mat: possible mechanism and characteristics, Nanoscale Research Letters 10(1) (2015) 207.
[59] J. Wang, K. Pan, Q. He, B. Cao, Polyacrylonitrile/polypyrrole core/shell nanofiber mat for the removal of hexavalent chromium from aqueous solution, Journal of Hazardous Materials 244-245 (2013) 121-129.
[60] N.M. Mahmoodi, Z. Mokhtari-Shourijeh, Preparation of PVA-chitosan blend nanofiber and its dye removal ability from colored wastewater, Fibers and Polymers 16(9) (2015) 1861-1869.
[61] P.K. Neghlani, M. Rafizadeh, F.A. Taromi, Preparation of aminated-polyacrylonitrile nanofiber membranes for the adsorption of metal ions: Comparison with microfibers, Journal of Hazardous Materials 186(1) (2011) 182-189.
[62] A. Gupta, V.S. Chauhan, N. Sankararamakrishnan, Preparation and evaluation of iron–chitosan composites for removal of As(III) and As(V) from arsenic contaminated real life groundwater, Water Research 43(15) (2009) 3862-3870.
[63] D. Vu, X. Li, C. Wang, Adsorption of As(III) from aqueous solution based on porous magnetic/chitosan/ferric hydroxide microspheres prepared via electrospraying, Science China Chemistry 56(5) (2013) 678-684.
[64] B.J. McAfee, W.D. Gould, J.C. Nadeau, A.C.A. da Costa, BIOSORPTION OF METAL IONS USING CHITOSAN, CHITIN, AND BIOMASS OF RHIZOPUS ORYZAE, Separation Science and Technology 36(14) (2001) 3207-3222.
[65] S. Saha, P. Sarkar, Arsenic remediation from drinking water by synthesized nano-alumina dispersed in chitosan-grafted polyacrylamide, Journal of Hazardous Materials 227-228 (2012) 68-78.
[66] A. Heidari, H. Younesi, Z. Mehraban, H. Heikkinen, Selective adsorption of Pb(II), Cd(II), and Ni(II) ions from aqueous solution using chitosan–MAA nanoparticles, International Journal of Biological Macromolecules 61 (2013) 251-263.
[67] Y. Zhu, J. Hu, J. Wang, Competitive adsorption of Pb(II), Cu(II) and Zn(II) onto xanthate-modified magnetic chitosan, Journal of Hazardous Materials 221-222 (2012) 155-161.
[68] M.-W. Wan, C.-C. Kan, B.D. Rogel, M.L.P. Dalida, Adsorption of copper (II) and lead (II) ions from aqueous solution on chitosan-coated sand, Carbohydrate Polymers 80(3) (2010) 891-899.
[69] S. Haider, S.-Y. Park, Preparation of the electrospun chitosan nanofibers and their applications to the adsorption of Cu(II) and Pb(II) ions from an aqueous solution, Journal of Membrane Science 328(1) (2009) 90-96.

[70] G. Huang, C. Yang, K. Zhang, J. Shi, Adsorptive Removal of Copper Ions from Aqueous Solution Using Cross-linked Magnetic Chitosan Beads, Chinese Journal of Chemical Engineering 17(6) (2009) 960-966.

CHAPTER 3 The mechanistic actions of different silver species at the surfaces of polyacrylonitrile nanofibers regarding antibacterial activities

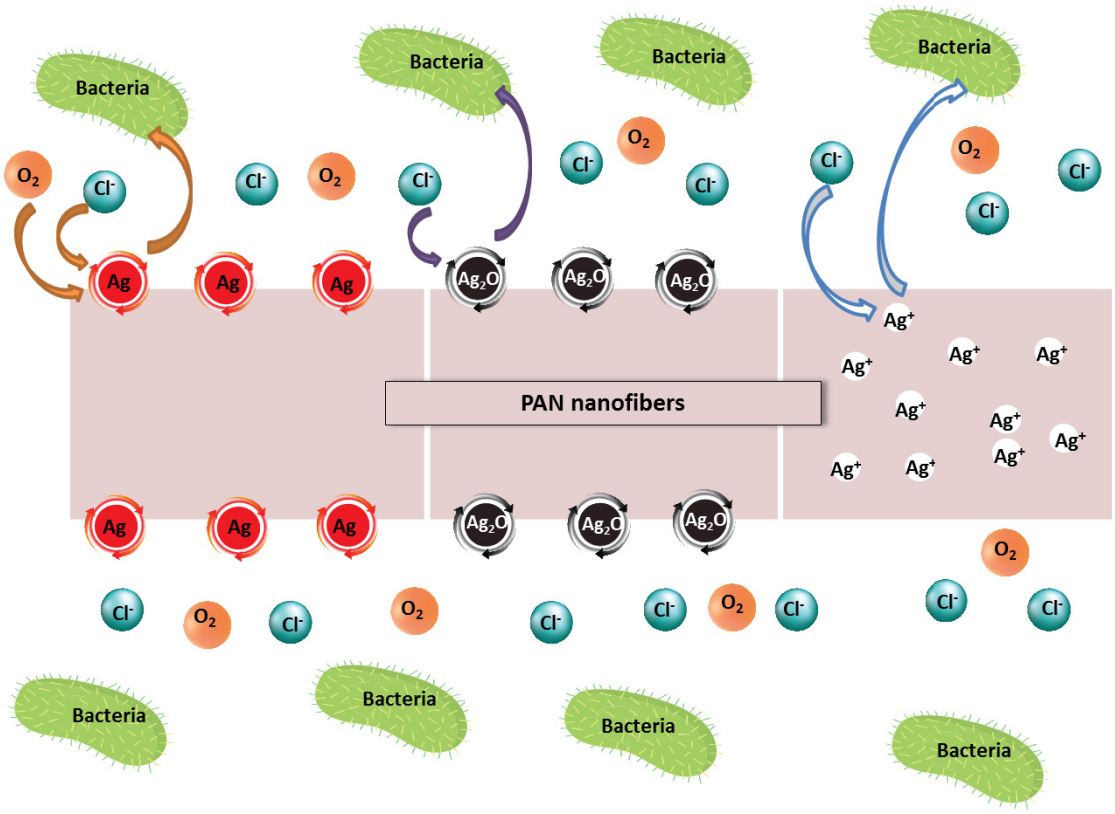

3.1. Introduction

Silver nanoparticles distributed on polymeric nanofiber scaffolds display specifically peculiar properties and have excellent potential to be used in biological applications, as well as chemical fields, electronics, energy storage, textile industries [1, 2]. One of the most common methods to incorporate metallic nanoparticles into the nanofibrous scaffolds is reactions between metallic salts and reducing agents [3]. Ag nanoparticles embedded nanofibers exhibit biomedical properties, which inherit from silver; and high surface-to-volume ratio, large numbers of reaction sites and water stability from nanofibers. Due to the unique property of silver on antibacterial activity, the silver composites have been used in medical devices, namely, cardiovascular implants [4], catheters [5], orthopedic implants [6], and dental composites [7], with antimicrobial and antibacterial characteristics. In the context of antibiotic-resistant bacteria, the medical world is in need of new antibiotic classes [8, 9]. Silver nanoparticles appeared as a very promising material to play this role; thus, extensive studies on silver nanoparticles, applied in bioengineering fields, have been conducted recently [10].

Silver can be embedded into the systems under different forms, silver salts, immobilized silver ions, zero-valent or mono-valent silver [11, 12]. Zero-valent silver and mono-valent silver at the form of silver nanoparticles are considered as a new class of antibacterial agent with effective antimicrobial properties and low toxicity toward human cells [13]. Metallic silver nanoparticles, containing zero-valent silver, exhibit bactericidal action through the mechanism linked to the oxidative dissolution of silver elements into the environment under oxic conditions. Zero-valent nano silver is sensitive to oxygen due to the size of nanometer and large surface area, thus, silver nanoparticles in aqueous environment will be partly

oxidized and play the role of silver-ion reservoir [14, 15]. Another report revealed the three stages of actions as follows; (i) when exposed to humid air or water, the silver nanoparticles, containing Ag^0, would be oxidized and dissolved; (ii) the silver ions then diffuse across liquid medium; and (iii) the formation of new smaller silver particles by chemical reduction or photoreduction [16]. Whereas, silver oxide nanoparticles containing mono-valent silver – Ag (+1) can be released by simple dissolution or ion exchange, a slightly acidic environment will speed up the decay of metal oxide and allow a faster release of Ag^+ [17]. In the case of silver ions, at the forms of entrapped silver ions or silver salts, they are highly toxic to a wide variety of organisms including bacteria, and the bactericidal mechanism is very well known [18]. The antibacterial comparison between silver ions and silver nanoparticles, therefore, is very appealing to scientific world.

Polyacrylonitrile (PAN) nanofibers possess hydrophilic property and active chelating groups - nitrile, which makes PAN nanofibers an appealing starting material for further modification into metal-adsorptive nanofibers [19, 20]. In addition, with high atomic percentage of carbon, PAN was implemented as a precursor for carbon nanofibers, which then exhibit a potential to be made into electrochemical electrodes or semiconductor devices [21-23]. Among many different nanoscale-capable synthesis methods such as melt-blown, drawing, template synthesis, phase separation, and self-assembly, electrospinning has risen as a simple yet versatile and cost-effective technique for fabricating nanofibers [24-28]. By applying an electric force on a drop of polymer solution to overcome the surface tension, nanofibers can be drawn and collected on a collector [29-31].

However, the antibacterial effect of such silver species is not significantly compared yet. Therefore, in our report, we investigated the antibacterial activity of

various silver species; silver nitrate, silver oxide nanoparticles, and silver nanoparticles, embedded in PAN nanofibrous scaffolds, against E. coli and B. subtilis. All the antibacterial tests were performed in triplicate and via three cycles to evaluate the bactericidal sustainability. The cytotoxicity against mouse cells – NIH3T3 dermal fibroblasts was examined over a 7-day course; the cytotoxicity of silver is considered dependent on cell lines, dose, and time of exposure [32].

3.2. Experimental

3.2.1 Materials

Polyacrylonitrile (PAN, Mw 150,000 g/mol) was acquired from Sigma-Aldrich, Tokyo, Japan. N,N-dimethylformamide (DMF), silver nitrate ($AgNO_3$ - 99.8%), sodium hydroxide (NaOH 97%), and sodium borohydride ($NaBH_4$) were purchased from Wako pure chemical industries, Osaka, Japan. Escherichia coli (Hfr 3000) was received from The Coli Genetic Stock (CGSC; Yale Univ., New Haven, CT, USA). Bacillus subtilis (168) was received from Dr. Ogasawara, Shinshu University, Japan. The petri dishes were provided by Sansei Medical Co., LTD., Japan.

3.2.2 Silver species incorporated in PAN nanofibers

Three different PAN solutions were prepared with 8 wt. % polymer in DMF and then vigorously stirred for 24 h. Subsequently, $AgNO_3$ was added to two solutions and they were further stirred for 2 h. The calculated silver-salt amounts were 1/20 and 1/5 corresponding to as-spun composite nanofibers in weight. Electrospinning was carried out for 24 h for each sample with same parameters, 15 cm distance from tip to collector, 40 % relative humidity, and 20 °C room temperature. The process ensured the relatively equal in thickness of all electrospun sheets. Three electrospun samples were denoted as PAN, $AgNO_3$-PAN 1/20, and $AgNO_3$-PAN 1/5.

To prepare silver (I) oxide nanoparticles incorporated PAN nanofibers, the $AgNO_3$-PAN 1/20 and 1/5 nanofibers were immersed in NaOH 1 M solutions for 2 h. The resulted samples were named as Ag_2O-PAN 1/20 and Ag_2O-PAN 1/5, respectively.

Similarly, the zero-valent silver nanoparticle/PAN composite nanofibers were achieved by treating $AgNO_3$-PAN 1/20 and 1/5 with $NaBH_4$ 0.5 M solutions to reduce silver salt to metallic silver nanoparticles. The resultant samples were indicated as Ag-PAN 1/20 and Ag-PAN 1/5.

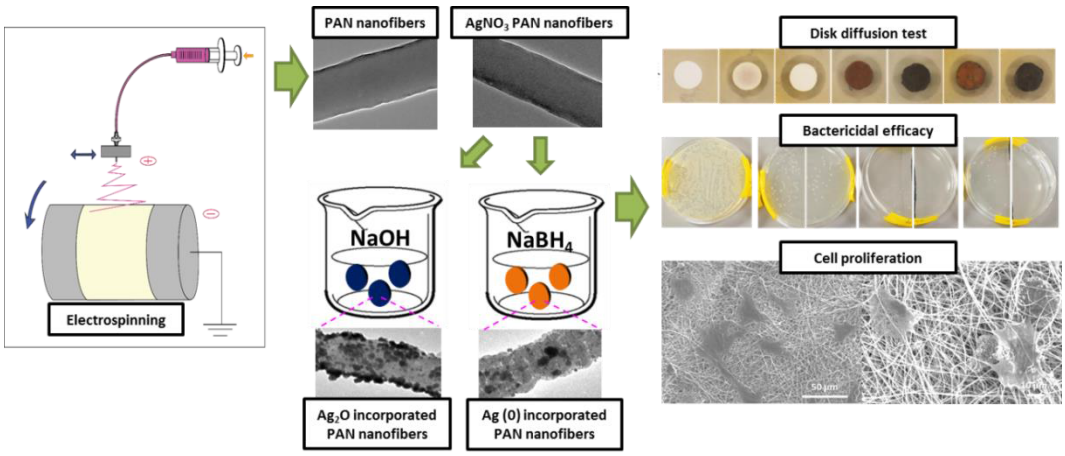

Scheme 3. 1 Experimental design

3.2.3 Characterization

Scanning Electron Microscope photographs and Energy Dispersive X-Ray Spectroscopy graphs were acquired on SEM-EDS (JSM-6010LA, JEOL, Japan). Transmission Electron Microscopy images were taken on TEM (2010 Fas TEM, JEOL, Tokyo, Japan). X-ray Photoelectron Spectroscopy surveys were collected on XPS (Kratos Axis-Ultra DLD, Kratos Analytical). Fourier Transform Infrared (FT-IR) spectra were acquired on Prestige-21, Shimadzu Co., Ltd., Japan. Wide-angle X-ray diffraction (XRD) graphs were taken on X-ray diffractometer (Miniflex 300, Rigaku Co., Ltd., Japan). Inductively coupled plasma-atomic emission spectroscopy (ICP-AES; Shimadzu ICPS-1000 IV; Shimadzu, Kyoto, Japan) was utilized for measuring silver release.

3.2.4 Silver release study and antibacterial effect

The silver release profiles were studied by immersing 0.02 g nanofibers in 50 mL distilled water under gentle agitation, 100 rpm during the period of 7 days. 5 mL liquid samples were extracted for ICP tests at certain time periods for examining the silver concentrations.

Disk diffusion tests and antimicrobial efficacy were assessed against Escherichia coli strain (Hfr 3000) and Bacillus subtilis strain (168). The bacteria were cultured in the LB liquid medium for 24 h, at 37 °C for E. coli and 30 °C for B. subtilis. The cultured bacteria were diluted with saline water to the bacterial concentration of 10^6 colony forming unit per milliliter - CFU/mL, confirmed by optical density at 600 nm.

In halo tests, 200 µL amounts of bacteria suspension (10^6 CFU/mL) were smeared over agar plates. Afterward, the rounded specimens were gently placed on agar plates, which were then cultured over 24 h. The diameters of inhibition zones were measured in mm.

The reduction of viability due to the effects of silver species was quantified by log reduction after 8 h immersion of silver composite samples in bacterial medium and 24 h culture of bacterial medium on agar plates subsequently in order to count viable bacteria cells. Precisely, 0.01 g nanofibers were incubated in 2 mL bacterial suspension at 37 °C for E. coli and 30 °C for B. subtilis. The log reduction was calculated as follows:

$$\text{Log Reduction} = \log_{10} \frac{A}{B}$$

Where A is the number of viable microorganisms of negative control sample, B is the number of viable microorganisms of tested samples.

After the first antibacterial tests, all samples were extracted and examined against with fresh bacteria. The antibacterial sustainability was assessed through two more

incubation cycles. The gradual decrease in antimicrobial activity was expected because of the reduction of silver loadings after each cycle.

3.2.5 In vitro cell adhesion

NIH3T3 cells used for biocompatible evaluation test were obtained from Riken Bioresource Center (ID: RCB1862, Riken Bioresource Center, Tsukuba, Japan). The specimens were cut into small pieces and tests were done in triplicate. Firstly, all specimens were sterilized by 70 % ethanol solution, then washed with PBS three times. For the cell adhesion tests, 1 mL cell suspension aqueous solution containing 50,000 cells was dripped over 0.001 mg nanofiber scaffolds, the specimens were kept for 3 h for cell attachment. Cell-seeded composite specimens were then rinsed with PBS to remove unattached cells and maintained in growth medium, using 96-well plates, at 37 °C, and 5% CO_2 for 7 days. The numbers of attached and grown cells on the nanofibers were quantified on days 1, 4, and 7; the method was described on section 2.5 of previous published article [33]. In detail, nanofiber specimens were placed in micro-tube, buffer solution (0.5% Triton X100 in PBS) was subsequently added to remove attached cells from the scaffolds. The buffer solutions containing cells were sampled and quantified at UV wavelength of 340 nm, using LDH assay method [34].

3.3. Results and discussion

3.3.1 Morphology study of nanofiber membranes

SEM images show thin and highly uniform PAN nanofibers with average diameters of 301 ± 63 nm, Figure 3.1 (a). The average diameters of the as-spun silver composite nanofibers slightly decreased as the higher silver-salt amounts added to the polymer solutions, 275 ± 52 and 243 ± 58 nm, Figure 3.1 (b) and (c) for $AgNO_3$-

PAN 1/20 and 1/5, respectively. It can be explained by the higher conductivity of the spinning solution, which decreases the electrostatic potential and produces thinner nanofibers [35].

For the silver nanoparticle/nanofiber composite samples, fine nano-sized silver nanoparticles can be spotted gathering on the PAN nanofibers, Figure 3.1 (d), (e), (f) and (g) corresponding to Ag_2O-PAN 1/20, Ag_2O-PAN 1/5, Ag-PAN 1/20, and Ag-PAN 1/5, respectively. The morphology of composite nanofibers was rough with grain-like particles attaching to the surfaces. More particles aggregated, after reactions, on the surfaces of nanofibers with the higher silver loadings, when we compared Figure 3.1 (e, g) against Figure 3.1 (d, f).

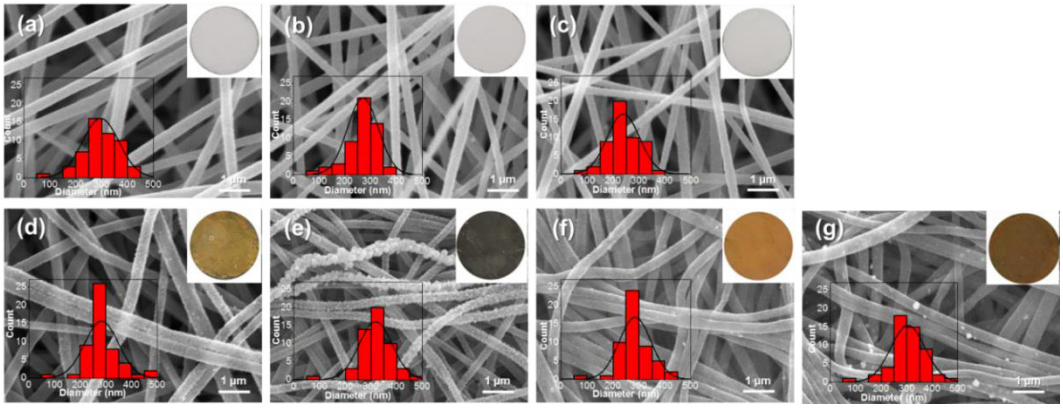

Figure 3. 1 - Morphology of (a) as-spun PAN nanofibers; $AgNO_3$-PAN (b) 1/20 and (c) 1/5, Ag_2O-PAN (d) 1/20 and (e) 1/5; Ag-PAN (f) 1/20 and (g) 1/5. Colors of samples are represented on inset photos.

For a closer look at the nano-size of silver particles, TEM images were obtained. TEM photographs depict the round-shaped silver nanoparticles embedded in/on nanofiber strands; the density and size of particles could be well distinguished; more particles with larger size on composite nanofiber samples containing higher silver amounts can be observed. The incorporation of silver nanoparticles into the polymer

matrix occurred following the reactions of silver salts with sodium hydroxide or sodium borohydride to form mono-valent or zero-valent silver nanoparticles.

As-spun PAN nanofiber, $AgNO_3$-PAN 1/20 nanofiber, and $AgNO_3$-PAN 1/5 nanofiber present images of smooth, translucent, and featureless fibers, Figure 3.2 (a), (b), and (c). Interestingly, at higher magnification, some silver particles at the size of few nanometers were detected in $AgNO_3$-PAN 1/20 and $AgNO_3$-PAN 1/5 nanofibers, inset pictures. This observation can be explained by the partial reduction of $AgNO_3$ by DMF solvent after adding silver salt into the PAN/DMF solutions or photoreduction attributed to the contact of silver salt with any sources of light, leading to the particulate formation.

In the cases of silver nanoparticle/PAN composite nanofibers, the size distributions of silver oxide nanoparticles and metallic silver nanoparticles were calculated from several TEM images to form the statistic histograms. The mean particulate sizes, measured and calculated on image J, with standard deviations were 12.01 ± 2.35 and 14.3 ± 4.88 nm for Ag_2O-PAN 1/20 and Ag-PAN 1/20 nanofibers, Figure 3.2 (d) and (f), respectively. For the Ag_2O-PAN 1/5 and Ag-PAN 1/5 samples, the bulkier particles aggregated after chemical reduction. In Figure 3.2 (e) and (g), the mean sizes with standard deviations were calculated as 34.57 ± 12.66 nm for Ag_2O-PAN 1/5 and 32.37 ± 22.59 for Ag-PAN 1/5. In Ag-PAN 1/5 samples, there were few particles with size larger than 100 nm, formed inside PAN nanofibers. It could be explained as the hydrogen generated from the hydrolysis of sodium borohydride penetrated into the PAN polymer matrix and reacted with $AgNO_3$ [36, 37]. The reduction could, therefore, happen inside the nanofibers and form 100-nm sized silver particles, Figure 3.2 (g).

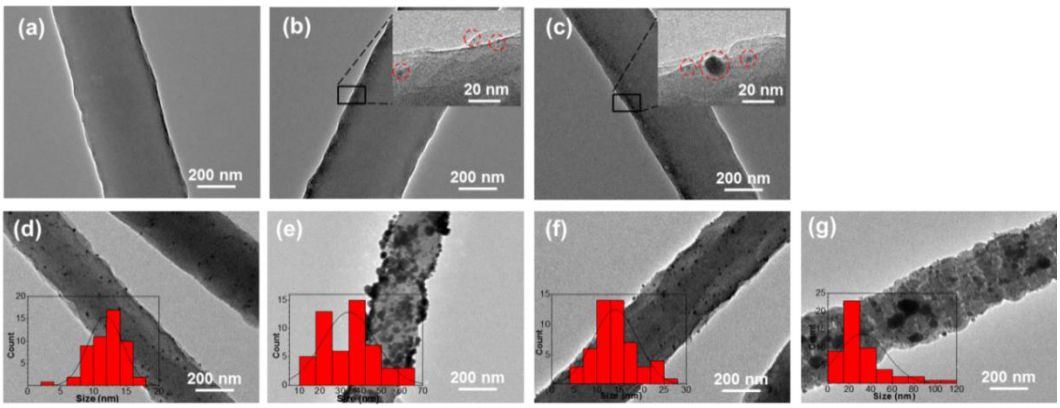

Figure 3. 2 - TEM images of (a) as-spun PAN, $AgNO_3$-PAN (b) 1/20 and (c) 1/5, Ag_2O-PAN (d) 1/20 and (e) 1/5, Ag-PAN (f) 1/20 and (g) 1/5 with particle size histograms.

3.3.2 FT-IR spectral analysis

In Figure 3.3, PAN nanofibers show typical peaks at 2930, 2245, 1450, 1070, and 1040 cm^{-1} characterizing CH_2 asymmetric stretching, C≡N symmetric stretching, CH_2 bending, C–C stretching, and C–C≡N combination mode, respectively [38]. Those peaks were also present in all silver-PAN composite nanofibers. Noticeably, there were slight negative shifts of CH_2 asymmetric stretching due to the interactive influences of silver salts toward the group, $AgNO_3$-PAN 1/20 and 1/5. [39].

In Figure 3.3 (B), peaks at 1410, 1390, 1305, and 1040 cm^{-1} could be ascribed for nitrate groups in $AgNO_3$ [40, 41]. Those peaks were eliminated from spectra of Ag_2O-PAN 1/20, Ag_2O-PAN 1/5, Ag-PAN 1/20, and Ag-PAN 1/5, demonstrating that the silver salt was depleted and the reaction between silver salt and NaOH or $NaBH_4$ happened completely.

The rising band at 3400-3500 cm^{-1} must be due to the vapor absorption into the PAN composite nanofibers. It is believed that the highly adsorptive properties of $AgNO_3$ and Ag nanoparticles toward vapor gave rise to this band, Figure 3.3 (A) [42].

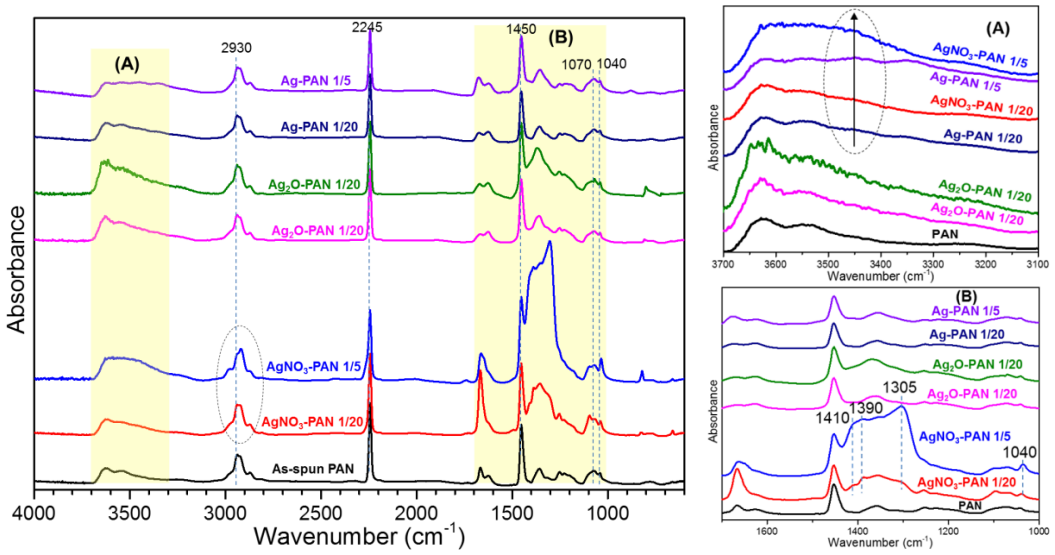

Figure 3. 3 - FT-IR spectra of PAN nanofibers, $AgNO_3$-PAN 1/20, 1/5, Ag_2O-PAN 1/20, 1/5, Ag-PAN 1/20, and 1/5.

3.3.3 X-ray diffraction study

To investigate the differences and the variations of crystallinity before and after chemical reactions, XRD characterization was performed. Pristine PAN nanofibers show 2 typical wide bands centered at 2θ = 17 ° and 26.5 °. The penetration of silver salt into the polymer matrix made positive shift for the 17 ° band and the decreasing intensity for 26.5 ° band. The penetration of silver nitrate into the polymer matrix were supposed to make these changes [43].

Two wide typical bands of PAN also appear in all chemical-reduced silver/PAN composite nanofibers, Figure 3.4 (d), (e), (f), and (g). Those two bands were positionally identical to two bands of pristine PAN. It could be perceived as the influences of silver salt to the crystalline structure of the polymer were eliminated, due to the complete reactions of $AgNO_3$ with reagents NaOH or $NaBH_4$.

The presence of silver oxide nanoparticles and silver nanoparticles manifested via two different sets of peaks. Figure 3.4 (d) and (e) illustrates XRD patterns of Ag_2O-PAN 1/20 and 1/5 with diffraction peaks at 2θ = 32.8 °, 38.1 °, 55.9 °, and 65.4 °

correlating to (111), (200), (220), and (311) crystal planes of cubic Ag_2O [44]. Figure 3.4 (g) and (h) demonstrates characteristic peaks of Ag-PAN 1/20 and 1/5; peaks at 38 °, 44 °, 64.5 °, and 77 ° could be indexed to (111), (200), (220), and (311) crystal planes of Ag(0) [45]. The intensities of those peaks increased due to the increase in size and number of silver nanoparticles. There was no shifting in peak positions of Ag_2O and Ag, thus, it can be interpreted as no changes in the interlayer of d-spacing of lattice caused by impurities [45, 46].

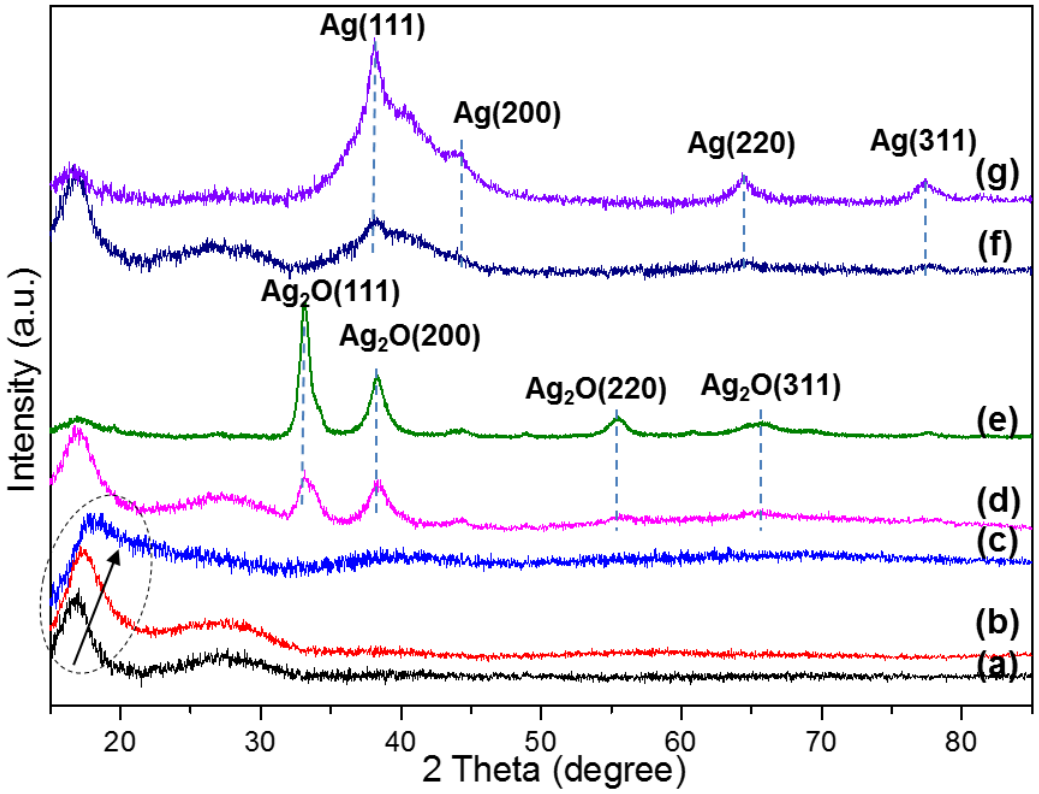

Figure 3. 4 - XRD spectra of (a) PAN nanofibers, $AgNO_3$-PAN (b) 1/20, (c) 1/5, Ag_2O-PAN (d) 1/20, (e) 1/5, Ag-PAN (f) 1/20, and (g) 1/5.

3.3.4 XPS analyses

The chemical properties of the nanofibrous surfaces were analyzed on XPS. Broad XPS surveys present O 1s (530 eV), N 1s (398 eV), Ag 3d (366-372 eV), and C 1s (284 eV) characteristic peaks on all composite samples graphs, confirming the existence of these elements in all samples, Figure 3.5. The presence of oxygen in

both Ag-PAN samples can be explained by the oxidation of silver (0) nanoparticles, the oxidation happened during the synthesis process. The silver nanoparticles presented very high surface area which facilitated the oxidation of metallic silver (Ag^0) to mono-valent silver oxide (Ag_2O). Moreover, the silver species chemisorbed on the zero-valent silver nanoparticles could also contribute to the peaks of oxygen in XPS data of Ag-PAN samples.

In Figure 3.5 (II), magnified XPS spectra of Ag 3d region show negative shifts, comparing Ag-PAN 1/5 against Ag-PAN 1/20 and Ag_2O-PAN 1/5 against Ag_2O-PAN 1/20. By contrast, the two silver peaks in $AgNO_3$-PAN 1/20 and 1/5 shifted positively. These shifts occurred due to the surface-chemistry changes of PAN nanofibers [47].

The oxygen signal (O 1s) shifted toward lower binding energy, which indicated that the electronic density around some surface oxygen atoms had increased.

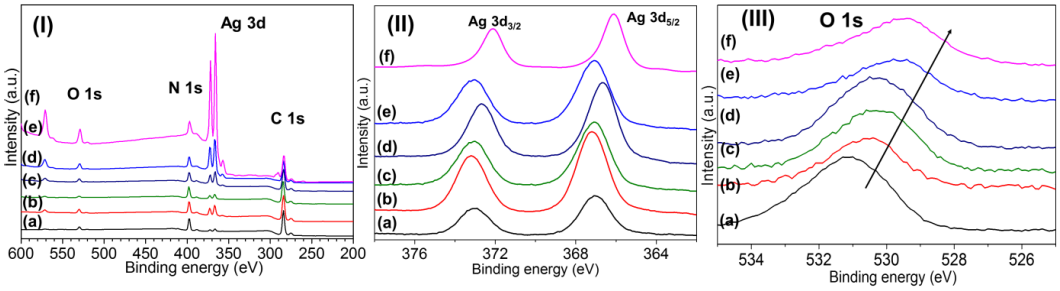

Figure 3. 5 - (I) XPS surveys, (II) XPS high resolution spectra over silver region, and (III) XPS high resolution spectra over oxygen region for $AgNO_3$-PAN (a) 1/20, (b) 1/5, Ag-PAN (c) 1/20, (d) 1/5, Ag_2O-PAN (e) 1/20, and (f) 1/5.

The C 1s signals could be interpreted as the combination of two major signals from carbon species of different functionality. The C 1s peak at BE = ~ 285 eV was assigned to C-C, C-H and C≡N chemical groups present in PAN without any specifically altered chemistry [48]. The second peak at around 283.5 eV, could be

assigned for those same chemical groups in PAN with shifted binding energy. It could be rationalized as the results of the interaction between some carbon atoms and silver. The interaction geometries are proposed in Scheme 3.1. The atomic interaction assumingly happened at the surface contact of PAN polymer matrix and silver. Atomic interactions led to electron transfer between carbon, nitrogen, oxygen, and silver [49]. The relatively changed intensities and the negative shifts of the second peak altered upon silver loadings on the top layer of the specimens. The trend, which could be deduced from observing the spectra, was with the higher silver doping on the surface layer of composite scaffolds, the atomic percentages of influenced carbon atoms increased. By calculating the ratios between split carbon signals, the atomic percentages of silver-influenced carbon atoms relative to the total number of carbon atoms were 14.85, 24.45, 25.62, 23.33, 18.16, and 40.82 at.% in $AgNO_3$-PAN 1/20, 1/5, Ag-PAN 1/20, 1/5, Ag_2O-PAN 1/20, and 1/5, Figure 3.6.

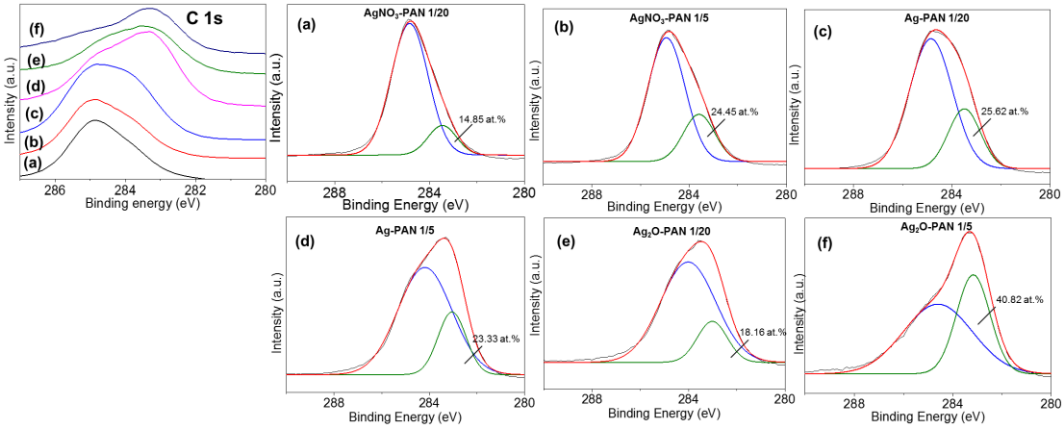

Figure 3. 6 - XPS spectra of C 1s peaks, and deconvoluted XPS $AgNO_3$-PAN (a) 1/20, (b) 1/5, Ag-PAN (c) 1/20, (d) 1/5, Ag_2O-PAN (e) 1/20, (f) 1/5.

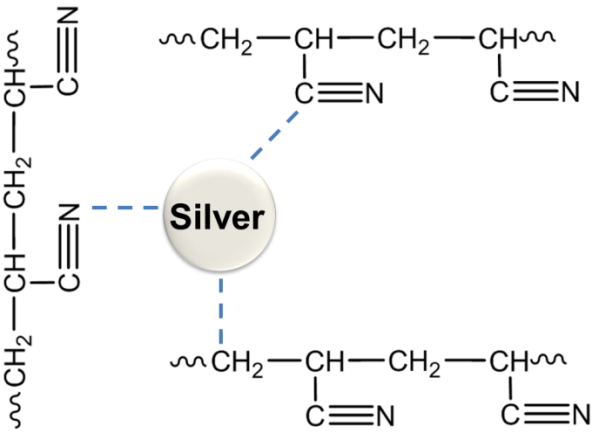

Scheme 3. 2 - Proposals for the interactive geometry of polyacrylonitrile and silver nanoparticles

For surface nitrogen chemistry, the N 1s spectra were split into three signals on XPS data of $AgNO_3$-PAN specimens and two signals for the rest. In Figure 3.7, the highest binding energy was attributed to the N^{+5} species from $AgNO_3$ [50], this peak was not present in other specimens due to the removal of silver salt after the reaction with NaOH or $NaBH_4$. The middle peak came from nitrile of PAN (C≡N), and the peak at lowest binding energy is characterized as the charged nitrogen atoms, belonging to C≡N groups of PAN polymer and having interaction with silver.

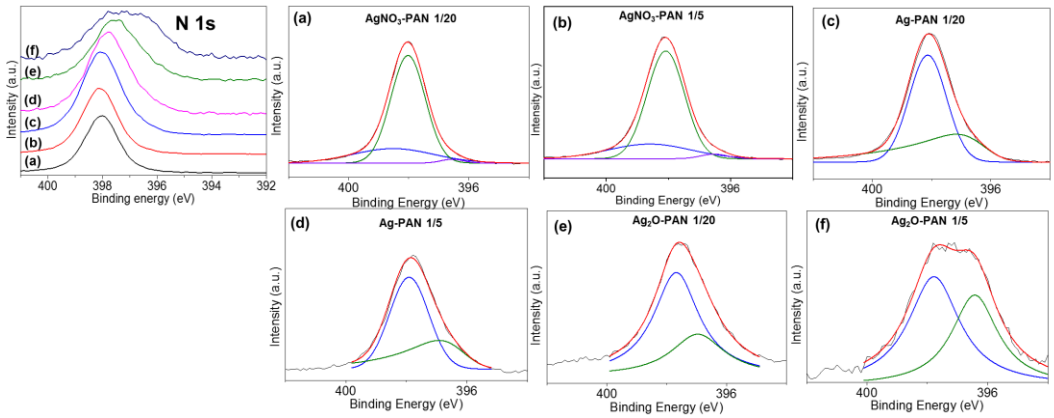

Figure 3. 7 - XPS spectra of N 1s, deconvoluted XPS $AgNO_3$-PAN (a) 1/20, (b) 1/5, Ag-PAN (c) 1/20, (d) 1/5, Ag_2O-PAN (e) 1/20, (f) 1/5.

3.3.5 Silver release profiles

Ag^+ release is considered the determining factor for the antibacterial effects, thus, it is important to investigate the silver release rates of all silver composite samples before carrying out antibacterial tests. In order to study the kinetics and quantitative release of silver from silver composite nanofibers, release tests were performed and the concentrations of dipping solutions were quantified on ICP. The data were acquired over the periods of seven days. Figure 3.8 (a) and (b) were cumulative silver release, using ppm as the unit on y axis. Figure 3.8 (c) and (d) exhibit percentages of silver releases against total silver-loading amounts, calculated based on the data on Figure 3.8 (a) for the course of 24 h and (b) for the course of 7 days.

$AgNO_3$-PAN 1/20 and 1/5 samples present rapid release profiles with more than 90 wt.% silver reserves after 1 h, 94.15 ± 2.65 and 92.25 ± 3.02 wt.%, respectively, Figure 3.8 (c) due to the high solubility of silver nitrate. Ag_2O-PAN 1/20 and 1/5 samples show considerable amounts discharged after the first 24 h, 42.90 ± 3.86 and 25.41 ± 0.83 wt.%, respectively. The mechanism of mono-valent silver species, which detached from the nanofiber specimens, could be ascribed to the leaching and the dissolution of silver oxide nanoparticles. Ag-PAN 1/20 and 1/5 demonstrated a slower initial release of silver and the release over the course of 7 days showed more gradual profiles, compared to Ag_2O-PAN 1/20 and 1/5. The amounts of silver releases were directly proportional to the silver-doping amounts of the composite nanofibers. After 7 days, the silver discharge was 15.19 ± 1.58 and 53.37 ± 1.88 ppm for Ag_2O-PAN 1/20 and 1/5. Zero-valent silver samples showcased 6.41 ± 1.35 and 11.27 ± 0.98 ppm of silver discharge, Ag-PAN 1/20 and 1/5, respectively. Similar to Ag_2O-PAN, higher silver doping amounts presented higher silver discharge.

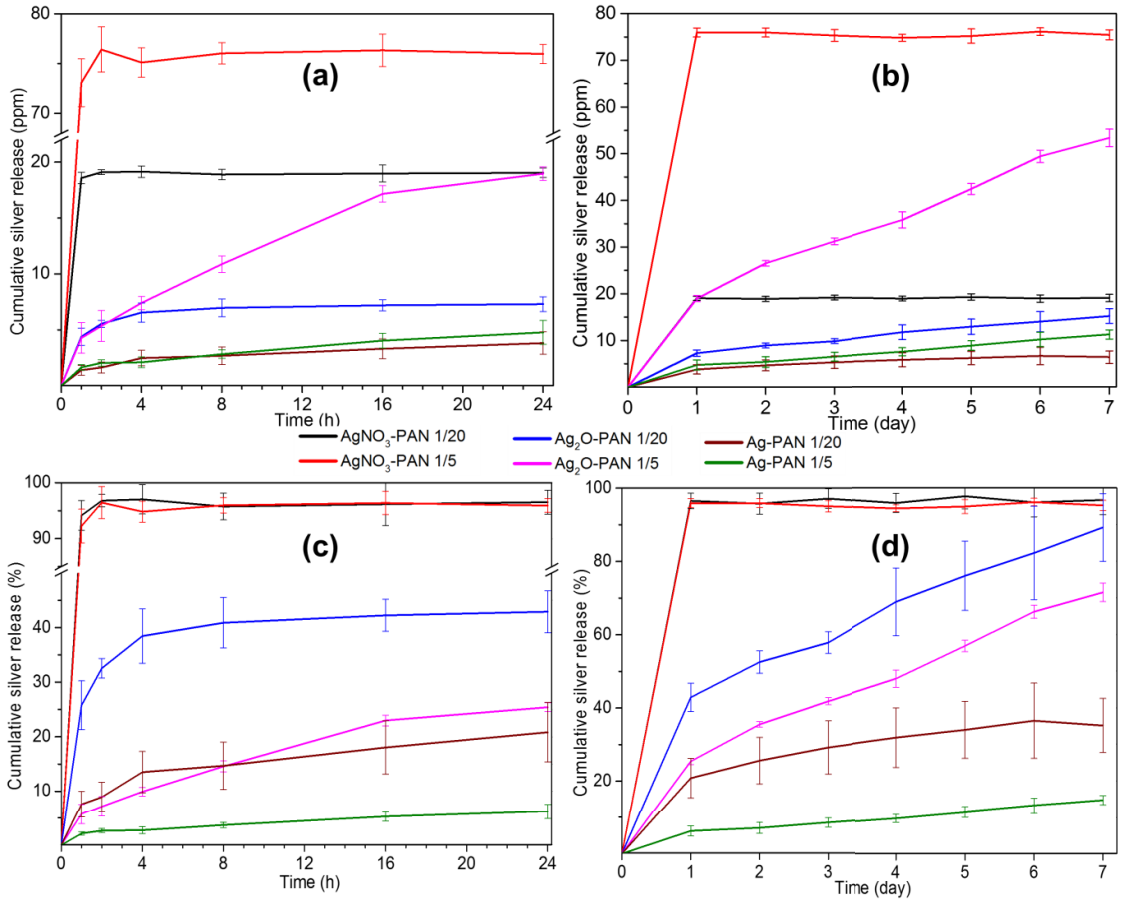

Figure 3. 8 - Silver release behavior of silver composite samples over the period of 24 h (a) and (c), and 7 days (b) and (d). The data in (c) and (d) were calculated based on (a) and (b).

3.3.6 Antibacterial activity of silver PAN composite nanofibers

The antibacterial effects of the composite nanofibers were assessed against typical gram negative and gram positive bacteria, E. coli and B. subtilis. The negative control tests were also performed to confirm the antimicrobial activities of the scaffolds were the effects of silver alone.

In Figure 3.9, on the first cycle, the clear halo zones were observed for all specimens of silver composite nanofibers. The Ag_2O-PAN 1/5 specimens exhibited the most expansive halo zones against both gram bacteria. The Ag_2O-PAN 1/20 showed secondly effective antibacterial activities against E. coli and the Ag-PAN 1/5

possessed the second largest inhibition zones against B. subtilis. Quantitatively and visually, the least expansive halo zones were demonstrated by $AgNO_3$-PAN 1/20 specimens, intriguingly, despite the silver-release results.

For the second and the third cycles, the Ag_2O-PAN 1/20, 1/5, the Ag-PAN 1/20, and 1/5 reduced the inhibitory halos sharply after each cycle. The Ag_2O-PAN 1/20 showed very small antibacterial zones on the third cycle. Similarly, the Ag_2O-PAN 1/5 also presented the significantly diminished antibacterial characteristics. We surmised that the silver loadings on Ag_2O-PAN samples were reduced faster after each cycle, attributed to the fast silver discharge. The robust antibacterial properties surprisingly belonged to $AgNO_3$-PAN samples. Comparing the halo zones between samples having the same silver loading, $AgNO_3$-PAN on the third cycle showed the most expansive inhibition zones.

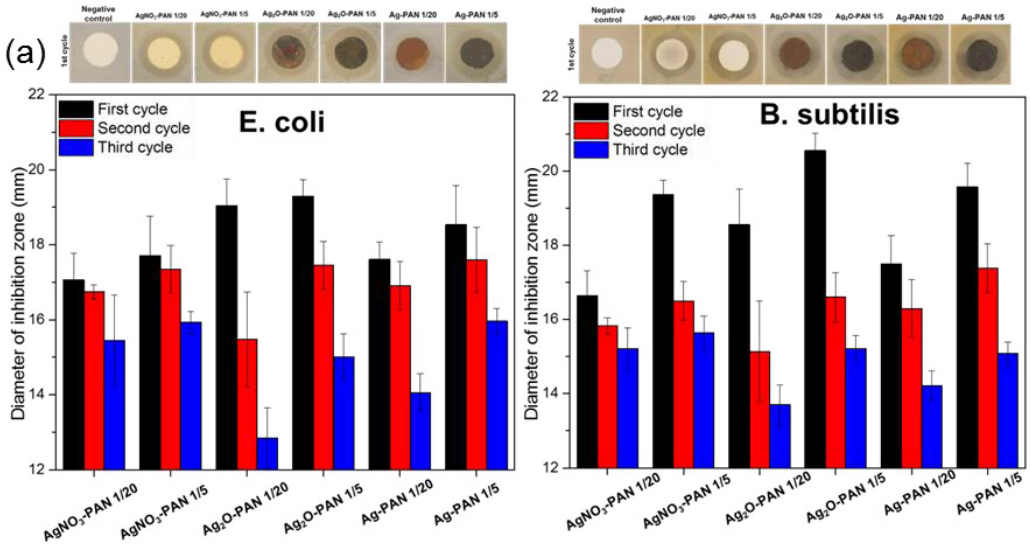

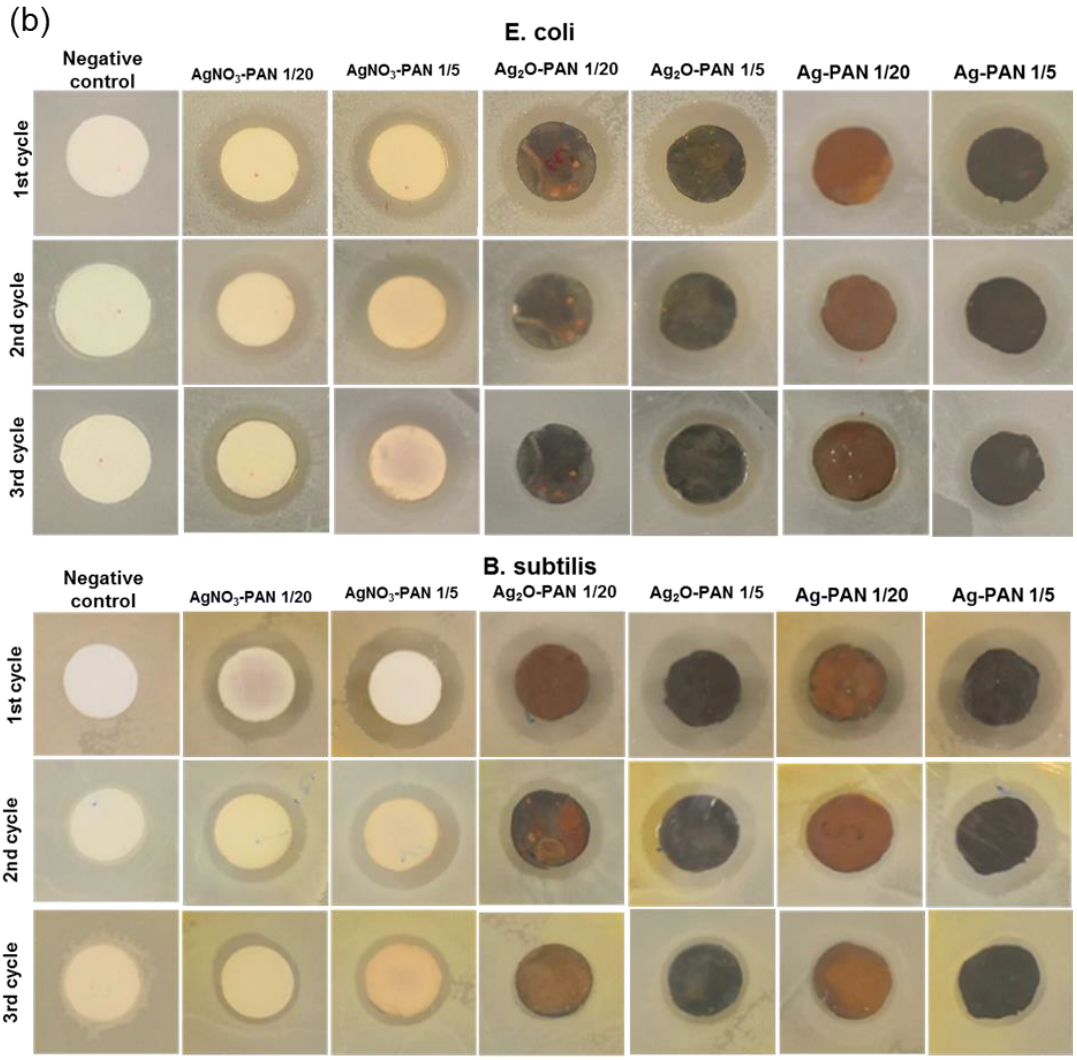

Figure 3. 9 - (a) Mean diameters of inhibition zones of disk diffusion test with standard deviations, (b) Representative images of inhibition zones for three cycles

Quantitative assessment of the bactericidal efficiency was also carried out for 3 cycles, each cycle in triplicate. The results demonstrated an impressive 3-log reduction for all silver composite scaffolds against E. coli and 4-log reduction against B. subtilis, on the first cycle. The Ag_2O-PAN 1/5 demonstrated the most potent bactericidal properties against both strain bacteria. Evaluating the bactericidal actions of all samples after 3 cycles, the robust toxicity of $AgNO_3$-PAN toward both bacterial strains was slightly better than Ag_2O-PAN and Ag-PAN samples,

comparing samples at the same silver loading amounts. The results were in line with the results of disk-diffusion tests.

The antibacterial results were opposite to the silver release in the case of $AgNO_3$-PAN, which showed rapid discharge of silver, but in antibacterial tests, the antibacterial effects of those samples were weaker than other composite samples on the first cycle. The phenomena must be attributed to the interference of NaCl in bacterial medium. The instant salt metathesis reaction between $AgNO_3$ and NaCl created AgCl, the silver halide then aggregated to form almost insoluble silver salt particles (the dissolution of AgCl is 1.9 mg/L) [51, 52]. However, the silver poly-chloride complexes, $[AgCl_2]^-$, $[AgCl_3]^{2-}$ and $[AgCl_4]^{3-}$ - products of reactions between AgCl and Cl^-, could form in the cases of Ag_2O-PAN and Ag-PAN samples in liquid medium; when the Cl^-/AgCl ratio is high enough, chloride (Cl^-) can react with AgCl and the dissolution of halide salt occurs [53].

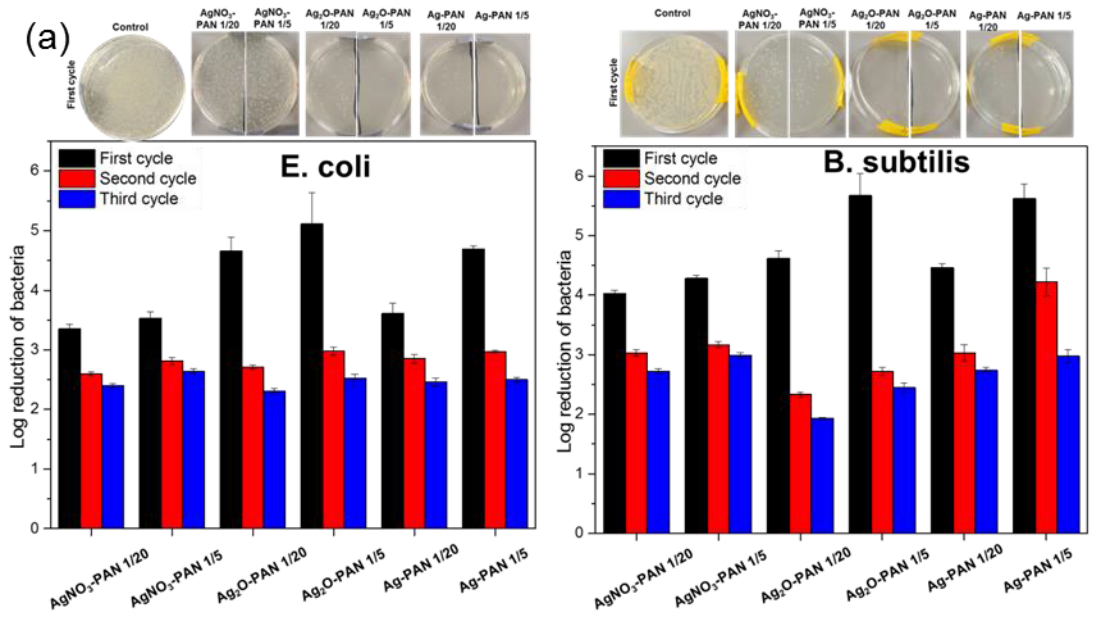

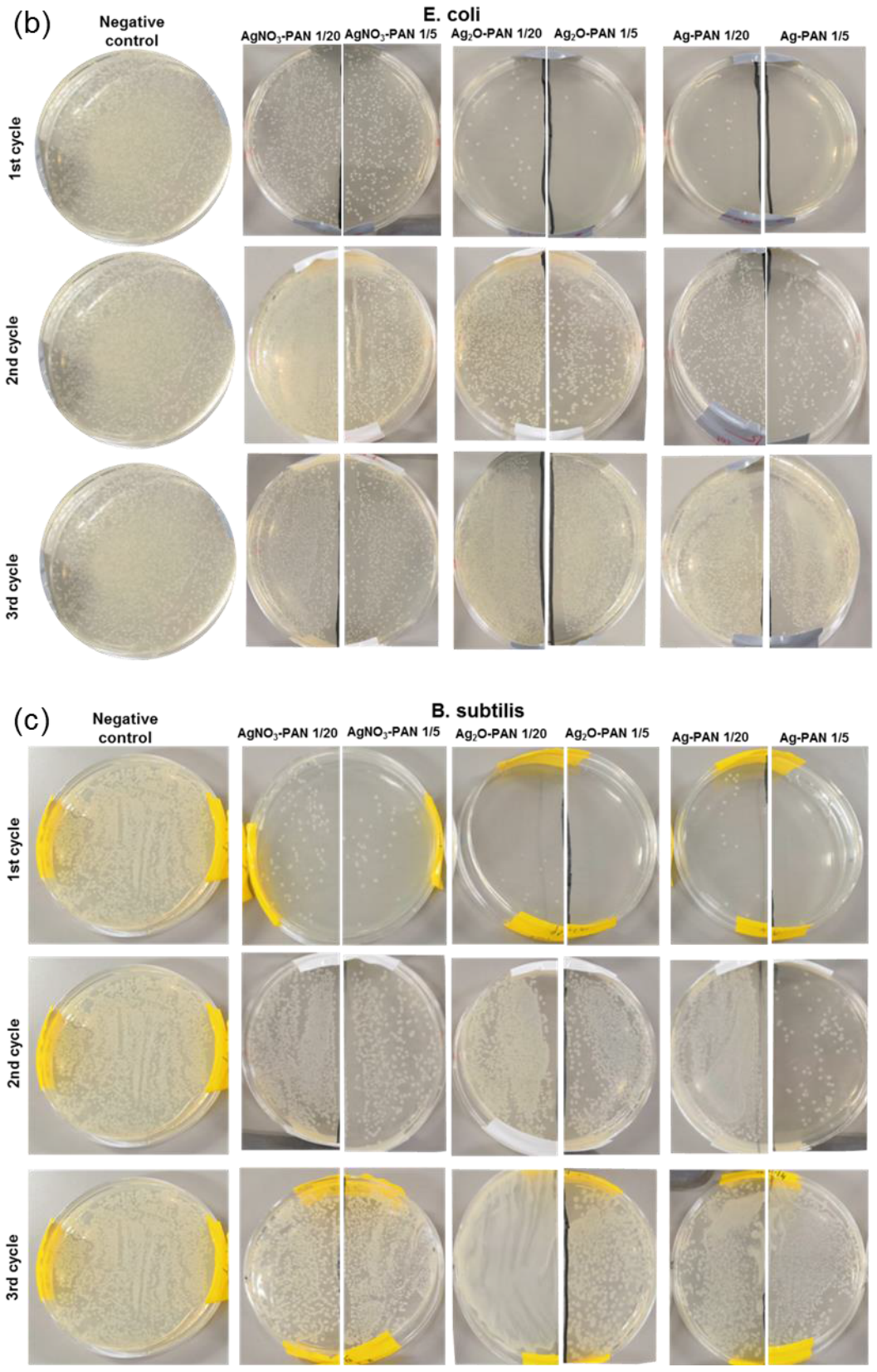

Figure 3. 10 - (a) Bactericidal efficacy based on agar plate counting method, representative images of bactericidal efficacy of all samples based on agar plate

counting method, negative control samples at 103 CFU/mL, other samples at 106 CFU/mL against (b) E. coli and (c) B. subtilis

3.3.7 Biocompatibility evaluation of composite nanofibers

Potential cytotoxicity of the silver composite samples toward mammalian cells while applying in wound dressings is of concern, due to argyria or blue-gray discoloration of the skin. Therefore, the cyto-compatibility was necessary to be evaluated. All samples were tested for 7 days with mouse fibroblast cells (NIH3T3). The viability of NIH3T3 cells grown on the nanofiber scaffolds was investigated on days 1, 4, and 7. Mouse fibroblast proliferation could take place on silver nanofiber composite scaffolds containing not too high silver concentrations; reportedly, there is no cytotoxic effect at concentration lower than 50 μg/mL [54]. On the Ag-PAN 1/5 sample, the constant cell reduction was observed, indicating the cell proliferation did not happen on this scaffold.

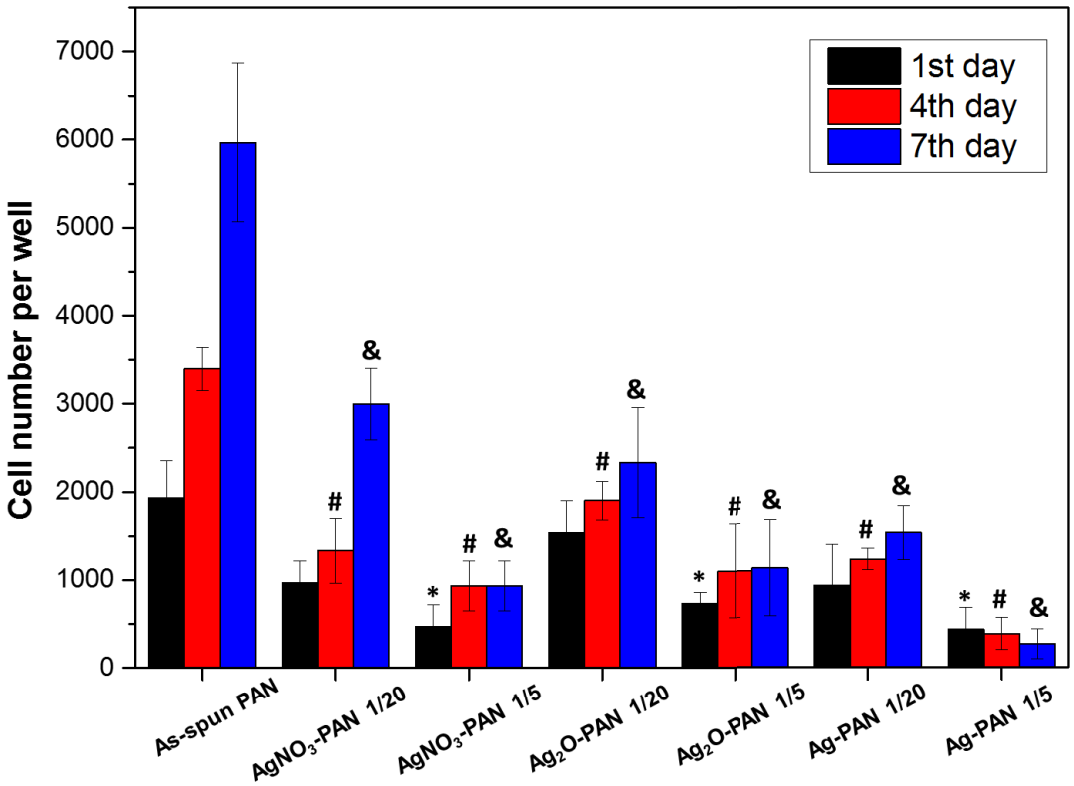

Figure 3. 11 - The proliferation of NIH3T3 cells on days 1, 4, and 7. Values are expressed as means ± standard deviation. *, #, & indicate significant difference ($P < 0.05$ compared with control).

In Figure 3.12, SEM analyses of mouse fibroblast cells on antibacterial scaffolds exhibited the cell adherence and the proliferation on the day 3. Due to the inhibitory actions of silver at high concentrations, the morphology of cells changed to round shape, Figure 3.12 (c), (e), (f), and (g), compared to spindle-like shape on Figure 3.12 (a), (b), and (d).

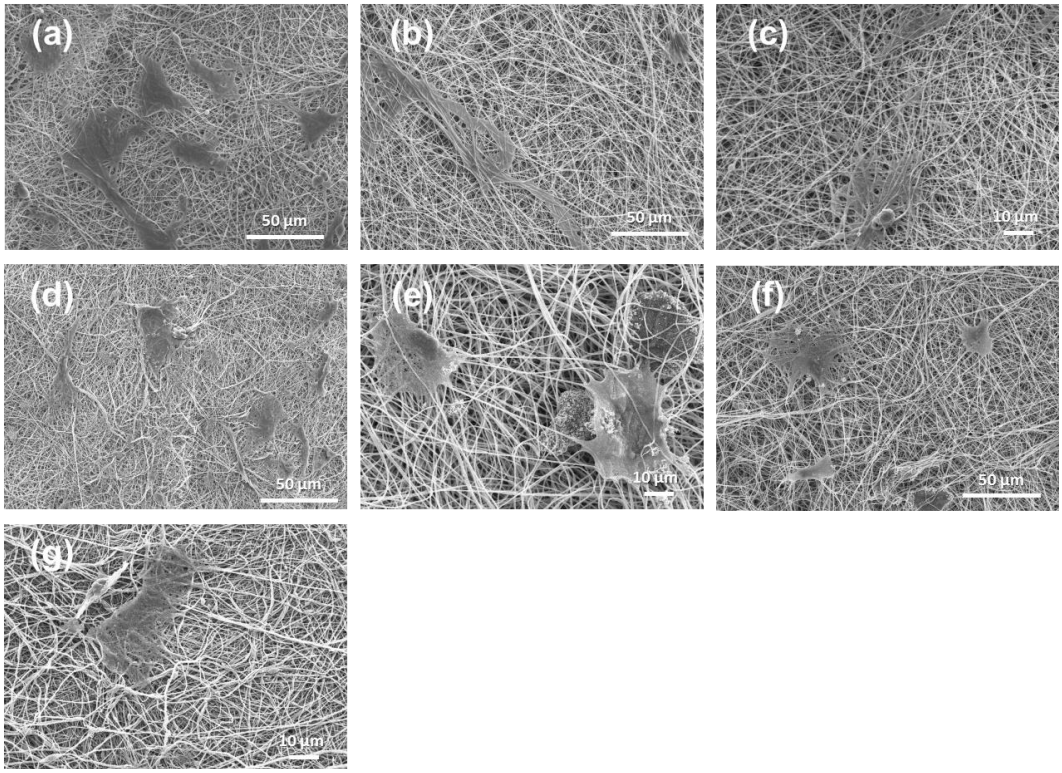

Figure 3. 12 - SEM images of NIH3T3 cells attached on nanofibers after 3-day culture; (a) as-spun PAN nanofibers; $AgNO_3$-PAN (b) 1/20 and (c) 1/5, Ag_2O-PAN (d) 1/20 and (e) 1/5; Ag-PAN (f) 1/20 and (g) 1/5

3.3.8 The formation of AgCl on the surfaces of $AgNO_3$-PAN 1/20 and 1/5 due to the interference of halide anions

All silver containing samples after the antibacterial assay were further characterized to examine the alteration of silver species and the morphology of the nanofibers. There were significant differences in the morphology of $AgNO_3$-PAN 1/20 and 1/5 samples with the newly formed of AgCl nanoparticles, Figure 3.13 (a). The confirmation of silver halide presence was further investigated by XRD and FTIR, Figure 3.13 (b) and (c). Due to the reaction with halide anions in the bacterial medium, the set of new peaks in XRD spectrum can be ascribed to the peak diffraction of AgCl. The removal of $–NO_3$ peaks in FTIR of the sample further demonstrated the depletion of $AgNO_3$ due to the reaction with halide salts.

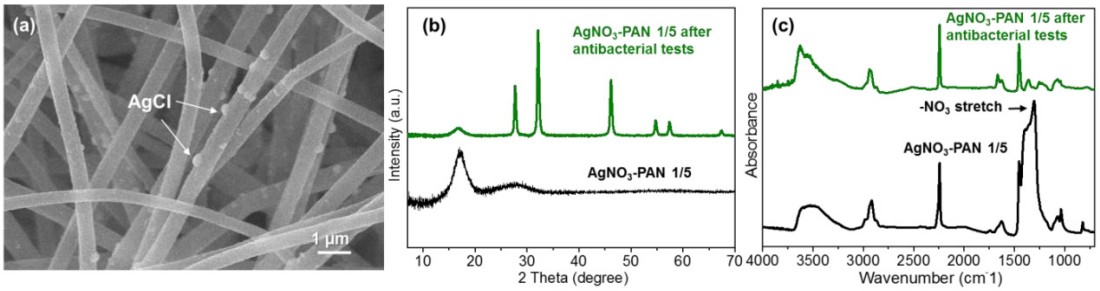

Figure 3. 13 - (a) SEM image of $AgNO_3$-PAN 1/5 nanofibers after the first cycle of antibacterial assay against E. coli with the newly formed AgCl nanoparticles detected on the surfaces, (b) XRD, and (c) FTIR spectra of $AgNO_3$-PAN nanofibers before and after the antibacterial tests.

3.4. Conclusion

Conclusively, three different silver species were successfully embedded into PAN nanofibers for the evaluation upon antimicrobial efficacy and NIH3T3 fibroblast compatibility. All samples were well characterized, TEM images displayed nanosized particles on all composite nanofibers, suggesting different reductive

mechanisms happened to aggregate silver nanoparticles. XRD verified the natures of different silver species via various synthesizing routes. Surprisingly, the silver salt composite nanofibers showed relatively weakest bactericidal properties against E. coli and B. subtilis. The interference of halide salt in bacterial medium could be the major explanation for the deterioration of antibacterial effects. Whereas, the passivation layer of AgCl instituting on Ag nanoparticles or Ag_2O nanoparticles, which presented a barrier to prevent the penetration of silver ions to the liquid environment, could be demolished by the formation of poly-chloride complexes. Ag_2O-PAN and Ag-PAN demonstrated good antibacterial efficiency on the first cycle. Noticeably, the bactericidal actions of zero-valent Ag nanoparticles against microbial organisms were less potent than Ag_2O nanocomposite samples on the first cycle, due to the slower release rate. To discharge silver, the zero-valent silver nanoparticles need to follow the oxidation and dissolution, whereas the silver oxide nanoparticles at the form of mono-valent silver could be released directly through the dissolution process.

References

[1] M. Gopiraman, D. Deng, S. Saravanamoorthy, I.-M. Chung, I.S. Kim, Gold, silver and nickel nanoparticle anchored cellulose nanofiber composites as highly active catalysts for the rapid and selective reduction of nitrophenols in water, RSC Advances 8(6) (2018) 3014-3023.
[2] M. Gopiraman, D. Deng, K.-Q. Zhang, W. Kai, I.-M. Chung, R. Karvembu, I.S. Kim, Utilization of Human Hair as a Synergistic Support for Ag, Au, Cu, Ni, and Ru Nanoparticles: Application in Catalysis, Industrial & Engineering Chemistry Research 56(8) (2017) 1926-1939.
[3] E. Lam, K.B. Male, J.H. Chong, A.C.W. Leung, J.H.T. Luong, Applications of functionalized and nanoparticle-modified nanocrystalline cellulose, Trends in Biotechnology 30(5) (2012) 283-290.
[4] M. Rafique, I. Sadaf, M.S. Rafique, M.B. Tahir, A review on green synthesis of silver nanoparticles and their applications, Artificial Cells, Nanomedicine, and Biotechnology 45(7) (2017) 1272-1291.
[5] B. Karandikar, B. Gibbins, D. Roe, N. Bonn-Savage, J.-B. Roullet, Antimicrobial surface functionalization of plastic catheters by silver nanoparticles, Journal of Antimicrobial Chemotherapy 61(4) (2008) 869-876.
[6] Y.a. Qing, L. Cheng, R. Li, G. Liu, Y. Zhang, X. Tang, J. Wang, H. Liu, Y. Qin, Potential antibacterial mechanism of silver nanoparticles and the optimization of orthopedic

implants by advanced modification technologies, International journal of nanomedicine 13 (2018) 3311-3327.
[7] Juliana Mattos Corrêa, Matsuyoshi Mori, Heloísa Lajas Sanches, Adriana Dibo da Cruz, Edgard Poiate Jr., and Isis Andréa Venturini Pola Poiate, Silver Nanoparticles in Dental Biomaterials, International Journal of Biomaterials 2015 (2015) 9.
[8] D.I. Andersson, D. Hughes, Antibiotic resistance and its cost: is it possible to reverse resistance?, Nature Reviews Microbiology 8 (2010) 260.
[9] M.A. Fischbach, C.T. Walsh, Antibiotics for Emerging Pathogens, Science 325(5944) (2009) 1089.
[10] M.K. Rai, S.D. Deshmukh, A.P. Ingle, A.K. Gade, Silver nanoparticles: the powerful nanoweapon against multidrug-resistant bacteria, Journal of Applied Microbiology 112(5) (2012) 841-852.
[11] A.P. Gondikas, A. Morris, B.C. Reinsch, S.M. Marinakos, G.V. Lowry, H. Hsu-Kim, Cysteine-Induced Modifications of Zero-valent Silver Nanomaterials: Implications for Particle Surface Chemistry, Aggregation, Dissolution, and Silver Speciation, Environmental Science & Technology 46(13) (2012) 7037-7045.
[12] J. Liu, Z. Wang, F.D. Liu, A.B. Kane, R.H. Hurt, Chemical transformations of nanosilver in biological environments, ACS nano 6(11) (2012) 9887-9899.
[13] O. Choi, K.K. Deng, N.-J. Kim, L. Ross, R.Y. Surampalli, Z. Hu, The inhibitory effects of silver nanoparticles, silver ions, and silver chloride colloids on microbial growth, Water Research 42(12) (2008) 3066-3074.
[14] C.-N. Lok, C.-M. Ho, R. Chen, Q.-Y. He, W.-Y. Yu, H. Sun, P.K.-H. Tam, J.-F. Chiu, C.-M. Che, Silver nanoparticles: partial oxidation and antibacterial activities, JBIC Journal of Biological Inorganic Chemistry 12(4) (2007) 527-534.
[15] J. Liu, R.H. Hurt, Ion Release Kinetics and Particle Persistence in Aqueous Nano-Silver Colloids, Environmental Science & Technology 44(6) (2010) 2169-2175.
[16] R.D. Glover, J.M. Miller, J.E. Hutchison, Generation of Metal Nanoparticles from Silver and Copper Objects: Nanoparticle Dynamics on Surfaces and Potential Sources of Nanoparticles in the Environment, ACS Nano 5(11) (2011) 8950-8957.
[17] G.A. Sotiriou, A. Meyer, J.T.N. Knijnenburg, S. Panke, S.E. Pratsinis, Quantifying the Origin of Released Ag+ Ions from Nanosilver, Langmuir 28(45) (2012) 15929-15936.
[18] C. Greulich, D. Braun, A. Peetsch, J. Diendorf, B. Siebers, M. Epple, M. Köller, The toxic effect of silver ions and silver nanoparticles towards bacteria and human cells occurs in the same concentration range, RSC Advances 2(17) (2012) 6981-6987.
[19] K. Saeed, S. Haider, T.-J. Oh, S.-Y. Park, Preparation of amidoxime-modified polyacrylonitrile (PAN-oxime) nanofibers and their applications to metal ions adsorption, Journal of Membrane Science 322(2) (2008) 400-405.
[20] E.F.C. Chaúque, L.N. Dlamini, A.A. Adelodun, C.J. Greyling, J. Catherine Ngila, Modification of electrospun polyacrylonitrile nanofibers with EDTA for the removal of Cd and Cr ions from water effluents, Applied Surface Science 369 (2016) 19-28.
[21] H. Wang, W. Wang, H. Wang, X. Jin, H. Niu, H. Wang, H. Zhou, T. Lin, High Performance Supercapacitor Electrode Materials from Electrospun Carbon Nanofibers in Situ Activated by High Decomposition Temperature Polymer, ACS Applied Energy Materials 1(2) (2018) 431-439.
[22] L.-F. Chen, X.-D. Zhang, H.-W. Liang, M. Kong, Q.-F. Guan, P. Chen, Z.-Y. Wu, S.-H. Yu, Synthesis of Nitrogen-Doped Porous Carbon Nanofibers as an Efficient Electrode Material for Supercapacitors, ACS Nano 6(8) (2012) 7092-7102.
[23] W. Na, J. Jun, J.W. Park, G. Lee, J. Jang, Highly porous carbon nanofibers co-doped with fluorine and nitrogen for outstanding supercapacitor performance, Journal of Materials Chemistry A 5(33) (2017) 17379-17387.
[24] K. Wei, J.-h. Xia, B.-S. Kim, I.-S. Kim, Multiwalled carbon nanotubes incorporated bombyx mori silk nanofibers by electrospinning, Journal of Polymer Research 18(4) (2011) 579-585.

[25] M. Gopiraman, H. Bang, G. Yuan, C. Yin, K.-H. Song, J.S. Lee, I.M. Chung, R. Karvembu, I.S. Kim, Noble metal/functionalized cellulose nanofiber composites for catalytic applications, Carbohydrate Polymers 132 (2015) 554-564.
[26] H. Lee, I.S. Kim, Nanofibers: Emerging Progress on Fabrication Using Mechanical Force and Recent Applications, Polymer Reviews 58(4) (2018) 688-716.
[27] D.-N. Phan, H. Lee, D. Choi, C.-Y. Kang, S.S. Im, I.S. Kim, Fabrication of Two Polyester Nanofiber Types Containing the Biobased Monomer Isosorbide: Poly (Ethylene Glycol 1,4-Cyclohexane Dimethylene Isosorbide Terephthalate) and Poly (1,4-Cyclohexane Dimethylene Isosorbide Terephthalate), Nanomaterials 8(2) (2018) 56.
[28] D.-N. Phan, H. Lee, B. Huang, Y. Mukai, I.-S. Kim, Fabrication of electrospun chitosan/cellulose nanofibers having adsorption property with enhanced mechanical property, Cellulose 26(3) (2019) 1781-1793.
[29] H. Lee, K. Watanabe, M. Kim, M. Gopiraman, K.-H. Song, J.S. Lee, I.S. Kim, Handspinning Enabled Highly Concentrated Carbon Nanotubes with Controlled Orientation in Nanofibers, Scientific Reports 6 (2016) 37590.
[30] J.A. Wahab, G. Xu, H. Lee, P.D. Nam, K. Wei, S.H. Kim, I.S. Kim, Fabrication of silk fibroin/eggshell nanofiber membranes for facemasks, Fibers and Polymers 17(11) (2016) 1776-1781.
[31] D.-N. Phan, N. Dorjjugder, M.Q. Khan, Y. Saito, G. Taguchi, H. Lee, Y. Mukai, I.-S. Kim, Synthesis and attachment of silver and copper nanoparticles on cellulose nanofibers and comparative antibacterial study, Cellulose 26(11) (2019) 6629-6640.
[32] S.G. Mukherjee, N. O'Claonadh, A. Casey, G. Chambers, Comparative in vitro cytotoxicity study of silver nanoparticle on two mammalian cell lines, Toxicology in Vitro 26(2) (2012) 238-251.
[33] R.A. Rebia, S. Rozet, Y. Tamada, T. Tanaka, Biodegradable PHBH/PVA blend nanofibers: Fabrication, characterization, in vitro degradation, and in vitro biocompatibility, Polymer Degradation and Stability 154 (2018) 124-136.
[34] Y. Tamada, E.A. Kulik, Y. Ikada, Simple method for platelet counting, Biomaterials 16(3) (1995) 259-261.
[35] H. Lee, K. Watanabe, M. Kim, M. Gopiraman, K.-H. Song, J.S. Lee, I.S. Kim, Handspinning Enabled Highly Concentrated Carbon Nanotubes with Controlled Orientation in Nanofibers, Scientific reports 6 (2016) 37590-37590.
[36] S. Iravani, H. Korbekandi, S.V. Mirmohammadi, B. Zolfaghari, Synthesis of silver nanoparticles: chemical, physical and biological methods, Research in pharmaceutical sciences 9(6) (2014) 385-406.
[37] W. Chen, L.Z. Ouyang, J.W. Liu, X.D. Yao, H. Wang, Z.W. Liu, M. Zhu, Hydrolysis and regeneration of sodium borohydride (NaBH4) – A combination of hydrogen production and storage, Journal of Power Sources 359 (2017) 400-407.
[38] E. Cipriani, M. Zanetti, P. Bracco, V. Brunella, M.P. Luda, L. Costa, Crosslinking and carbonization processes in PAN films and nanofibers, Polymer Degradation and Stability 123 (2016) 178-188.
[39] Y. Shi, Y. Li, J. Zhang, Z. Yu, D. Yang, Electrospun polyacrylonitrile nanofibers loaded with silver nanoparticles by silver mirror reaction, Materials Science and Engineering: C 51 (2015) 346-355.
[40] S. Akmaz, D. Ad, #x131, #xfc, E. zel, M. Yasar, O. Erguven, The Effect of Ag Content of the Chitosan-Silver Nanoparticle Composite Material on the Structure and Antibacterial Activity, Advances in Materials Science and Engineering 2013 (2013) 6.
[41] Y. Wei, L. Li, X. Yang, G. Pan, G. Yan, X. Yu, One-Step UV-Induced Synthesis of Polypyrrole/Ag Nanocomposites at the Water/Ionic Liquid Interface, Nanoscale Research Letters 5(2) (2009) 433.
[42] D. Manikprabhu, K. Lingappa, Microwave Assisted Rapid and Green Synthesis of Silver Nanoparticles Using a Pigment Produced by Streptomyces coelicolor klmp33, Bioinorganic Chemistry and Applications 2013 (2013) 5.

[43] Y. Tong, X. Lu, W. Sun, G. Nie, L. Yang, C. Wang, Electrospun polyacrylonitrile nanofibers supported Ag/Pd nanoparticles for hydrogen generation from the hydrolysis of ammonia borane, Journal of Power Sources 261 (2014) 221-226.
[44] K.T. Sullivan, C. Wu, N.W. Piekiel, K. Gaskell, M.R. Zachariah, Synthesis and reactivity of nano-Ag2O as an oxidizer for energetic systems yielding antimicrobial products, Combustion and Flame 160(2) (2013) 438-446.
[45] M. Goudarzi, N. Mir, M. Mousavi-Kamazani, S. Bagheri, M. Salavati-Niasari, Biosynthesis and characterization of silver nanoparticles prepared from two novel natural precursors by facile thermal decomposition methods, Scientific Reports 6 (2016) 32539.
[46] K. Shameli, M.B. Ahmad, S.D. Jazayeri, S. Sedaghat, P. Shabanzadeh, H. Jahangirian, M. Mahdavi, Y. Abdollahi, Synthesis and characterization of polyethylene glycol mediated silver nanoparticles by the green method, International journal of molecular sciences 13(6) (2012) 6639-6650.
[47] R.H. Bradley, G. Beamson, X. Ling, I. Sutherland, Surface nitrogen chemistry of PAN carbon fibres, Applied Surface Science 72(3) (1993) 273-276.
[48] S. Tas, O. Kaynan, E. Ozden-Yenigun, K. Nijmeijer, Polyacrylonitrile (PAN)/crown ether composite nanofibers for the selective adsorption of cations, RSC Advances 6(5) (2016) 3608-3616.
[49] X. Crispin, C. Bureau, V.M. Geskin, R. Lazzaroni, W.R. Salaneck, J.L. Brédas, Chemisorption of acrylonitrile on the Cu(100) surface: A local density functional study, The Journal of Chemical Physics 111(7) (1999) 3237-3251.
[50] S. W. Huang, K. G. Neoh, E. T. Kang, H. S. Han, K. L. Tan, Palladium-containing polyaniline and polypyrrole microparticles, Journal of Materials Chemistry 8(8) (1998) 1743-1748.
[51] M.G. Espinoza, M.L. Hinks, A.M. Mendoza, D.P. Pullman, K.I. Peterson, Kinetics of Halide-Induced Decomposition and Aggregation of Silver Nanoparticles, The Journal of Physical Chemistry C 116(14) (2012) 8305-8313.
[52] B. Le Ouay, F. Stellacci, Antibacterial activity of silver nanoparticles: A surface science insight, Nano Today 10(3) (2015) 339-354.
[53] C. Levard, S. Mitra, T. Yang, A.D. Jew, A.R. Badireddy, G.V. Lowry, G.E. Brown, Effect of Chloride on the Dissolution Rate of Silver Nanoparticles and Toxicity to E. coli, Environmental Science & Technology 47(11) (2013) 5738-5745.
[54] A. Syed, S. Saraswati, G.C. Kundu, A. Ahmad, Biological synthesis of silver nanoparticles using the fungus Humicola sp. and evaluation of their cytoxicity using normal and cancer cell lines, Spectrochimica Acta Part A: Molecular and Biomolecular Spectroscopy 114 (2013) 144-147.

CHAPTER 4 Synthesis and attachment of silver and copper nanoparticles on cellulose nanofibers and comparative antibacterial study works

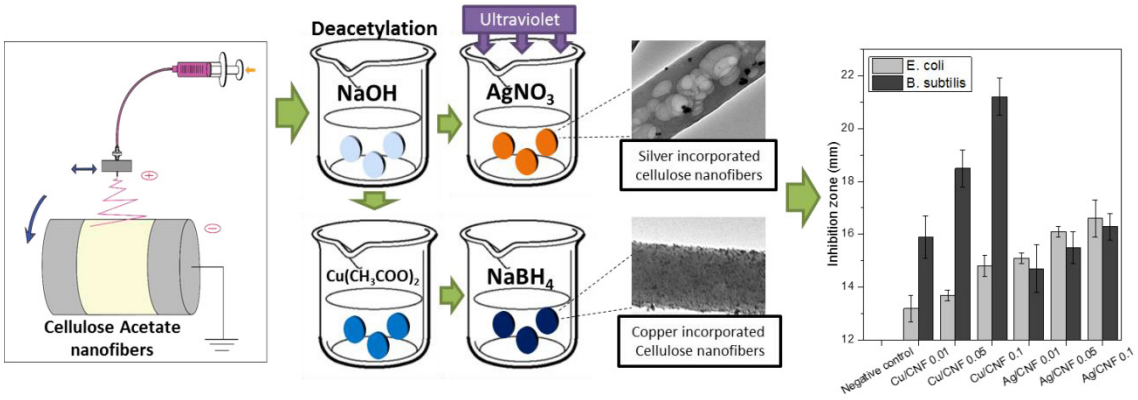

4.1 Introduction

Cellulose is a natural material thus considered environmentally friendly in contrast to fossil fuel-based commodity polymers regarding biodegradability and the environmental consequences [1]. In consideration of new composite materials with low environmental impact, cellulose is rising as a promising alternative for oil-derived polymers and has attracted much interest in academia, as well as industrial sectors. In recent years, cellulose or cellulosic derivatives have been widely utilized for electrospinning to fabricate nano-sized fibers with multiple functions [2]. Cellulose nanofibers offer good mechanical properties – approximately 5 MPa in the tensile test [3], chemical resistance, and thermal stability [4]. Cellulose nanofibers have presented great potential in filtration, food packaging, electronic devices, food additives, and medical and cosmetic products [5].

Pathogenic bacteria are the root of numerous diseases and infections which cause human sickness. To cure those infectious diseases, diverse antibacterial agents have been utilized, including metallic nanoparticles [6]. Silver nanoparticles are considered as a new class of antibacterial agent, with sustainable activity against a wide spectrum of bacteria [7]; until now no life-threatening risks ensuing from inhalation, ingestion or dermal application of AgNPs have been reported hence AgNPs in suitable doses are considered to be safe for humans [8]. For thousands of years, copper has been used as a powerful antibiotic agent and liquid disinfection [9]. Moreover, copper promotes human cell and tissue regeneration during wound treatment and has been combined with other materials to improve the healing effects [10]. Copper in small doses exhibits negligible cytotoxicity on human cells, yet lethal effects on bacteria [11].

There are several well-reported routes to synthesizing metallic nanoparticles,

including chemical, physical, photochemical and biological methods [12]. Chemical methods, with three main elements involved metal precursors, reducing agents, and stabilizing agents, can be used to regulate metal nanoparticles in a variety of sizes and shapes with high uniformity and time-saving feature [13]. The physical route has been described as implementing heat generating systems [14], electric discharge plasma [15], and an electric arc discharge [16] to reduce metal precursor to metal nanoparticles. Recently, biological methods, employing bacteria or substances extracted from plants for silver or copper nanoparticle synthesis, have emerged as an environmentally friendly, economical, and promising route [17-19]. When integrating into medical devices, it is a necessity to eliminate any consequent risk for human health, as well as environments. Therefore, photochemical approaches without the use of additional reagents are regarded as sustainable alternatives for silver nanoparticles syntheses.

The electrospinning method is an effective approach to fabricate ultra-thin fibers with high specific surface area and controllable porosity, hence ideal for applications in tissue engineering scaffolds, wound dressings, and drug delivery [20]. To conduct electrospinning, the desired polymers are first dissolved in solvent systems, single or co-solvent. A high voltage power supply with adjustable voltages and a rotary collector to obtain fibers in random orientation are the required apparatus. The former one produces electrical force to overcome the surface tension of the droplet, and an electrified fluid jet is subsequently spun and elongated. While the jet is traveling through the air, the solvent evaporation takes place, and thin fibers accumulate at the collector [21, 22].

Attempts to incorporate metal nanoparticles into the polymer matrix of nanofibers have made significant progress [23, 24]. Metal nanoparticle-based composite

nanofibers demonstrate great advantages to facilitate the uniform distribution and the controllable release of silver or copper at the bacteria contact surfaces [25]. For this reason, we opted for silver and copper nanoparticles loaded on cellulosic nanofibers as a functional composite material with antibacterial effects. There have been several scientific articles investigating the synthesis and growth of silver nanoparticles on fibers via the UV-induced method [26-29]. The absorption of silver ions in cellulose was governed by the hydroxyl groups on cellulose nanofibers [30], and the UV light played the role of reducing agent. The introduction of copper nanoparticles and their antibacterial properties have also been presented on other research papers [31, 32]. In our study, we successfully coating the silver and copper metals in the nanofibrous cellulosic framework and juxtaposed the UV-facilitating synthesis of AgNPs and the chemical synthesis of CuNPs regarding the metal loading effectiveness on the nanofibrous scaffolds, the metal release properties, and the antibacterial activity against two representative bacteria strains, E. coli and B. subtilis.

4.2 Experimental

4.2.1 Materials

Cellulose acetate (39.8 acetyl weight content, average Mw = 30,000 g mol^{-1}) was purchased from Sigma Aldrich Chemical Co., Ltd (USA). Dimethylformamide (DMF 99.8 %), acetone (99.5%), 65 wt% nitric acid (HNO_3) of analytical grade, silver nitrate ($AgNO_3$) (99.8%), and copper (II) acetate ($Cu(CH_3COO)_2$) (97%) were obtained from Wako Pure Chemical Industries, Ltd. (Japan). All chemicals were used without any additional purification. Escherichia coli strain (Hrf 3000) was received from the Coli Genetic Stock (CGSC; Yale Univ., New Haven, CT, USA). Bacillus subtilis strain (168) was provided by Dr. Ogasawara, Shinshu University,

Japan. The Cell Counting Kit-8 (CCK-8) was purchased from Dojindo Laboratories Japan. The Luria-Bertani broth was purchased in an analytical grade from Nacalai Tesque, INC., Kyoto, Japan. The Petri dishes were supplied by Sansei Medical Co., LTD., Japan.

4.2.2 Fabrication of cellulose nanofibers

Firstly, cellulose acetate was dissolved in the mixture of Acetone/DMF with the weight ratio between two solvents 2/3 to prepare a 20 wt% solution of the polymer. The solution was vigorously agitated for 24 h to ensure all components mixed thoroughly. The electrospinning was set up with a high voltage power supply (Har-100*12, Matsusada Co., Tokyo, Japan), a collector, and a syringe pump. A 20-ml plastic syringe, with a metallic needle affixed to it, was used to contain the prepared solution. The inner diameter of the needle was 1.2 mm, and the distance between the tip of the needle and the collector was adjusted to 18 cm. The syringe pump was set to a flow-rate of 1 ml h^{-1}, and the spinning was performed for 48 h. The parameters were set as voltage of 15 kV, room temperatures, and humidity of approximately 40%.

Once the spinning process was completed, the cellulose acetate nanofibrous sheet was removed from the collector and immersed in sodium hydroxide solution 0.1 M for 36 h. The deacetylation reaction took place slowly to transform CANFs to CNFs. The CNFs were then submerged in dilute nitric acid 0.001 M for 1 h to remove all excessive amount of NaOH and subsequently washed several times with distilled water. Afterward, the resulted nanofiber mat was cut into round-shaped specimens with a diameter of 12 mm in preparation for further processes.

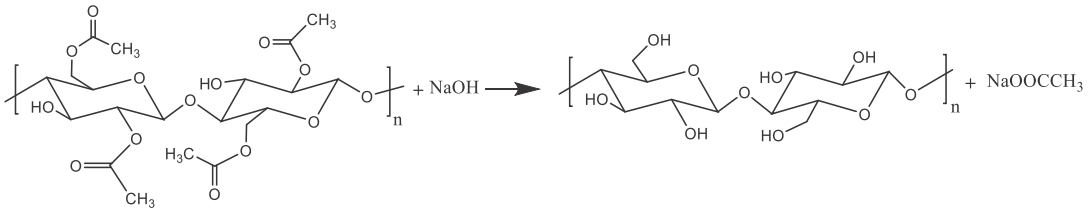

Scheme 4. 1 - Deacetylation reaction to transforming cellulose acetate nanofibers to cellulose nanofibers

4.2.3 The synthesis of silver nanoparticles and copper nanoparticles on the surfaces of cellulose nanofibers

For the formation of silver nanoparticles on the surfaces of CNFs, we opted for the UV facilitation method, which was employed by shaking circular cellulose specimens in $AgNO_3$ solutions 0.01, 0.05, and 0.1 M under the radiation of UV light for 24 h, gradually activated the reduction of $AgNO_3$ to AgNPs on the surfaces of the CNFs. Samples were denoted as Ag/CNFs 0.01, 0.05, and 0.1.

To embed CuNPs in the CNFs, rounded cellulosic specimens were immersed in $Cu(CH_3COO)_2$ solutions 0.01, 0.05, and 0.1 M under gentle agitation for 24 h. Those specimens were taken out and dried at room temperature for 48 h. The chemical reduction to copper nanoparticles was implemented by immersing dried specimens in $NaBH_4$ 0.5 M. Resultant samples were indicated as Cu/CNFs 0.01, 0.05, and 0.1.

After the metal nanoparticle incorporation, all specimens were washed with DI water several times and dried in program control oven (AS ONE DOV-600P, MonotaRo Co., Ltd., Japan) for 24 h at 60 °C.

4.2.4 Characterization

Scanning Electron Microscope (SEM, JSM-6010LA, JEOL, Japan) and Transmission Electron Microscopy (TEM, JEOL 2010 Fas TEM, Tokyo, Japan) were

employed for morphological study. Fourier Transform Infrared (FT-IR, Prestige-21, Shimadzu Co., Ltd., Japan) was used for chemical compositions. Elemental analysis was studied on X-ray Photoelectron Spectroscopy (XPS, Kratos Axis-Ultra DLD, Kratos Analytical) and Energy Dispersive X-Ray Spectroscopy (SEM-EDS, JSM-6010LA, JEOL, Japan).

Inductively Coupled Plasma-Atomic Emission Spectroscopy (ICP-AES, Shimadzu ICPS-1000 IV, Shimadzu, Kyoto, Japan) was implemented to determine the silver and copper release in solutions and the metal contents of all treated samples. To investigate the silver or copper contents of composite nanofiber samples, samples were first immersed in concentrated HNO_3 solutions, the reactions between silver or copper species and HNO_3 ensued to dissolve all metal nanoparticles to the solutions. The resultant solutions were then sampled and quantified on ICP.

4.2.5 Silver and copper release kinetics and antibacterial assessment assay

The metal release profiles of nanofibrous samples were examined by submerging 0.15 g CNFs containing silver or copper in 50 mL distilled water under the gentle shaking condition - 100 rpm for 7 days. 2 mL of liquid specimens were extracted after certain periods of time in order to measure the silver or copper release.

The E. coli and B. subtilis were chosen as subjects of the antibacterial evaluation. The bacteria were cultured in the LB liquid medium for 24 h, at 37 °C in the case of E. coli and 30 °C in the case of B. subtilis. Subsequently, the cultures were diluted with saline solution to about 10^6 colony forming unit (CFU)/ml, verified by optical density at 600 nm.

In regard to the inhibition zone test, 200 µL bacteria suspension at the density of 10^6 CFU/mL was spread on each agar plate; then specimens were gently placed on

top of that. Agar plates were, subsequently, cultured for 24 h before being evaluated.

For bactericidal efficacy evaluation, 0.01 g of nanofiber webs were soaked in 1 mL LB broth inoculated with bacteria at the concentration of 10^6 (CFU)/ml under mild shaking of 50 rpm for 8 h. Afterward, bacterial broths were sampled, properly diluted, and spread on the agar plates for 24-h culture in order to count the live bacteria cells. The log reduction was calculated as follows:

$$\text{Log Reduction} = \log_{10} (A/B)$$

Where A is the number of bacteria colonies counted and calculated on the agar disk after culturing the negative control sample with bacterial broths. B is the number of bacteria colonies counted and calculated on the agar disk after culturing cellulosic samples containing metal with bacteria.

4.3 Results and discussion

4.3.1 Morphology and color study of nanofibers

Figure 4.1 (a) and (b) show SEM micrographs of electrospun CANFs and CNFs, no significant changes in the morphologies were observed between them. CANFs and CNFs presented the smooth, featureless morphology with mean diameters of 393±98 nm and 411±120 nm, respectively. The cellulosic nanofibers displayed a wide range of diameter distribution. The nanoparticulate formation on the surfaces of the cellulose nanofibers can be observed in Figure 4.1 (c, d, e, f, g, and h). The mean diameters of Ag/CNFs 0.01, 0.05, and 0.1 were 430 ± 153, 440 ± 115, and 456 ± 100 nm, whereas the mean diameters of Cu/CNFs 0.01, 0.05, and 0.1 were 407 ± 73, 428 ± 79, and 506 ± 77, respectively. These composite fibers presented coarser diameters, compared to CANFs and CNFs, due to the swelling on account of the penetration of silver nitrate and copper (II) acetate into the polymer matrix, as well as the newly

formed nanoparticles on the fiber scaffold could also affect the nanofiber diameters. The nanoparticles were observed to be well distributed on CNFs.

Ag/CNFs 0.01, 0.05, and 0.1 samples exhibited a range of brown colors, with or without yellow tints, the yellow tints could be spotted in the case of Ag/CNFs 0.1 – Figure 4.1 (e*). These colors were ascribed to partly the interactions between silver ions and cellulose, as well as the nanoparticulate formation of silver. Whereas Cu/CNFs presented a range from grey to black colors, the saturated black color belonged to Cu/CNFs 0.1, Figure 4.1 (h*).

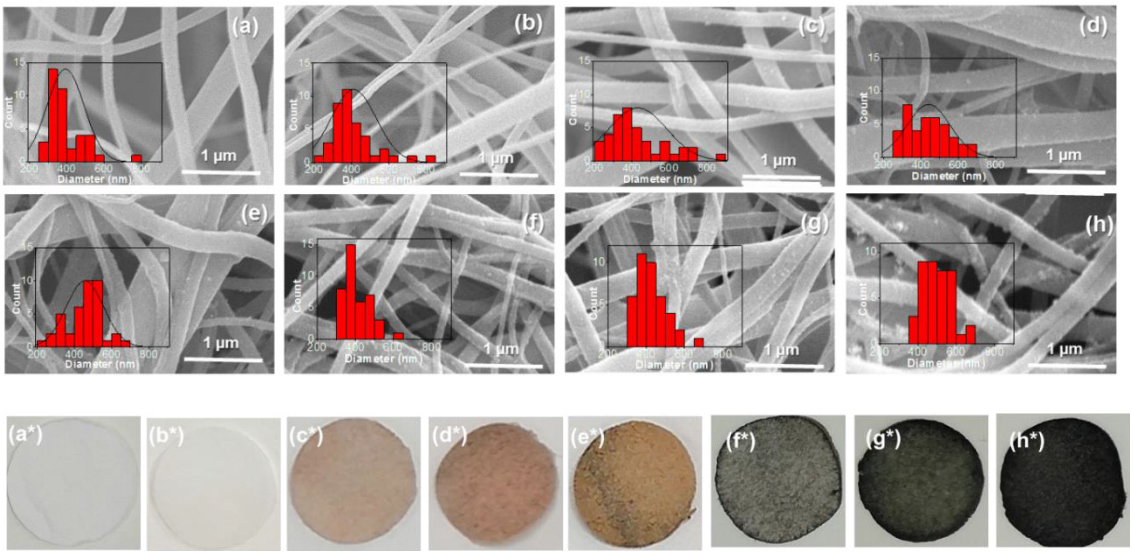

Figure 4. 1 - Morphology and color appearances of (a, a*) cellulose acetate nanofibers; (b, b*) cellulose nanofibers; Ag/CNFs 0.01 (c, c*), 0.05 (d, d*), and 0.1 (e, e*); Cu/CNFs 0.01 (f, f*), 0.05 (g, g*), and 0.1 (h, h*)

TEM images revealed the porous structure of the CANFs which was also reported in [33], and all post-treated CNFs inherently adopted that porous feature. The high porosity of CANFs could be explained by the phase separation occurred in a co-solvent system of DMF and acetone. This phenomenon sometimes happens in a single solvent system but the polymer solution is electrospun in a high humidity

environment, in which water plays the role of the second solvent. Scheme 4.2 illustrates the pore-forming phenomenon in cellulosic nanofibers. In essence, the phase separation occurs due to the intrinsic distinctions between two solvents, which lead to the heterogeneity in polymer density from area to area. After solvents have been removed by the evaporation process, the pores form at lower polymer-density spots.

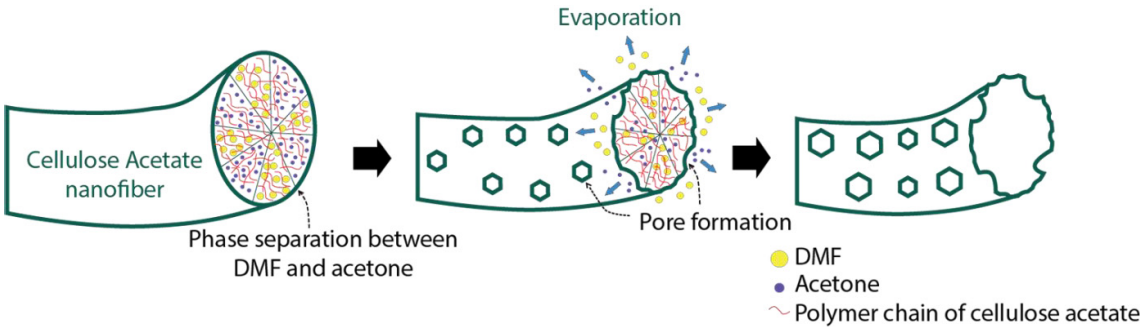

Scheme 4. 2 - A schematic model explaining the progress of pore formation in cellulose acetate nanofibers

AgNPs and CuNPs were detected on the surfaces of CNFs after the photo-induced treatment or chemical reduction. The sizes of silver particles were measured from several TEM photographs and the results were charted in Figure 4.2 (c, d, e, f, g, and h). The average sizes of AgNPs were 8.2 ± 2.3, 12.9 ± 4.3, and 18.5 ± 5.3 nm respective to treatment in $AgNO_3$ solutions 0.01, 0.05, and 0.1 M under UV radiation. The concentrations of silver salt treating solutions positively influenced the sizes of the AgNPs, the higher the concentrations the larger the particle sizes. In the case of Cu/CNFs samples, the average sizes of CuNPs were 6.5 ± 1.7, 6.7 ± 1.6, and 9.6 ± 2.8, respectively. The CuNPs possessed a more uniform size, and the difference between copper decorated cellulose samples was less significant.

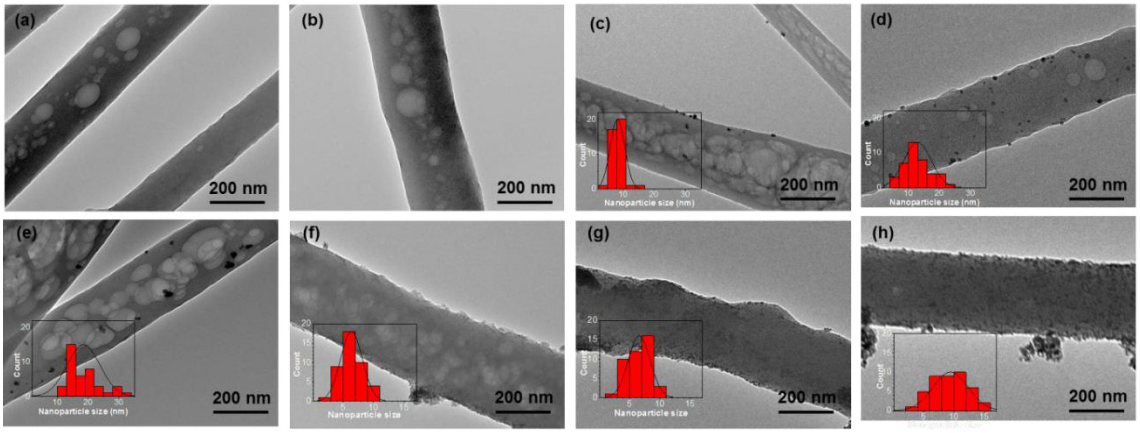

Figure 4. 2 - TEM images of (a) CANFs; (b) CNFs; Ag/CNFs (c) 0.01, (d) 0.05, (e) 0.1; Cu/CNFs (f) 0.01, (g) 0.05, and (h) 0.1.

4.3.2 Silver and copper contents

To determine the metal contents in all treated CNFs samples, 0.015 g of metal composite nanofibers was immersed in 50 mL concentrated HNO_3 solution for 24 h. ICP was subsequently performed on these solutions to quantify the silver or copper concentrations. The results from the ICP analysis disclosed the metal contents of all composite samples as follows: 0.4 ± 0.2, 3.8 ± 1.0, 6.8 ± 1.7 wt% for Cu/CNFs 0.01, 0.05, and 0.1; whereas, Ag/CNFs 0.01, 0.05, and 0.1 possessed silver contents of 6.0 ± 1.4, 8.7 ± 0.8, and 13.6 ± 0.9 wt%, respectively, Figure 4.3. The UV induced synthesis method proved to be effective on loading silver on the nanofiber platforms with the highest silver content of 13.6 wt%, treated in $AgNO_3$ 0.1 M solution. The highest copper loading amount was 6.8 ± 1.7 wt% for Cu/CNFs 0.1. There was a strong correlation between metal contents against the concentrations of treating solutions.

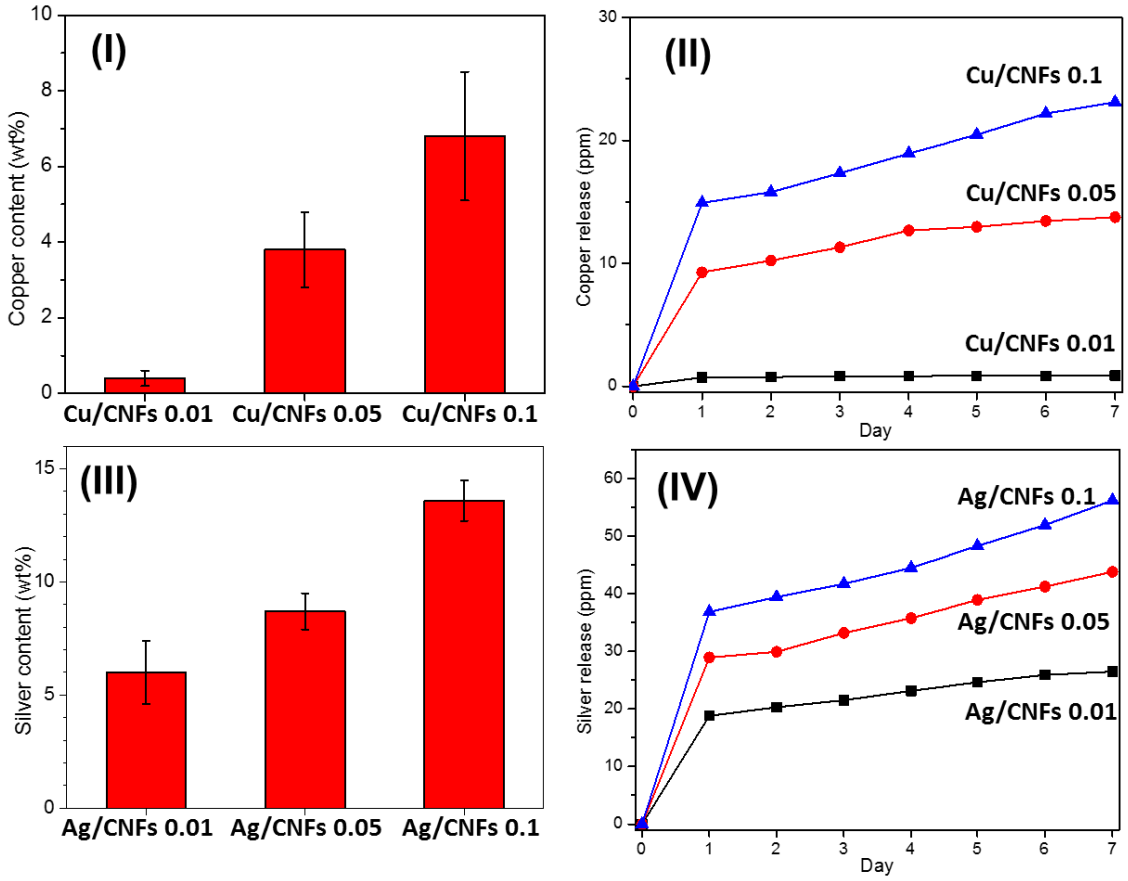

Figure 4. 3 - (I) Copper contents; (II) copper release profiles of Cu/CNFs 0.01, 0.05, and 0.1; (III) Silver contents; and (IV) silver release profiles of Ag/CNFs 0.01, 0.05, and 0.1.

4.3.3 FT-IR spectral study

The FT-IR spectroscopy graphs of CANFs and CNFs reported in Figure 4.4, verified the transformation of cellulose acetate into cellulose. The FTIR spectrum of CANFs presented three distinctive peaks at 1750, 1375, and 1230 cm^{-1} which characterized carbonyl C=O stretching, C-CH_3 bending, and C-O stretching of acetyl groups in cellulose acetate, respectively [34]. The two peaks at 1750 and 1230 disappeared in the spectroscopy of CNFs, indicating that the acetyl groups were completely removed after the deacetylation reaction with NaOH. The wide-stretching band at 3500-3600, ascribed to the O-H group in CA nanofiber graph, shifted to the

new position at 3200-3500 in the case of CNFs nanofiber, and the intensity noticeably increased. Conclusively, the CANFs were fully converted into CNFs.

CNFs showed the typical band at 3200-3500 and peaks of CNFs at 2890, 1640, 1375, 1160, and 1020, attributed to O-H stretching, C-H stretching, H-O-H bending of absorbed water, C-OH bending, C-O antisymmetric bridge stretching, and C-O-C pyranose ring skeletal vibration, respectively [35]. For CNFs treated in $AgNO_3$ under UV excitation, the peak at 820, ascribed to $-NO_3$ bending [36], indicated the presence of nitrate group in Ag/CNF samples. We surmise that a small amount of $AgNO_3$ penetrated into the CNFs during immersion treatment. The difference in intensity of the 820 cm^{-1} peak must be due to the difference in the quantities of silver nitrate absorbed in the nanofibers; hence, the results suggested that the concentration variation of the treating solutions is one of the factors to alter the silver contents. After immersing CNFs in copper (II) acetate, the acetyl groups were present on CNFs, identified by peaks at 1750, 1375, 1230, and 1050; those peaks were similar to CANFs. After the reduction of copper (II) acetate by sodium borohydride, these peaks disappeared in Cu/CNFs samples, which demonstrated the absolute conversion of copper (II) acetate to zerovalent copper nanoparticles – Cu (0) nanoparticles.

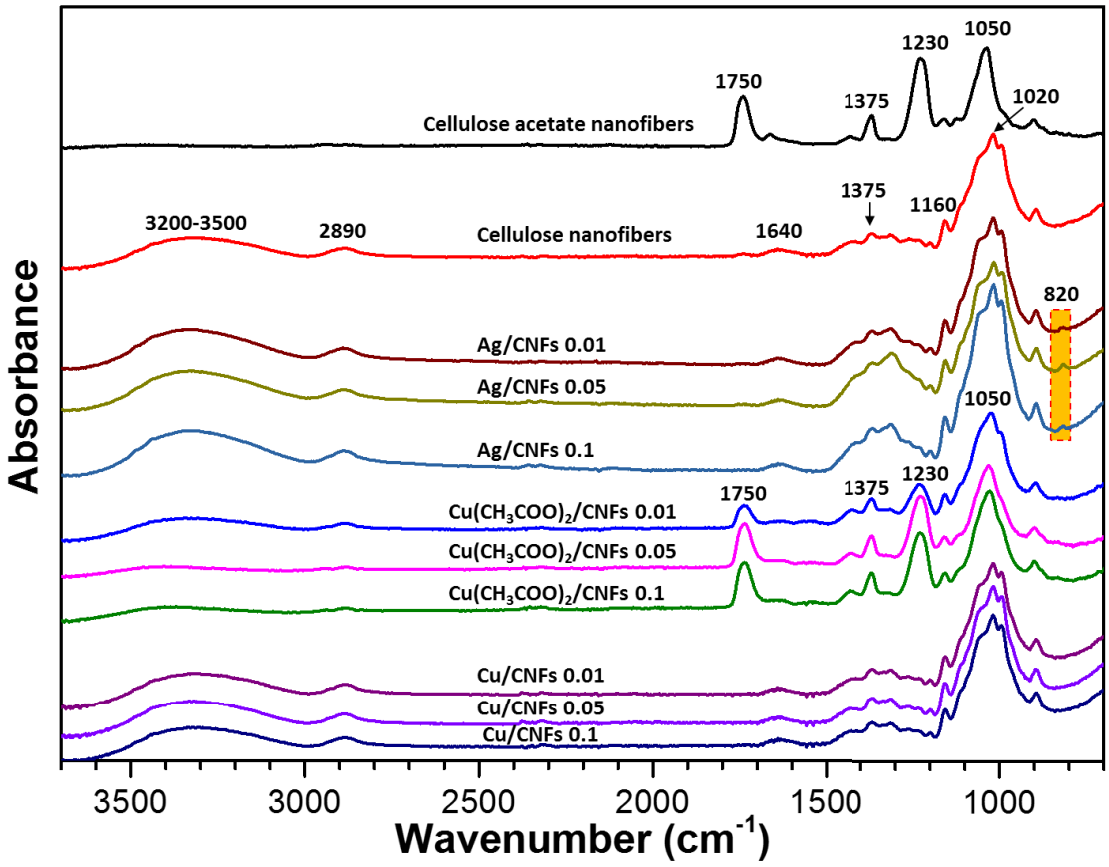

Figure 4. 4 - FT-IR spectra of CANFs, CNFs, Ag/CNFs, copper (II) acetate CNFs, and Cu/CNFs.

4.3.4 X-ray diffraction study

To identify the nature of metallic nanoparticles, X-ray diffraction patterns were acquired. CANFs presented two typical diffraction peaks, centered at 2θ = 9° and 22.5°, which characterized semi-crystallinity of acetylated structure of cellulose acetate [37]. After the deacetylation reaction, the CNFs displayed peaks which can be ascribed to cellulose II crystallites [38, 39]. No Ag/CNF samples showed diffraction peaks for silver, from which we surmised that the nature of silver nanoparticles reduced by UV-excitation was a mixture of zerovalent silver, monovalent silver, and silver salt - $AgNO_3$; therefore, specific diffraction silver peaks did not appear on silver composite nanofibers. This heterogeneity of AgNPs

was thought to cause the difficulty of detecting the silver by XRD. By contrast, CuNPs, reduced by chemical method, could be characterized by 3 typical diffraction peaks at 2θ = 44°, 51.5°, and 75°, corresponding to 111, 200, and 220 planes of copper nanoparticles [40].

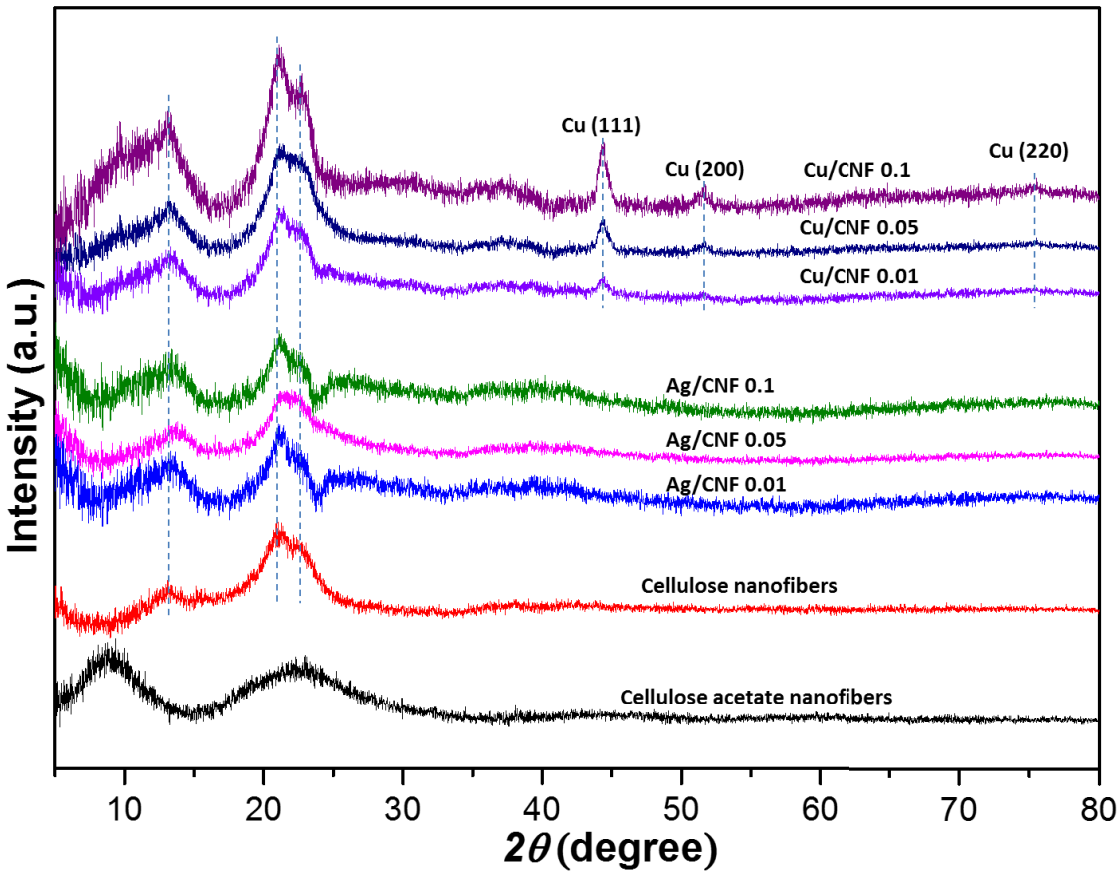

Figure 4. 5 - XRD spectra of CANFs, CNFs, Ag/CNFs, and Cu/CNFs.

4.3.5 XPS analysis

The presence of metal nanoparticles on CNF samples under UV treatment or chemical synthesis method was further verified by XPS spectra analysis. In Figure 4.5 (I) and (III), the peaks of O 1s (530.0 eV), C 1s (280.0 eV), and either Ag 3d (from 372.1 eV to 366.1 eV) or Cu 2p (from 952.3 eV to 932.4 eV) could be observed in all wide spectra. There are noticeable differences in the intensity of the metal element peaks between samples. Figure 4.5 (II), the magnified area at 378 –

362 eV identifies the silver element, peak positions at 372.1 and 366.1, the gap between two peaks was 6 eV. The $Cu2p_{1/2}$ and $Cu2p_{3/2}$ signals at 950.6 and 930.6 eV, which were assigned to Cu^0, demonstrated the reduction of copper (II) acetate to metallic copper. The peak gap was recorded to be about 20 eV [41].

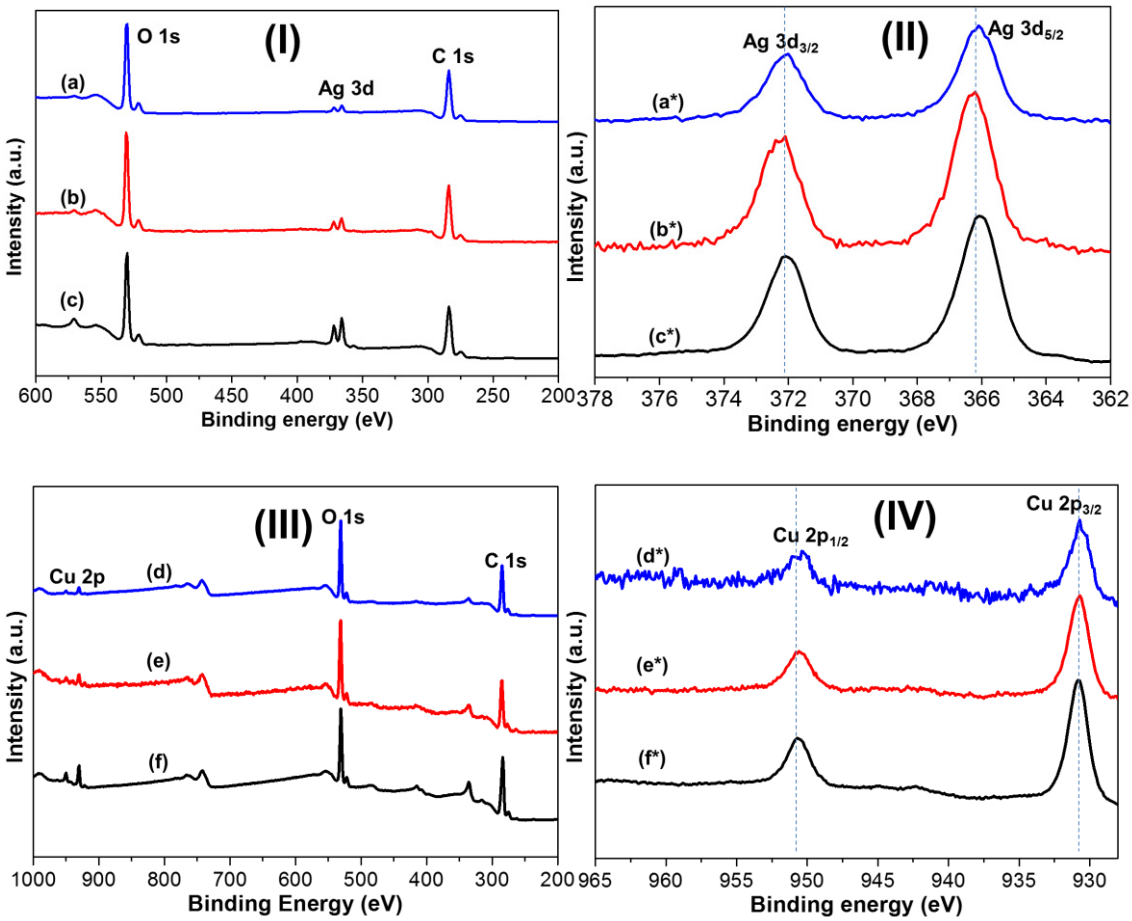

Figure 4. 6 - (I, III) XPS wide spectra, and XPS high resolution spectra of the silver region (II) and copper region (IV) for Ag/CNFs 0.01 (a, a*), 0.05 (b, b*), 0.1 (c, c*), and Cu/CNFs 0.01 (d, d*), 0.05 (e, e*), 0.1 (f, f*)

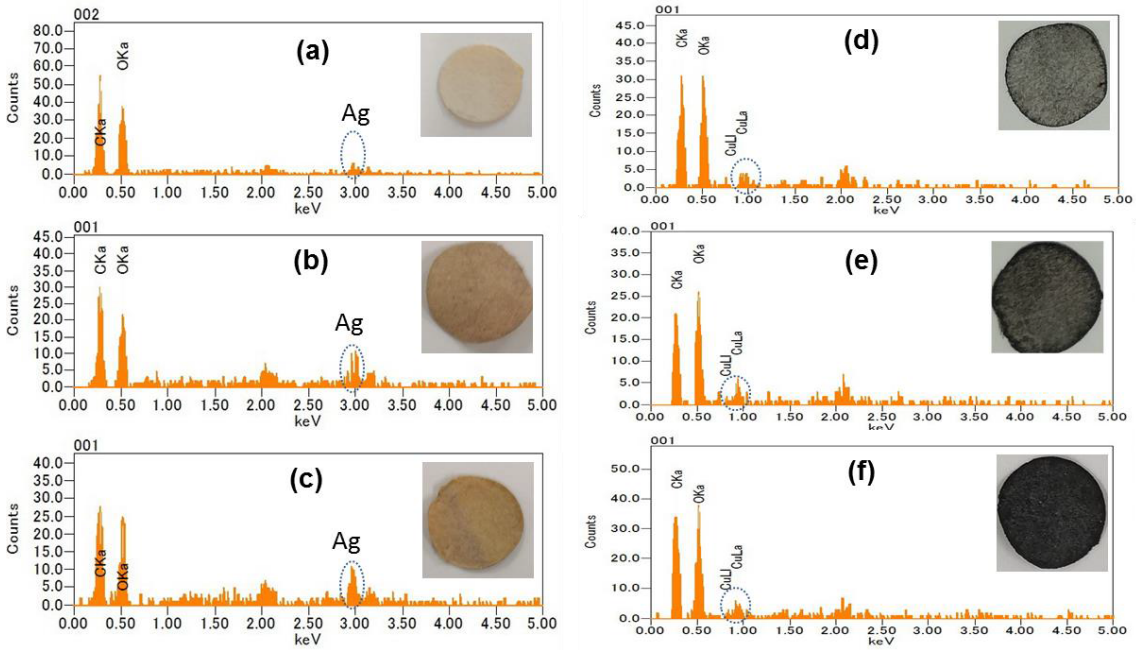

Figure 4. 7 - EDS spectra of Ag/CNFs 0.01 (a), 0.05 (b), 0.1 (c), Cu/CNFs 0.01 (d), 0.05 (e), and 0.1 (f)

4.3.6 Metal release kinetics

The release of metal ions over time from the nanoparticles was evaluated to anticipate the bactericidal effects of cellulose composite samples. On the one hand, a speedy release of copper or silver is necessary for the application of wound dressing, thus, the wound is instantaneously cleaned off contaminating organisms; but on the other hand, a slow rate of release ensures a sustainable feature for the membrane in long-term applications. Figure 4.3 (II) and (IV) indicates a rapid initial release at the first day for all Cu/CNFs and Ag/CNFs samples, followed by a more gradual discharge of copper or silver into the aqueous environment. The copper release of Cu/CNFs 0.01 sample was stable and almost unchanged during the 7-day course, Figure 4.3 (II). The maximum amounts of silver, discharged at the point of time of 7 days, were 26.47, 43.78, and 56.18 ppm for Ag/CNFs 0.01, 0.05, and 0.1, respectively; whereas they were 0.87, 13.76, and 23.11 for Cu/CNFs 0.01, 0.05, and

0.1. These values accounted for 8.79, 10.04, and 8.25 wt% of the total silver loading amounts on the respective Ag/CNF samples; and 4.5, 8.98, and 8.3 wt% of the total copper loading amounts on respective Cu/CNF samples.

4.3.7 Antibacterial activity against Escherichia coli and Bacillus subtilis

The antibacterial performance of the composite nanofibers was evaluated against E. coli (gram-negative) and B. subtilis (gram-positive) bacteria. To confirm that CNFs have no antibacterial activity, CNF specimens were used as the negative control. For all composite samples, disk diffusion test was done in triplicate and the inhibition zones were measured three times. The expansive degrees of halo zones along with standard deviation are illustrated in Figure 4.8 Cu/CNFs 0.01, 0.05, 0.1, Ag/CNFs 0.01, 0.05, and 0.1 distinctively demonstrated inhibitory zones against bacteria. There was a correlation between the metal release of the silver or copper composite nanofibers and the sizes of the bacterial inhibition zones, to some extent. With the higher metal release amounts, the sizes of inhibition zone were observed to be more expansive. The results indicated that the antibacterial properties of the composite nanofibers were proportionally related to the amounts of the silver or copper releases.

Noticeably, better comparatively expansive inhibition zones against E. coli than B. subtilis could be observed in the antibacterial assay of Ag/CNF specimens. However, Cu/CNFs exhibited better antibacterial activity against gram-positive bacteria. The inhibition zones of Cu/CNFs were 15.9 ± 0.8, 18.5 ± 0.7, and 21.2 ± 0.7 mm against B. subtilis, while only 13.2 ± 0.5, 13.7 ± 0.2, and 14.8 ± 0.4 mm against E. coli. The antibacterial results of CuNPs against B. subtilis were even higher than those of AgNPs. The resultant data agreed well with other scientific reports [42, 43].

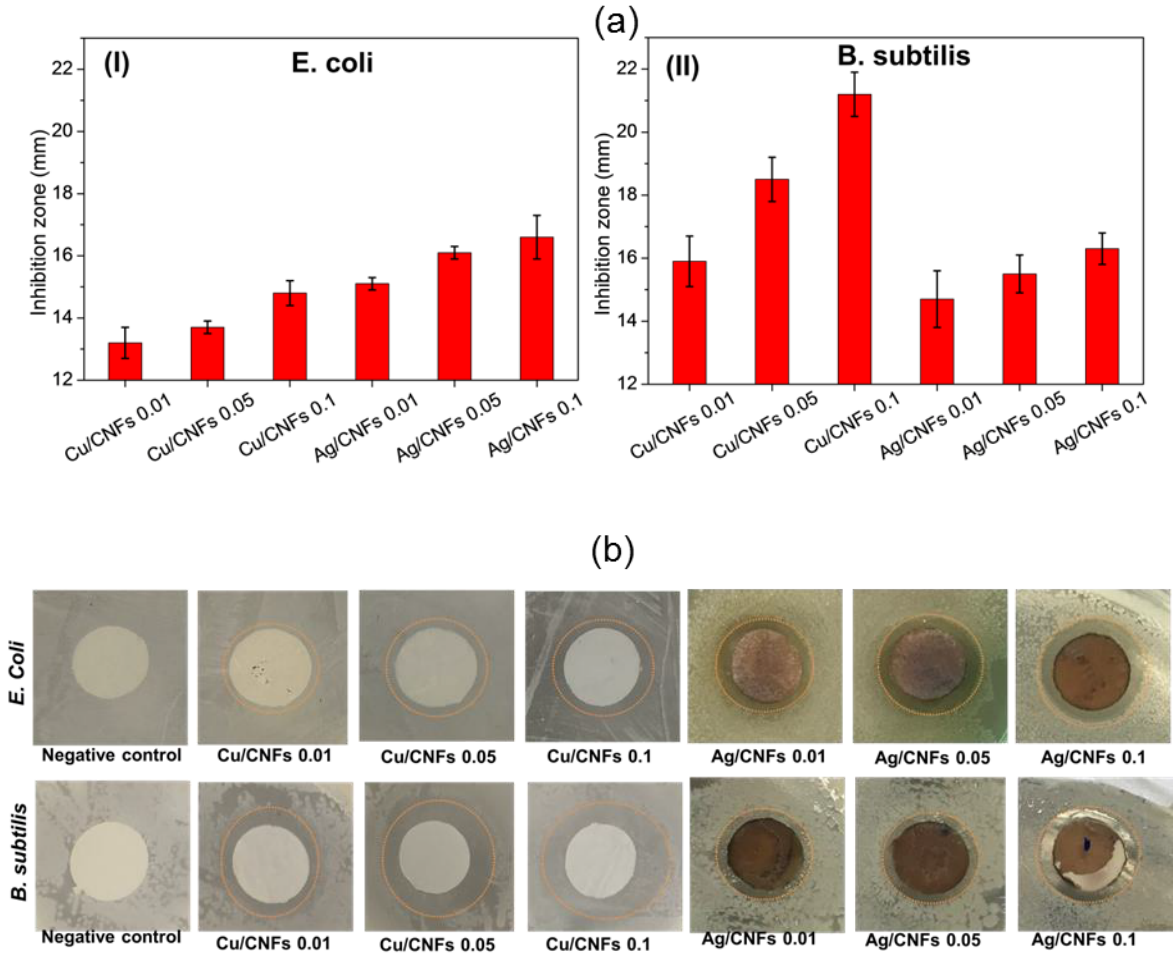

Figure 4. 8 – (a) Mean diameters of inhibition zones with standard deviations against (I) E. coli and (II) B. subtilis of the composite specimens, (b) Representative photographs of inhibition zone of CNFs – as the negative control, Cu/CNFs 0.01, 0.05, 0.1, Ag/CNFs 0.01, 0.05, and 0.1

The bactericidal efficacy against gram-negative E. coli and gram-positive B. subtilis for the specimen/bacterial broth ratio at 0.01 g/mL was evaluated by agar plate counting as shown in Figure 4.9. The pristine CNF specimens were also prepared as negative controls. Quantitative analyses were carried out in triplicate exhibited an impressive more than 2-log reduction for all composite samples. The disk counting method also demonstrated better bactericidal activity against E. coli with silver but copper showed better antibacterial properties against B. subtilis. The

results were in line with those of disk diffusion tests and other reports [43, 44].

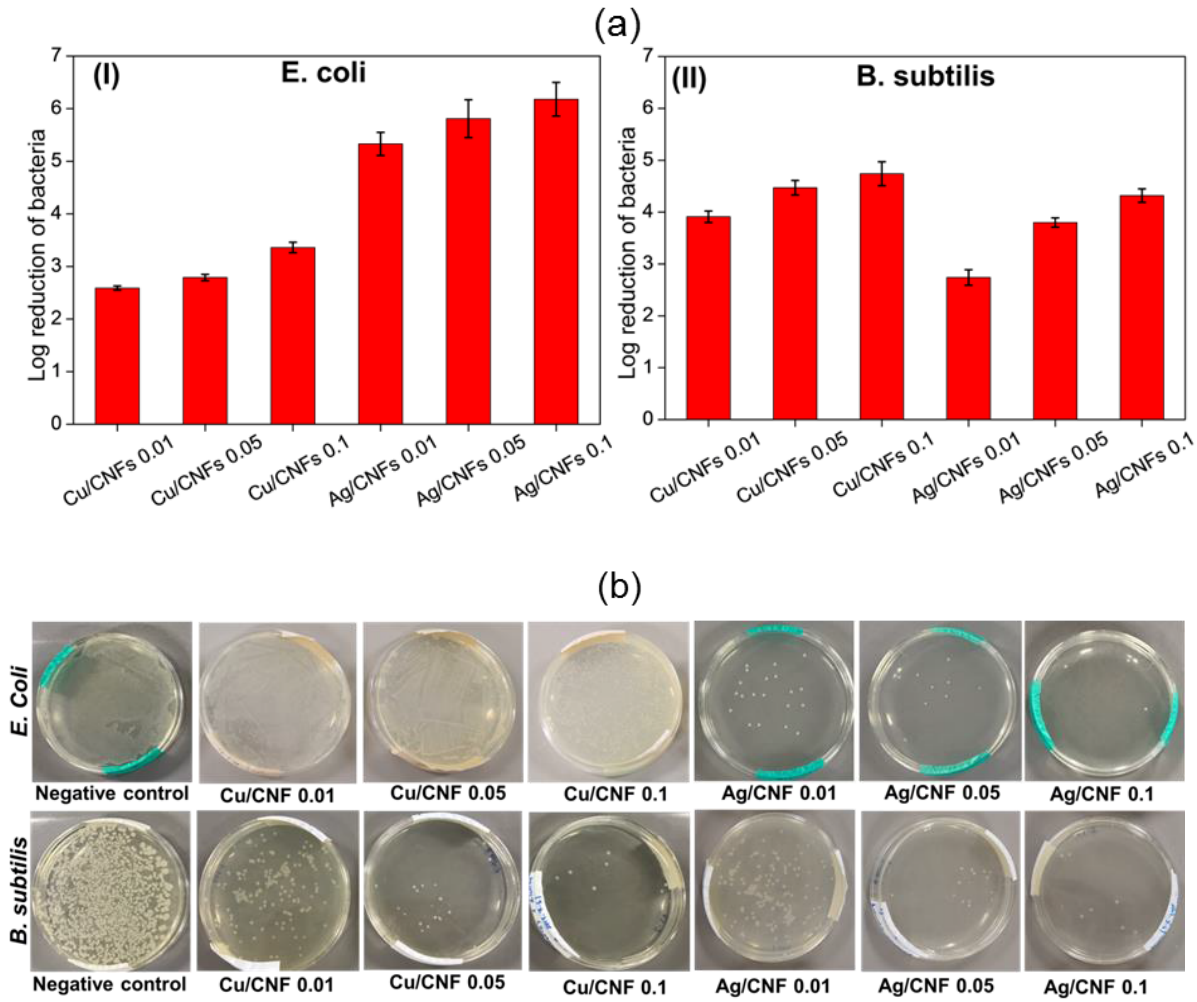

Figure 4. 9 – (a) Bactericidal efficacy of the composite specimens based on agar plate counting method, (b) Representative photographs of bactericidal efficacy of all samples based on agar plate counting method

It was concluded that composites of AgNPs and CNFs synthesized via UV-inducing method exhibited a superior antibacterial activity than the composite material Cu/CNFs synthesized via chemical route against gram-negative bacteria – E. coli. However, the copper composite samples showed better antibacterial activity against gram-positive bacteria – B. subtilis.

4.4 Conclusion

The syntheses of silver and copper nanoparticles decorated cellulose nanofibers via two routes, induced through UV excitation or reduced by the chemical reaction, were reported. The study demonstrated that silver and copper nanoparticles loaded on cellulosic scaffolds had potential to exert good antimicrobial properties against E. coli and B. subtilis. The metal release amounts were observed to be proportionally related to the contents of copper or silver loaded. All metal/cellulose composite nanofibers exhibited good antibacterial activity in terms of inhibition zones and log reduction. Against E. coli, silver samples displayed superior antibacterial activity, whereas, against B. subtilis, the copper samples demonstrated better.

References

[1] Y. Zhu, C. Romain, C.K. Williams, Sustainable polymers from renewable resources, Nature 540 (2016) 354.
[2] M. Gopiraman, A.W. Jatoi, S. Hiromichi, K. Yamaguchi, H.-Y. Jeon, I.-M. Chung, K. Ick Soo, Silver coated anionic cellulose nanofiber composites for an efficient antimicrobial activity, Carbohydrate Polymers 149 (2016) 51-59.
[3] D.-N. Phan, H. Lee, B. Huang, Y. Mukai, I.-S. Kim, Fabrication of electrospun chitosan/cellulose nanofibers having adsorption property with enhanced mechanical property, Cellulose 26(3) (2019) 1781-1793.
[4] Y.E. Greish, M.A. Meetani, E.A. Al Matroushi, B.A. Shamsi, Effects of thermal and chemical treatments on the structural stability of cellulose acetate nanofibers, Carbohydrate Polymers 82(3) (2010) 569-577.
[5] A. Rezaei, A. Nasirpour, M. Fathi, Application of Cellulosic Nanofibers in Food Science Using Electrospinning and Its Potential Risk, Comprehensive Reviews in Food Science and Food Safety 14(3) (2015) 269-284.
[6] M.A. Kohanski, D.J. Dwyer, J.J. Collins, How antibiotics kill bacteria: from targets to networks, Nature reviews. Microbiology 8(6) (2010) 423-435.
[7] G. Franci, A. Falanga, S. Galdiero, L. Palomba, M. Rai, G. Morelli, M. Galdiero, Silver Nanoparticles as Potential Antibacterial Agents, Molecules 20(5) (2015) 8856.
[8] B. Calderón-Jiménez, M.E. Johnson, A.R. Montoro Bustos, K.E. Murphy, M.R. Winchester, J.R. Vega Baudrit, Silver Nanoparticles: Technological Advances, Societal Impacts, and Metrological Challenges, Frontiers in chemistry 5 (2017) 6-6.
[9] J. Yang, H. Xu, L. Zhang, Y. Zhong, X. Sui, Z. Mao, Lasting superhydrophobicity and antibacterial activity of Cu nanoparticles immobilized on the surface of dopamine modified cotton fabrics, Surface and Coatings Technology 309 (2017) 149-154.
[10] A.C. Lokhande, A. Shelke, P.T. Babar, J. Kim, D.J. Lee, I.-C. Kim, C.D. Lokhande, J.H. Kim, Novel antibacterial application of photovoltaic Cu2SnS3 (CTS) nanoparticles, RSC Advances 7(54) (2017) 33737-33744.

[11] N. Beyth, Y. Houri-Haddad, A. Domb, W. Khan, R. Hazan, Alternative antimicrobial approach: nano-antimicrobial materials, Evidence-based complementary and alternative medicine : eCAM 2015 (2015) 246012-246012.
[12] S. Iravani, H. Korbekandi, S.V. Mirmohammadi, B. Zolfaghari, Synthesis of silver nanoparticles: chemical, physical and biological methods, Research in pharmaceutical sciences 9(6) (2014) 385-406.
[13] A. Zielińska, E. Skwarek, A. Zaleska, M. Gazda, J. Hupka, Preparation of silver nanoparticles with controlled particle size, Procedia Chemistry 1(2) (2009) 1560-1566.
[14] T.A. Dankovich, Microwave-assisted incorporation of silver nanoparticles in paper for point-of-use water purification, Environmental Science: Nano 1(4) (2014) 367-378.
[15] S.-W. Lee, S.-H. Chang, Y.-S. Lai, C.-C. Lin, C.-M. Tsai, Y.-C. Lee, J.-C. Chen, C.-L. Huang, Effect of Temperature on the Growth of Silver Nanoparticles Using Plasmon-Mediated Method under the Irradiation of Green LEDs, Materials 7(12) (2014) 7781.
[16] H. Kawamura, K. Moritani, Y. lto, Discharge electrolysis in molten chloride: formation of fine silver particles, Plasmas & Ions 1(1) (1998) 29-36.
[17] P. Kuppusamy, M.M. Yusoff, G.P. Maniam, N. Govindan, Biosynthesis of metallic nanoparticles using plant derivatives and their new avenues in pharmacological applications - An updated report, Saudi pharmaceutical journal : SPJ : the official publication of the Saudi Pharmaceutical Society 24(4) (2016) 473-484.
[18] S. Iravani, Green synthesis of metal nanoparticles using plants, Green Chemistry 13(10) (2011) 2638-2650.
[19] H.-J. Lee, J.Y. Song, B.S. Kim, Biological synthesis of copper nanoparticles using Magnolia kobus leaf extract and their antibacterial activity, Journal of Chemical Technology & Biotechnology 88(11) (2013) 1971-1977.
[20] D.-N. Phan, H. Lee, D. Choi, C.-Y. Kang, S. Im, I. Kim, Fabrication of Two Polyester Nanofiber Types Containing the Biobased Monomer Isosorbide: Poly (Ethylene Glycol 1,4-Cyclohexane Dimethylene Isosorbide Terephthalate) and Poly (1,4-Cyclohexane Dimethylene Isosorbide Terephthalate), Nanomaterials 8(2) (2018) 56.
[21] H. Lee, G. Xu, D. Kharaghani, M. Nishino, K.H. Song, J.S. Lee, I.S. Kim, Electrospun tri-layered zein/PVP-GO/zein nanofiber mats for providing biphasic drug release profiles, International Journal of Pharmaceutics 531(1) (2017) 101-107.
[22] C. Zhu, T. Nagaishi, J. Shi, H. Lee, P.Y. Wong, J. Sui, K. Hyodo, I.S. Kim, Enhanced Wettability and Thermal Stability of a Novel Polyethylene Terephthalate-Based Poly(Vinylidene Fluoride) Nanofiber Hybrid Membrane for the Separator of Lithium-Ion Batteries, ACS Applied Materials & Interfaces 9(31) (2017) 26400-26406.
[23] I. Kohsari, Z. Shariatinia, S.M. Pourmortazavi, Antibacterial electrospun chitosan–polyethylene oxide nanocomposite mats containing bioactive silver nanoparticles, Carbohydrate Polymers 140 (2016) 287-298.
[24] S. Ifuku, Y. Tsukiyama, T. Yukawa, M. Egusa, H. Kaminaka, H. Izawa, M. Morimoto, H. Saimoto, Facile preparation of silver nanoparticles immobilized on chitin nanofiber surfaces to endow antifungal activities, Carbohydrate Polymers 117 (2015) 813-817.
[25] L. Chen, X. Peng, Silver nanoparticle decorated cellulose nanofibrous membrane with good antibacterial ability and high water permeability, Applied Materials Today 9 (2017) 130-135.
[26] A.A. Omrani, N. Taghavinia, Photo-induced growth of silver nanoparticles using UV sensitivity of cellulose fibers, Applied Surface Science 258(7) (2012) 2373-2377.
[27] M. Kozicki, E. Sąsiadek, M. Kołodziejczyk, J. Komasa, A. Adamus, W. Maniukiewicz, A. Pawlaczyk, M. Szynkowska, J. Rogowski, E. Rybicki, Facile and durable antimicrobial finishing of cotton textiles using a silver salt and UV light, Carbohydrate Polymers 91(1) (2013) 115-127.
[28] M. Rehan, A. Barhoum, G. Van Assche, A. Dufresne, L. Gätjen, R. Wilken, Towards multifunctional cellulosic fabric: UV photo-reduction and in-situ synthesis of silver nanoparticles into cellulose fabrics, International Journal of Biological Macromolecules 98 (2017) 877-886.

[29] S. Perera, B. Bhushan, R. Bandara, G. Rajapakse, S. Rajapakse, C. Bandara, Morphological, antimicrobial, durability, and physical properties of untreated and treated textiles using silver-nanoparticles, Colloids and Surfaces A: Physicochemical and Engineering Aspects 436 (2013) 975-989.
[30] A.W. Jatoi, I.S. Kim, Q.Q. Ni, A comparative study on synthesis of AgNPs on cellulose nanofibers by thermal treatment and DMF for antibacterial activities, Materials Science and Engineering: C 98 (2019) 1179-1195.
[31] B. Jia, Y. Mei, L. Cheng, J. Zhou, L. Zhang, Preparation of copper nanoparticles coated cellulose films with antibacterial properties through one-step reduction, ACS Applied Materials & Interfaces 4(6) (2012) 2897-2902.
[32] O. Rubilar, M. Rai, G. Tortella, M.C. Diez, A.B. Seabra, N. Durán, Biogenic nanoparticles: copper, copper oxides, copper sulphides, complex copper nanostructures and their applications, Biotechnology Letters 35(9) (2013) 1365-1375.
[33] H. Lee, M. Nishino, D. Sohn, J.S. Lee, I.S. Kim, Control of the morphology of cellulose acetate nanofibers via electrospinning, Cellulose 25(5) (2018) 2829-2837.
[34] J. Song, N.L. Birbach, J.P. Hinestroza, Deposition of silver nanoparticles on cellulosic fibers via stabilization of carboxymethyl groups, Cellulose 19(2) (2012) 411-424.
[35] J. Li, L.-P. Zhang, F. Peng, J. Bian, T.-Q. Yuan, F. Xu, R.-C. Sun, Microwave-Assisted Solvent-Free Acetylation of Cellulose with Acetic Anhydride in the Presence of Iodine as a Catalyst, Molecules 14(9) (2009) 3551.
[36] Y. Oyumi, T.B. Brill, A.L. Rheingold, C. Lowe-Ma, Thermal decomposition of energetic materials. 2. The thermolysis of nitrate and perchlorate salts of the pentaerythrityltetrammonium ion, C(CH2NH3)44+, by rapid-scan FTIR spectroscopy. The crystal structure of pentaerythrityltetrammonium nitrate ([C(CH2NH3)4](NO3)4), The Journal of Physical Chemistry 89(11) (1985) 2309-2315.
[37] C.-H. Hong, S.-J. Ki, J.-H. Jeon, H.-l. Che, I.-K. Park, C.-D. Kee, I.-K. Oh, Electroactive bio-composite actuators based on cellulose acetate nanofibers with specially chopped polyaniline nanoparticles through electrospinning, Composites Science and Technology 87 (2013) 135-141.
[38] A.D. French, M. Santiago Cintrón, Cellulose polymorphy, crystallite size, and the Segal Crystallinity Index, Cellulose 20(1) (2013) 583-588.
[39] A.D. French, Idealized powder diffraction patterns for cellulose polymorphs, Cellulose 21(2) (2014) 885-896.
[40] M. Raffi, S. Mehrwan, T.M. Bhatti, J.I. Akhter, A. Hameed, W. Yawar, M.M. ul Hasan, Investigations into the antibacterial behavior of copper nanoparticles against Escherichia coli, Annals of Microbiology 60(1) (2010) 75-80.
[41] F.A. Akgul, G. Akgul, N. Yildirim, H.E. Unalan, R. Turan, Influence of thermal annealing on microstructural, morphological, optical properties and surface electronic structure of copper oxide thin films, Materials Chemistry and Physics 147(3) (2014) 987-995.
[42] T. Kruk, K. Szczepanowicz, J. Stefańska, R.P. Socha, P. Warszyński, Synthesis and antimicrobial activity of monodisperse copper nanoparticles, Colloids and Surfaces B: Biointerfaces 128 (2015) 17-22.
[43] K.-Y. Yoon, J. Hoon Byeon, J.-H. Park, J. Hwang, Susceptibility constants of Escherichia coli and Bacillus subtilis to silver and copper nanoparticles, Science of The Total Environment 373(2) (2007) 572-575.
[44] J.P. Ruparelia, A.K. Chatterjee, S.P. Duttagupta, S. Mukherji, Strain specificity in antimicrobial activity of silver and copper nanoparticles, Acta Biomaterialia 4(3) (2008) 707-716.

CHAPTER 5 Zinc oxide nanoparticles attached to polyacrylonitrile nanofibers with hinokitiol as gluing agent for synergistic antibacterial activities and effective dye removal

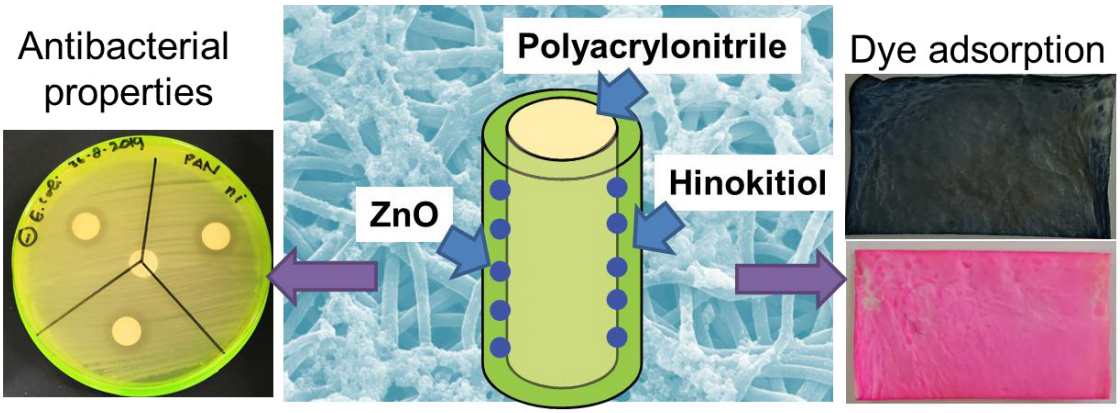

5.1. Introduction

Nanofibers with the advantages of nanoscale structures, have demonstrated improved chemical and mechanical properties compared to bulk materials, and acted as an ideal scaffold for loading functional agents such as antibiotics with enhanced contact area to pathogenic organisms. Ag, Cu, TiO_2, and ZnO can be incorporated in nanofibers to exert antibiotic effects on membranes. ZnO with varied morphologies was reported to display powerful antifungal and antibacterial activities against a wide range of pathogens but observed to be negligibly toxic toward human cells [1]. ZnO in microscale or nanoscale also exhibits high chemical activity due to their surface properties which produce reactive oxygen species via Haber-Weiss and Fenton reaction mechanisms [2].

Recently, different forms of antimicrobial materials, extracted from plants and marine creatures including polysaccharides, peptides, oils, polyphenols, and chitosan, have been extensively studied because they have a propensity of being non-toxic and environmentally benign [3]. Hinokitiol is a natural compound, being extracted from Chamaecyparis, which possesses antibacterial characteristics without significant cytotoxicity against human endothelial cells and epithelial cells [4]. The antibacterial activities of hinokitiol, partly due to the metabolic suppression toward cell membranes and respiration inhibition, have been reported toward pathogenic bacteria including *legionella pneumophila*, *aggregatibacter actinomycetemcomitans*, *staphylococcus aureus*, and *fusobacterium nucleatum* [5]. Furthermore, hinokitiol was demonstrated to exhibit antifungal effects against *helicibasidium mompa* and *roselliania necatrix*. The anti-inflammatory effects in various cells were also studied and proved to be significant by numerous mechanisms [6].

Organic dyes used for production of textiles, leather, and plastics have been

released excessively into the environment posing severe problems to the ecosystem. Among common water treatment techniques, adsorption has been employed effectively for removing toxic dyes. In this study, we successfully utilized zinc oxide as a bifunctional agent for the antibacterial application and dye removal. Antibacterial assessment was performed against *Escherichia coli* and *Staphylococcus aureus*, they represent gram negative and gram positive bacteria. S. aureus can cause bacteremia and endocarditis, whereas E. coli accounts for approximately 85% of urinary tract infections [7]. Zinc oxide has been reported to presents highly adsorptive behavior toward anionic dyes at around neutral pH [8], but according to our experiments ZnO nanoparticles were slowly discharged into water leading to the dwindling adsorptive capacity. The addition of hinokitiol to the composite nanofibers was proved to show synergistic bactericidal actions and help to hold ZnO particles firmly on the nanofibers.

5.2. Experimental

5.2.1 Materials

Polyacrylonitrile (PAN, Mw 150,000 g/mol) was purchased from Sigma-Aldrich, Tokyo, Japan. N,N-dimethylformamide (DMF), zinc chloride ($ZnCl_2$ - 96%), sodium hydroxide (NaOH 97%), ethanol (99.5%), and Hinokitiol (HT) were acquired from Wako pure chemical industries, Osaka, Japan. Staphylococcus aureus (NBRC 12732) and Escherichia coli (NBRC 3972) were received from the National Institute of Technology and Evaluation, Biological Resource Center (NBRC), Japan. The petri dishes were provided by Sansei Medical Co., LTD., Japan. CI reactive blue 19 (vinylsulfone) and CI reactive red 195 (monoazo-monochlorotriazine + vinylsulfone) were provided by Sumitomo Chemical Co., Ltd., Japan.

5.2.2 Zinc oxide and hinokitiol integrated in PAN nanofibers

Three bottles containg PAN polymer at 8 wt. % in DMF solvent were prepared. The PAN solutions were vigorously stirred for 24 h to dissolve the solute completely. $ZnCl_2$ were then added to two bottles to produce the salt polymer solutions in order that the weight ratios between Zn and PAN would be 1/8 and 1/2. Electrospinning was performed for 24 h for all three different nanofiber samples namely PAN, $ZnCl_2$-PAN_Lo, and $ZnCl_2$-PAN_Hi. $ZnCl_2$-PAN_Lo and $ZnCl_2$-PAN_Hi were related to the ratios between Zn and PAN of 1/8 and 1/2, respectively. The electrospinning fundamental parameters were selected as the tip to collector distance was 15 cm, relative humidity was 40 %, and room temperature was kept at 25°C.

ZnO-PAN nanofibers were prepared by dropping NaOH dissolved in ethanol over $ZnCl_2$-PAN nanofibers. The NaOH-Ethanol solution was prepared with the concentration of 1 g NaOH in 50 mL ethanol. The dribbling amounts of NaOH solution needed were calculated so that the reaction between alkali and zinc salt happened completely. The resulted $Zn(OH)_2$-PAN nanofibers was further gone through dehydration treatment at 150°C for 2 h, employing electric furnace (AMF-9P-III THV, Asahi Rika Seisakujo), to produce ZnO nanoparticles. Afterward, the soaking nanofibers were let for the reaction to happen completely and to dry at room temperature for a few hours before being washed with ethanol and distilled water several times, removing all impurities. Eventually, ZnO-PAN_Lo and ZnO-PAN_Hi were acquired.

To prepare nanofibers containing hinokitiol, hinokitiol solutions with two concentrations were prepared by adding 1 g or 4 g in 50 mL ethanol. The solution containing lower Hinokitiol concentration was denoted as HT_Lo and the higher one was named as HT_Hi. Afterward, PAN nanofibers were treated with HT_Lo or

HT_Hi solutions by slowly dropping 1 mL solution over each 0.1 g nanofibers, resulting in HT-PAN_Lo and HT-PAN_Hi samples. Similarly, ZnO-HT-PAN_Lo and ZnO-HT-PAN_Hi nanofibers were obtained from ZnO-PAN_Lo treated with lower HT solution and ZnO-PAN_Hi treated with higher HT solution, respectively.

5.2.3 Antibacterial assays

Disk diffusion tests were evaluated against *Escherichia coli* strain (NBRC 3972) and *Staphylococcus aureus* (NBRC 12732) for PAN sample - as negative control, ZnO-PAN, HT-PAN, and ZnO-HT-PAN samples in triplicate. Both bacteria were cultured in the LB broth for 24 h at 37°C. The bacterial mediums were then diluted to suitable concentrations by saline water. The used bacterial concentration in our tests was 10^6 colony forming unit per milliliter – CFU/mL. Thereafter, 200 μL volume of bacterial suspension with concentration of 10^6 CFU/mL were spread over the agar plates. The nanofibrous specimens were then placed on agar plates to measure halo zones after culturing over the 24-h course. The diameters of the inhibition zones were presented in mm with standard deviations.

5.2.4 Characterizations

The morphology of nanofibers was observed by scanning electron microscopy (SEM, JSM-6010LA by JEOL, Japan) and transmission electron microscopy (TEM, 2010 Fas TEM, JEOL, Tokyo, Japan) with the voltage of 200 kV. The average diameters of nanofibers were measured over 100 nanofiber strands for each sample and the size of ZnO nanoparticles were sampled for 500 particles. The calculations were implemented on analysis software (Image J) and Excel, and the results were displayed with mean values and standard deviations. Fourier Transform Infrared (FT-

IR) spectrophotometer (Prestige-21, Shimadzu Co., Ltd., Japan) was performed to verify distinctions between chemical groups of all samples, the range of wavelength was from 400 to 4000 cm^{-1} with accumulation over 20 scans for each graph. X-ray diffraction instrument (XRD) with CuKα anode (Miniflex 300, Rigaku Co., Ltd., Japan), operating at 30 kV and 500 mA, was utilized to detect diffraction angles and thus exhibit crystallinity of all nanofibrous samples. Elemental analysis was studied on energy dispersive X-ray spectroscopy (SEM-EDS, JSM-6010LA, JEOL, Japan).

5.2.5 Batch adsorption

The adsorption of blue and red dyes was examined using batch adsorption test for PAN, HT-PAN_Hi, ZnO-PAN_Hi and ZnO-HT-PAN_Hi samples. The amount of 10 mg nanofibers was immersed in 15 mL solutions containing either reactive blue dye or reactive red dye with the initial concentration of 0.01 g/L. During the adsorption process, all solutions were shaken at room temperature of 25 °C, the agitation speed of 150 rpm, for 26 h. All solutions were sampled for UV-Vis spectrophotometer (Shimadzu UV-2600 spectrophotometer, Japan) after every 2 h time interval.

5.3. Results and discussion

5.3.1 Morphology study of nanofiber membranes

SEM images of neat PAN, HT-PAN_Lo, HT-PAN_Hi, $ZnCl_2$-PAN_Lo and $ZnCl_2$-PAN_Hi were taken to show uniform, smooth, and bead-free nanofibers with the average diameters of 469±78, 474±84, 481±83, 398±89, 349±85 nm, from Figure 5.1 (a) to (e). The addition of $ZnCl_2$ to the PAN solution increased the conductivity and thus the stretching of the nanofibers, resulted in smaller fiber diameters for $ZnCl_2$-PAN samples. In Figure 5.1 (f) to (i), the success of ZnO synthesis could be

confirmed with the well decoration of spherical particles on nanofibers. The diameters of nanofibers containing ZnO increased slightly due to the additional size of ZnO nanoparticle clusters. The immersion treatment in Hinokitiol solutions did not make recognizable changes to the nanofibrous morphology. The diameters of ZnO-PAN_Lo, ZnO-PAN_Hi, ZnO-PAN-HT_Lo, and ZnO-PAN-HT_Hi were 410±105, 421±103, 415±87, and 430±90, respectively.

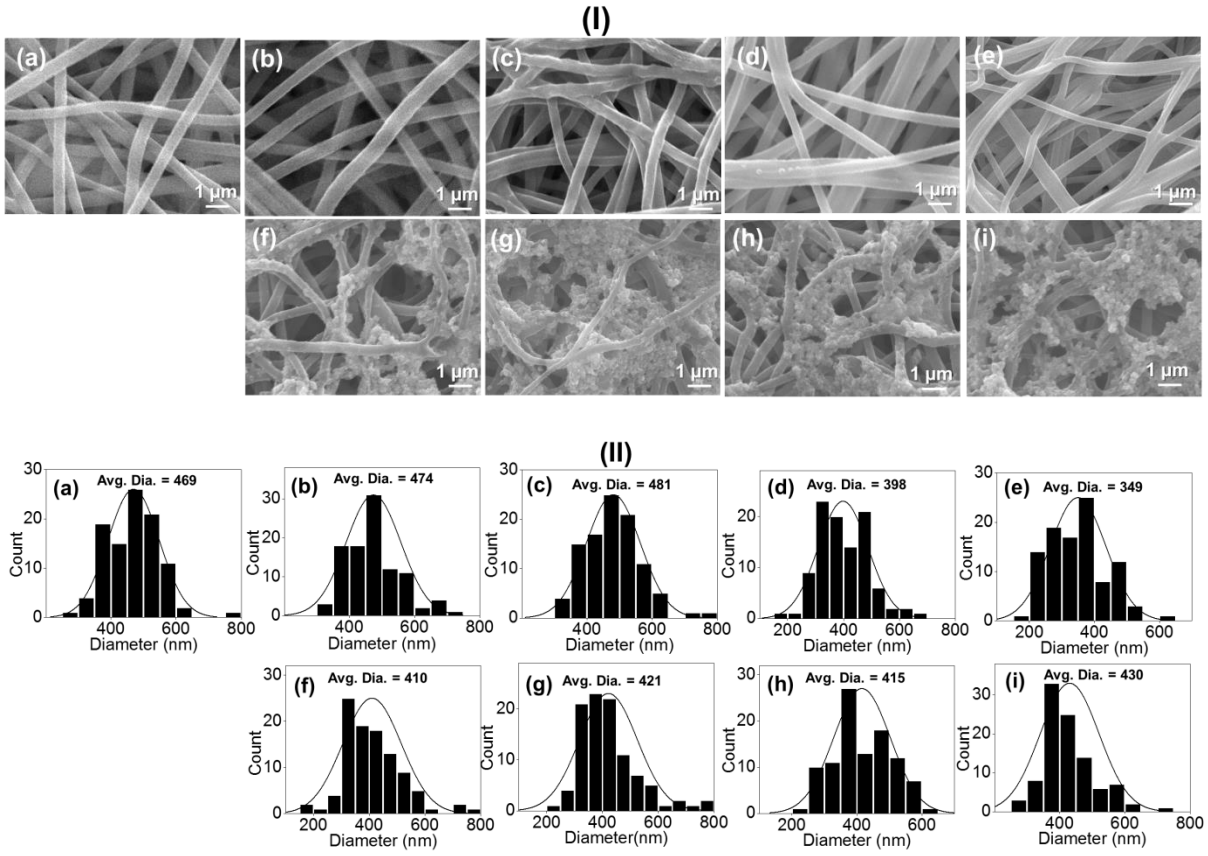

Figure 5. 1 - Morphology of (a) neat PAN nanofibers, (b)HT-PAN_Lo, (c) HT-PAN_Hi, (d) $ZnCl_2$-PAN_Lo, (e) $ZnCl_2$-PAN_Hi, (f) ZnO-PAN_Lo, (g) ZnO-PAN_Hi, (h) ZnO-HT-PAN_Lo, and (i) ZnO-HT-PAN_Hi nanofibers

To have better-detailed observation of ZnO nanoparticles and the covering layer of Hinokitiol, TEM analysis was performed, Figure 5.2. PAN and $ZnCl_2$-PAN nanofibers exhibit featureless and regular images. By contrast, the results given in

Figure 5.2 (b) and (c) show thin layer of Hinokitiol over the surface of PAN nanofibers and in Figure 5.2 (f) and (g) the decoration of ZnO nanoparticles at nanosize, aggregating together to form nanoparticulate clusters. Due to lack of bonding or adhesive agents to connect nanoparticles together, ZnO might leach out form the nanofibrous scaffold irreversibly. Therefore, Hinokitiol coating could maintain and secure ZnO nanoparticles to the surface of PAN nanofibers via metal-oxygen bonding complexes [9]. Hinokitiol ligand with two oxygen atoms forms complexes with Zn, involving minimal intermolecular interaction between ligand and metal, and thus complexes can hinder solubility [10]. In Figure 5.2 (i), HT layer covering ZnO nanoparticle cluster could help to avoid ZnO nanoparticles from dispersing into the aqueous environment.

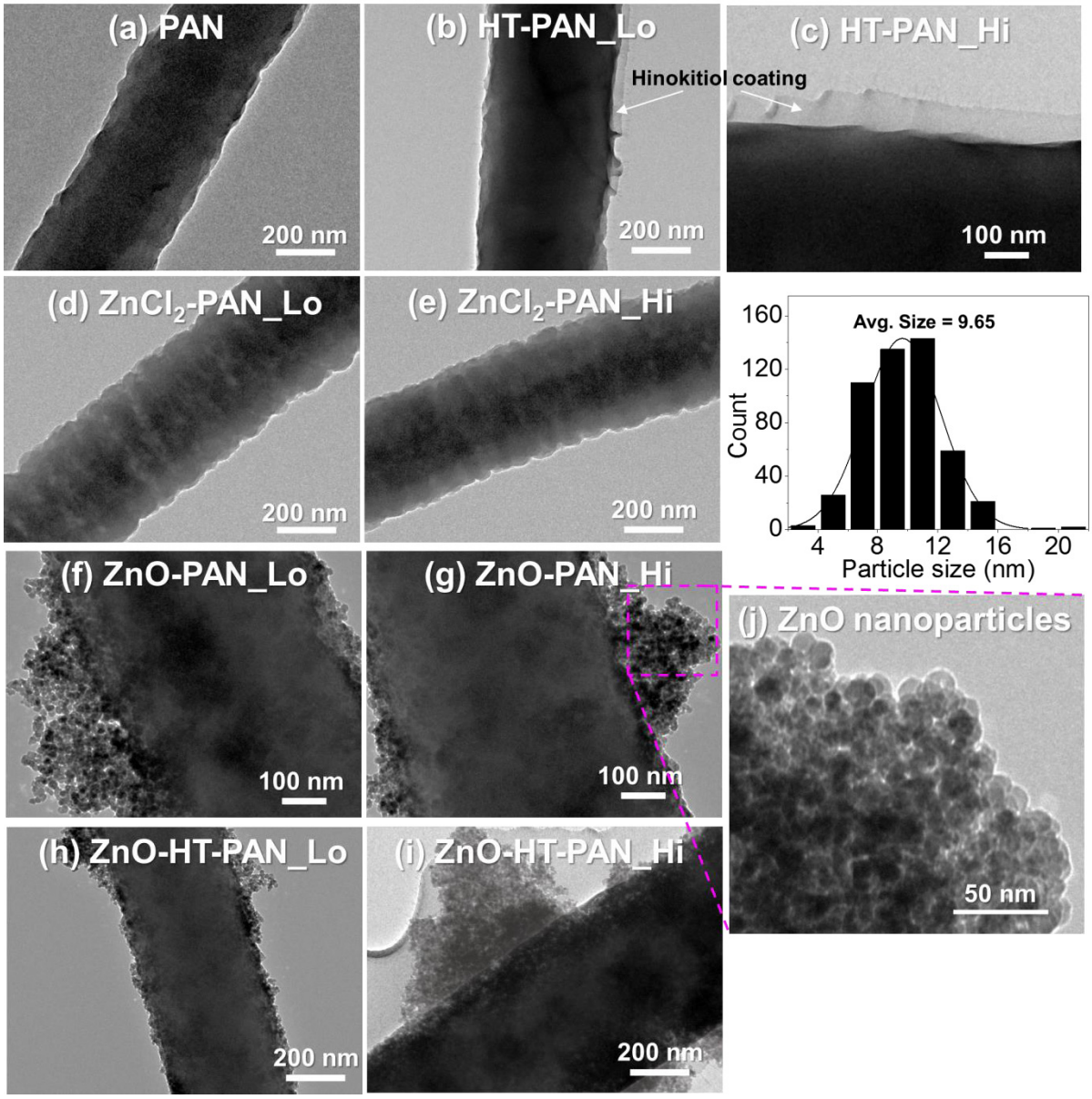

Figure 5. 2 - TEM images of (a) as-spun PAN, HT-PAN (b) _Lo and (c) _Hi, $ZnCl_2$_PAN (d) _Lo and (e) _Hi, ZnO-PAN (f) _Lo and (g) _Hi, (j) ZnO nanoparticles with particle size histogram, ZnO-HT-PAN (h)_Lo and (i)_Hi

5.3.2 FT-IR spectral analysis

In Figure 5.3, the typical FTIR peaks of PAN nanofibers were recorded at 2930, 2245, 1450 cm^{-1} assigned to CH_2 asymmetric stretching, C≡N symmetric stretching, and CH_2 bending [11] and these peaks appeared in all sample spectra. The rising of

peak at 1655 cm^{-1} and the band 3200-3600 cm^{-1} in the spectra of $ZnCl_2$-PAN nanofibers due to the high capacity of vapor absorption from surroundings in zinc salt. The diminution of these peak and band in ZnO-PAN nanofibers demonstrated that the reaction between $ZnCl_2$ and NaOH had happened completely. In Figure 5.3 (f), (g), (h), and (i), peaks at ca. 1590, ca. 1500, and ca. 1220 cm^{-1} characterized C=O stretching, C=C stretching, and C-O stretching, which confirmed the success of Hinokitiol incorporated in the nanofibers [4, 12].

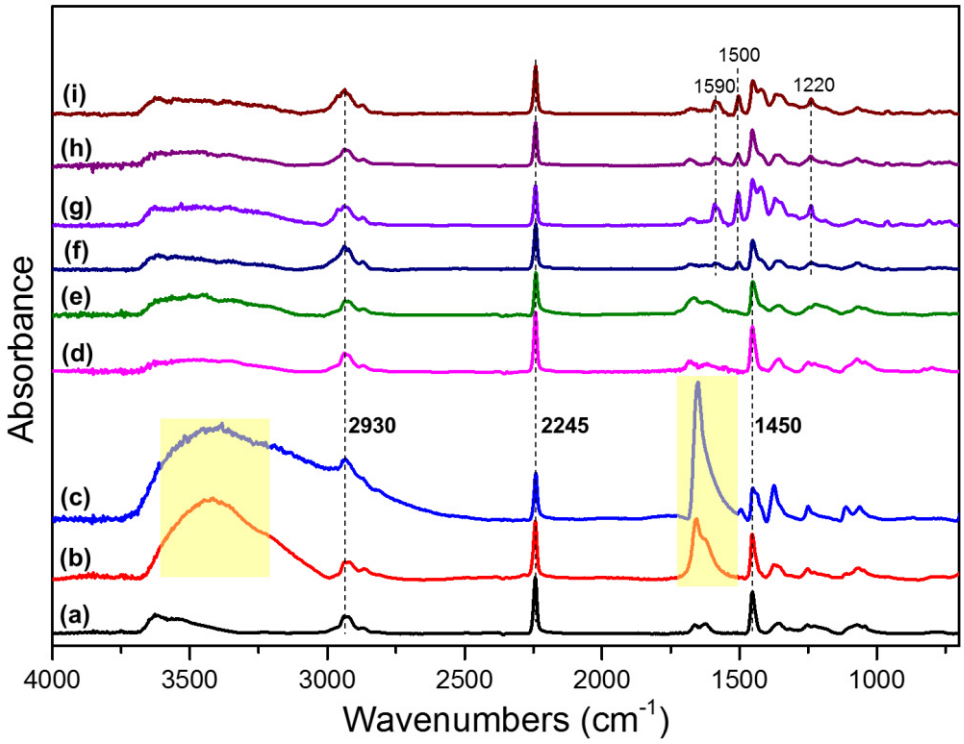

Figure 5. 3 - FT-IR spectra of (a) PAN nanofibers, (b) $ZnCl_2$-PAN_Lo, (c) $ZnCl_2$-PAN_Hi, (d) ZnO-PAN_Lo, (e) ZnO-PAN_Hi, (f) HT-PAN_Lo, (g) HT-PAN_Hi, (h) ZnO-HT-PAN_Lo, and (i) ZnO-HT-PAN_Hi nanofibers

5.3.3 X-ray diffraction study

Neat PAN nanofibers present 2 wide bands centered at around 2θ = 17° and 26.5°, which was reported in our previous report [11]. Due to the influences of $ZnCl_2$ to the

polymer matrix, $ZnCl_2$-PAN samples show some positive shifts of the 17° band to the new positions. The success of synthesizing ZnO could be assuredly confirmed by XRD analysis with the results given in Figure 5.4, displaying sharp peaks at Bragg's angles of approximate 32.5°, 35°, 37°, 48°,57.5°, 63.5°, and 68.5° indexed as (100), (002), (101), (102), (110), (103), and (112) of hexagonal zinc oxide. At the temperature of 150 °C, the zinc hydroxide decomposed to zinc oxide, characterized as nano-scale structure. The presence of ZnO in ZnO-HT-PAN_Lo and ZnO-HT-PAN_Hi with identical set of peaks regarding Bragg's angles and intensities demonstrated that integrating Hinokitiol did not affect the crystallinity of ZnO nanoparticles.Moreover, Hinokitiol also did not exhibit any influences toward the crystalline nature of the PAN nanofibers in HT-PAN samples, Fig 5.4. (f) and (g).

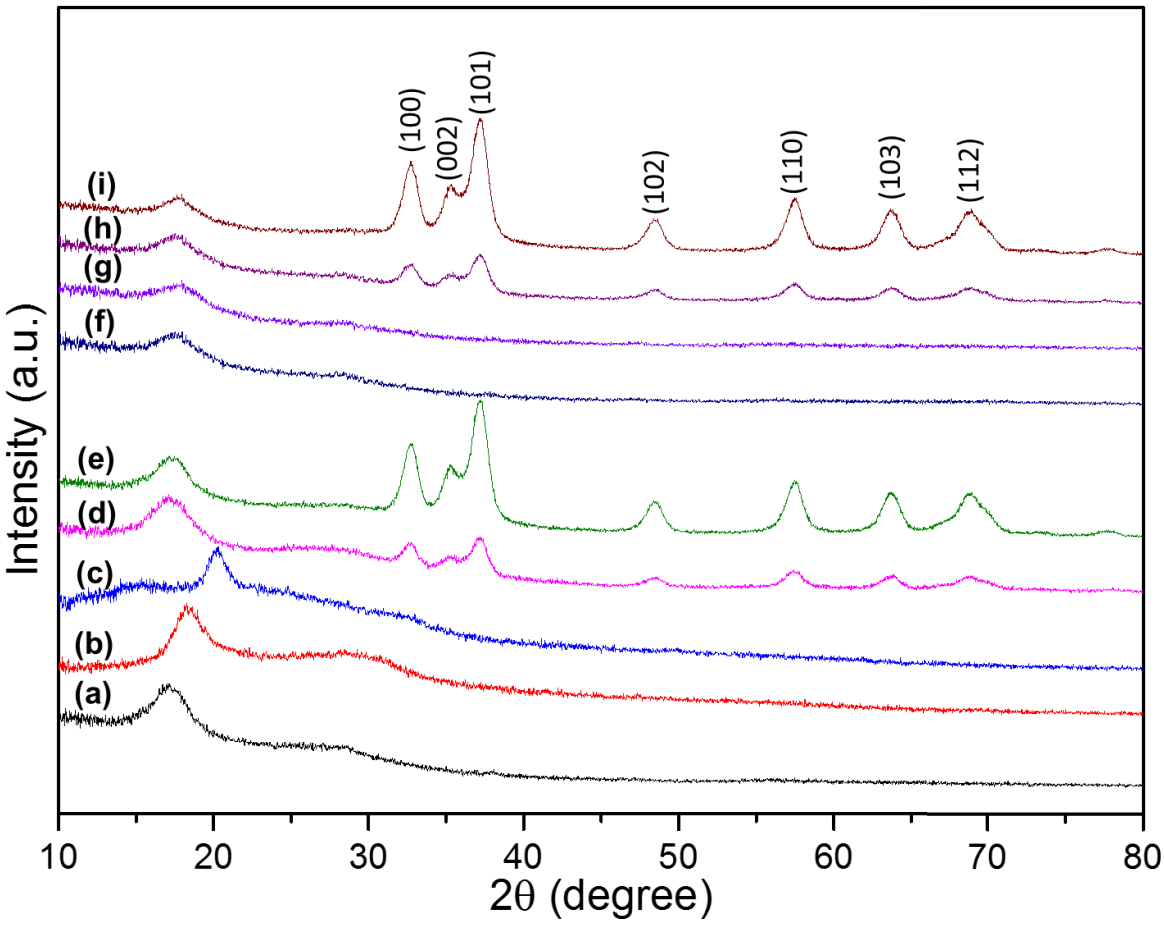

Figure 5. 4 - XRD spectra of (a) PAN nanofibers, (b) $ZnCl_2$-PAN_Lo, (c) $ZnCl_2$-PAN_Hi, (d) ZnO-PAN_Lo, (e) ZnO-PAN_Hi, (f) HT-PAN_Lo, (g) HT-PAN_Hi, (h) ZnO-HT-PAN_Lo, and (i) ZnO-HT-PAN_Hi nanofibers

5.3.4 EDS analyses

The Energy Dispersive X-Ray Spectroscopy (SEM-EDS) analysis presents the elemental composition on the surfaces of the nanofibers, Figure 5.5. There were no significant changes between PAN, HT-PAN_Lo, and HT-PAN_Hi samples in terms of elemental ratios which indicated that the integration of Hinokitiol in the nanofibers did not disturb noticeably the chemical composition of the nanofibers. The existence of zinc element was evidently proved in Figure 5.6 (d-i). The disappearance of chlorine peaks in ZnO containing samples demonstrated the reactions between $ZnCl_2$ and NaOH happened completely. Moreover, the newly-formed oxygen peak, as well as the remaining high intensity of zinc peak, verified the success of ZnO synthesis and clarified the attachment of zinc nanoparticles on the nanofibers, Figure 5.5 (f-i).

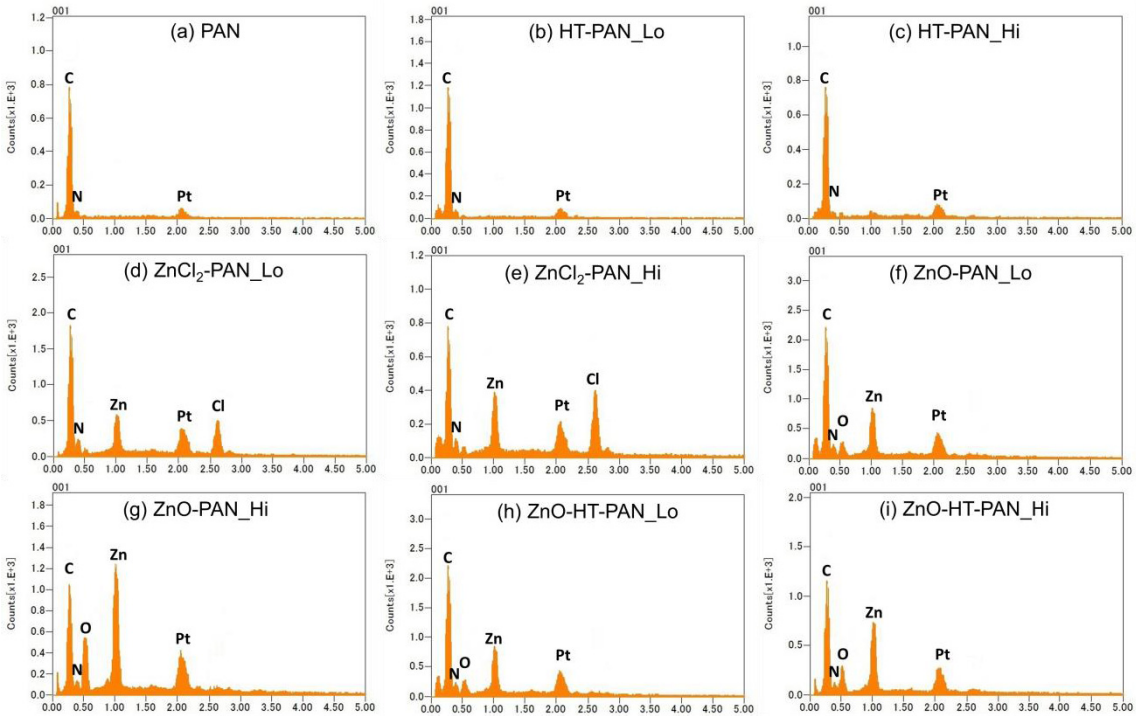

Figure 5. 5 - EDS spectra of (a) PAN, (b) HT-PAN_Lo, (c) HT-PAN_Hi, (d) $ZnCl_2$-PAN_Lo, (e) $ZnCl_2$-PAN_Hi, (f) ZnO-PAN_Lo, (g) ZnO-PAN_Hi, (h) ZnO-HT-PAN_Lo, and (i) ZnO-HT-PAN_Hi nanofibers

5.3.5 Surface wettability

Neat PAN nanofibers were found to be slightly hydrophilic with the average water contact angle of 65°, Figure 5.6. After treating in Hinokitiol solution, the surface of HT-PAN nanofibers reduced hydrophilic performance marginally. In published reports, Hinokitiol was considered as hydrophobic agents, thus the integration of it to the nanofibers impairs the hydrophilic characteristic [13]. Moreover, the hydrophilicity of PAN was significantly decreased with the introduction of ZnO nanoparticles adhered to PAN nanofibers. With the potential to be used as surface functional agent, ZnO coating provides the controllable hydrophobic property for the nanofibrous membranes.

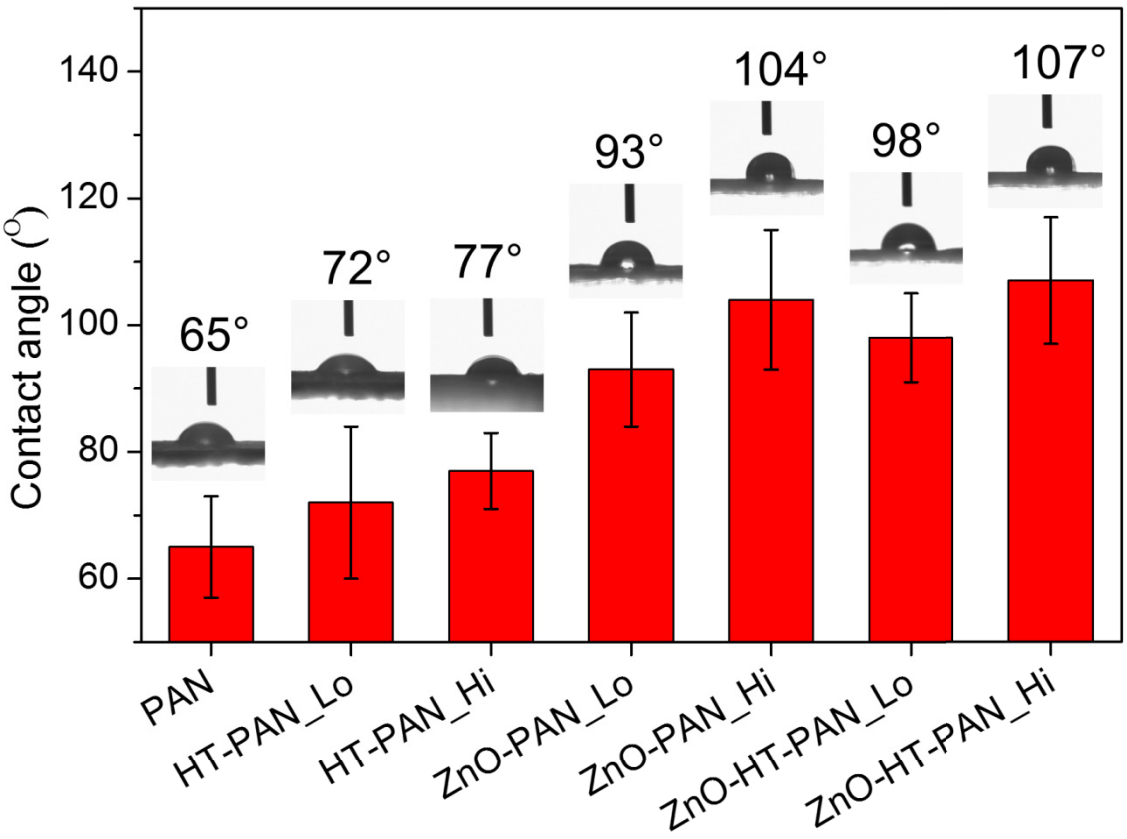

Figure 5. 6 - Contact angle measurement of nanofiber sheets with reproduction on ten specimens each sample, the results were presented on average values with standard deviations

5.3.6 Antibacterial activity of silver PAN composite nanofibers

Antibacterial effects of nanofibrous samples were evaluated following disk diffusion test method, Figure 5.7. Inhibition zones were obviously visible for samples containing HT or ZnO. Hinokitiol has been demonstrated to show antimicrobial properties against a wide spectrum of oral bacteria, fungi, and germs. The inhibition zones against both bacterial strains were significantly larger for PAN nanofibers consisting HT or ZnO with higher contents, 13.4 ± 0.6 mm for HT-PAN_Hi compared to 11.7 ± 0.8 mm for HT-PAN_Lo, similarly 15.8 ± 1.4 mm for ZnO-PAN_Hi in comparison with 13.2 ± 0.7 ZnO-PAN_Lo, all were against E. coli.

Similarly for S. aureus, the zone diameters were 11.3 ± 0.6, 13.6 ± 1, 13.3 ± 0.9, and 15.5 ± 0.5 for HT-PAN_Lo, HT-PAN_Hi, ZnO-PAN_Lo, and ZnO-PAN_Hi, respectively. The combination of HT and ZnO resulted in strong synergistic action against S. aureus. The sizes of the inhibition zones of ZnO-HT-PAN samples extensively expanded. It has been reported that HT could have synergistic effects if combined with transition metals due to metal-oxygen bonding interaction [14, 15]. However, the synergism of HT and ZnO was not clearly exhibited in the case of E. coli. We surmised that distinctions in the membrane structures between gram-negative and gram-positive had affected the results. Generally, gram-negative bacteria have been proven to have an outer membrane, which serves as the barrier for protection and exhibits strong resistance toward hydrophobic agents such as ZnO and Hinokitiol. The presence of both hydrophobic agents in PAN nanofibers decreased the wettability of the ZnO-HT-PAN_Lo and ZnO-HT-PAN_Hi samples, which in turn deteriorated the synergism.

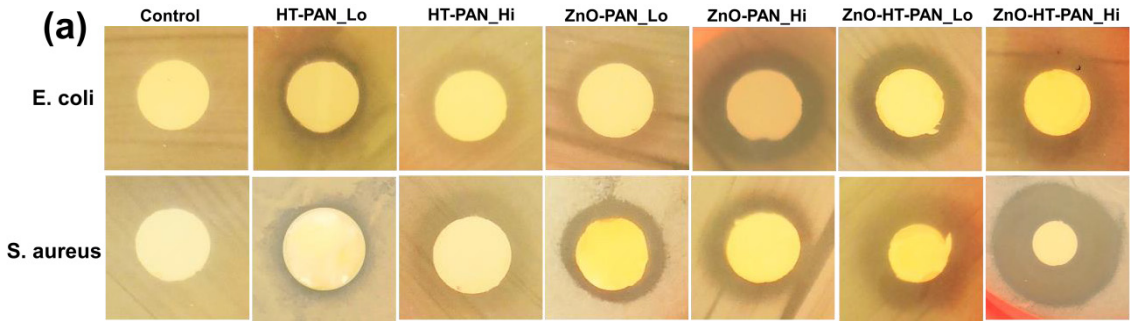

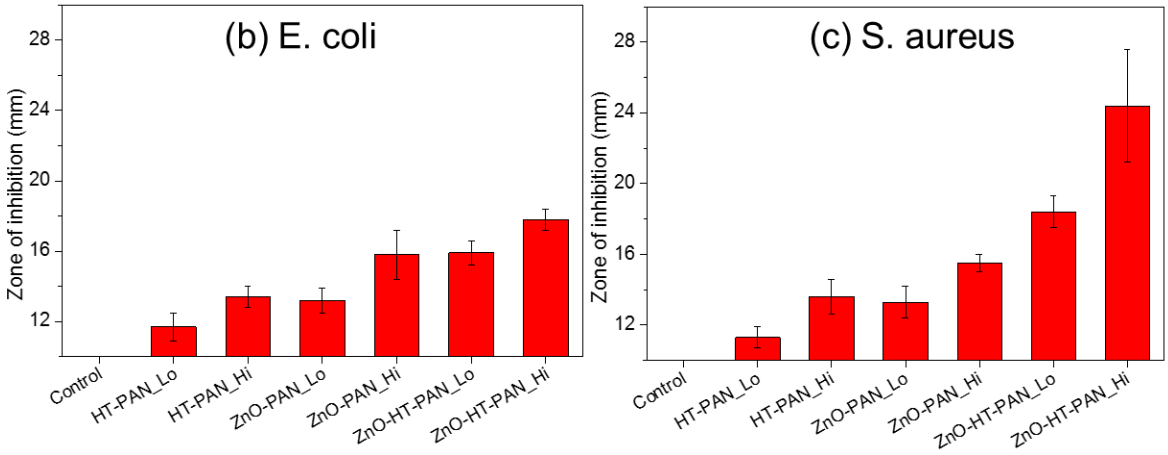

Figure 5. 7 - (a) Representative images of inhibition zones, (b) and (c) Calculated inhibition zones of nanofibrous samples based on disk diffusion test with standard deviations

5.3.7 Dye absorption kinetics and the leaching phenomena of ZnO into solutions

As a function of time, the dye adsorption was inspected over the course of 26 h, Figure 5.8 and 5.9. The reducing in intensity of UV peaks confirmed the adsorption of dye into ZnO containing samples, Figure 5.8 (c), (d), (g), and (h). Whereas, PAN and HT-PAN_Hi samples did not show any adsorptive properties, which was demonstrated by unvaried intensity of absorptive peaks, Figure 5.8 (a), (b), (e), and (f). The alteration of color could be qualitatively reported by monitoring the dye solutions, photos of dye solutions were taken at the appointed time before UV-vis tests were taken. The dye solutions gradually became less colored as a result of ZnO removing effects. However, due to the leaching disadvantage of ZnO, the blue-dye and red-dye solutions including ZnO-PAN_Hi nanofibers were slightly opaque, Figure 5.9-I (a) and (c) - representative images at the 8 h time point after contact. We believe that ZnO nanoparticles were discharged into the solution due to the combined effect of the agitation at 150 rpm and the affinity of dye molecules. Whereas, solutions containing ZnO-HT-PAN were clear, proving that the zinc oxide particles

were well retained within the nanofibrous webs, Figure 5.9-I (b) and (d).

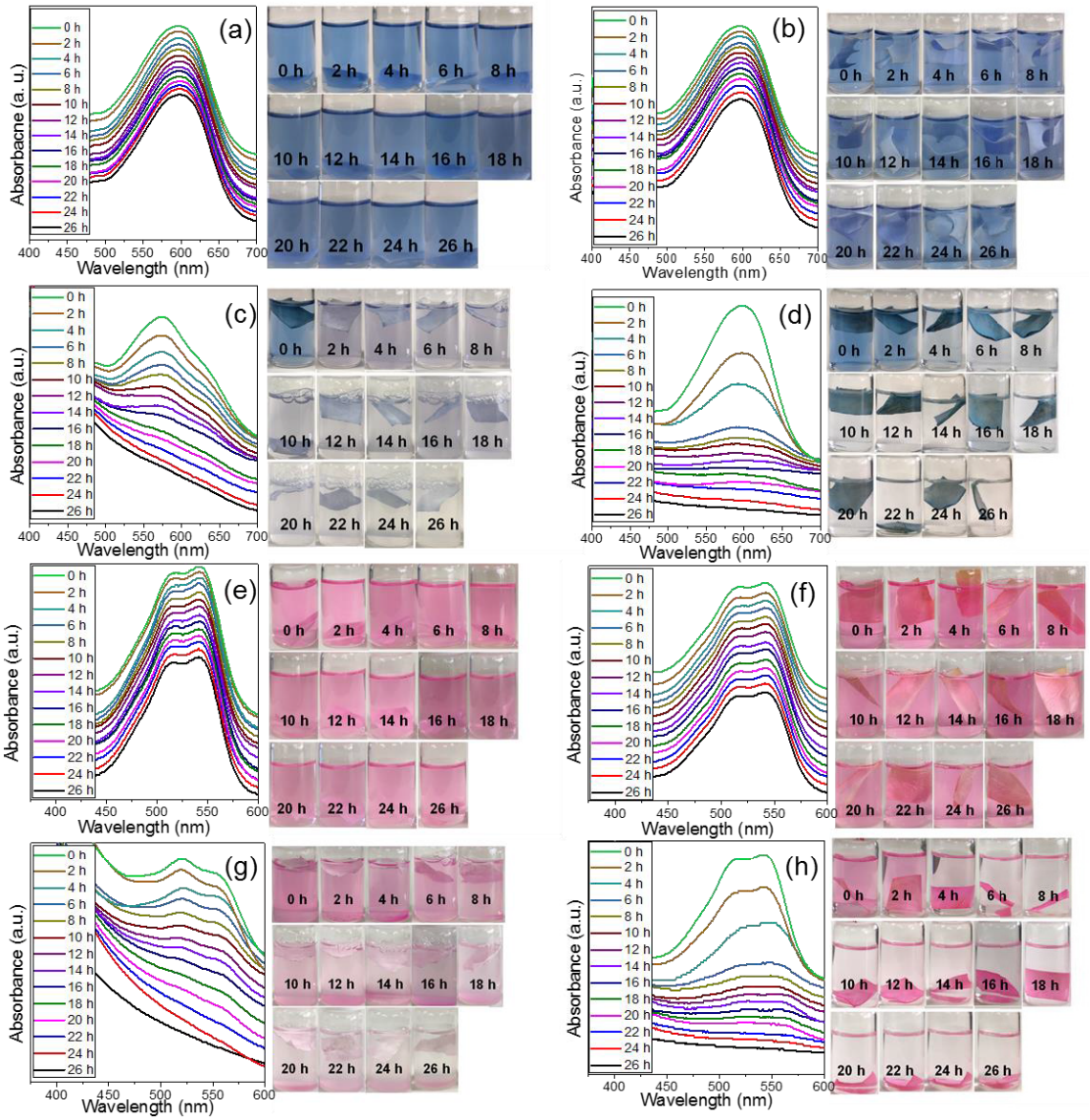

Figure 5. 8 - UV-Visible spectra of reactive-dye solutions in relation to time of contact with (a) and (e) PAN, (b) and (f) HT-PAN_Hi, (c) and (g) ZnO-PAN_Hi, (d) and (h) ZnO-HT-PAN_Hi

For quantitative assessment, the percentages of dye removal by adsorption were calculated based on the reducing intensities of UV peaks. The removed amount of dye went up sharply in the first 6 h for ZnO-HT-PAN_Hi samples, demonstrating the adsorptive nature of ZnO toward both reactive dyes, Figure 5.9-II. After that, the

removed percentages increased gradually and reached 100% at the time point of 24 h. In the case of ZnO-PAN_Hi, due to the dispersion of ZnO from nanofibers to the liquid environment, dye molecules adsorbed to ZnO were simultaneously released back to the solution. In Figure 5.9-I (c), the precipitation of ZnO nanoparticles, which had captured dye molecules, were detected.

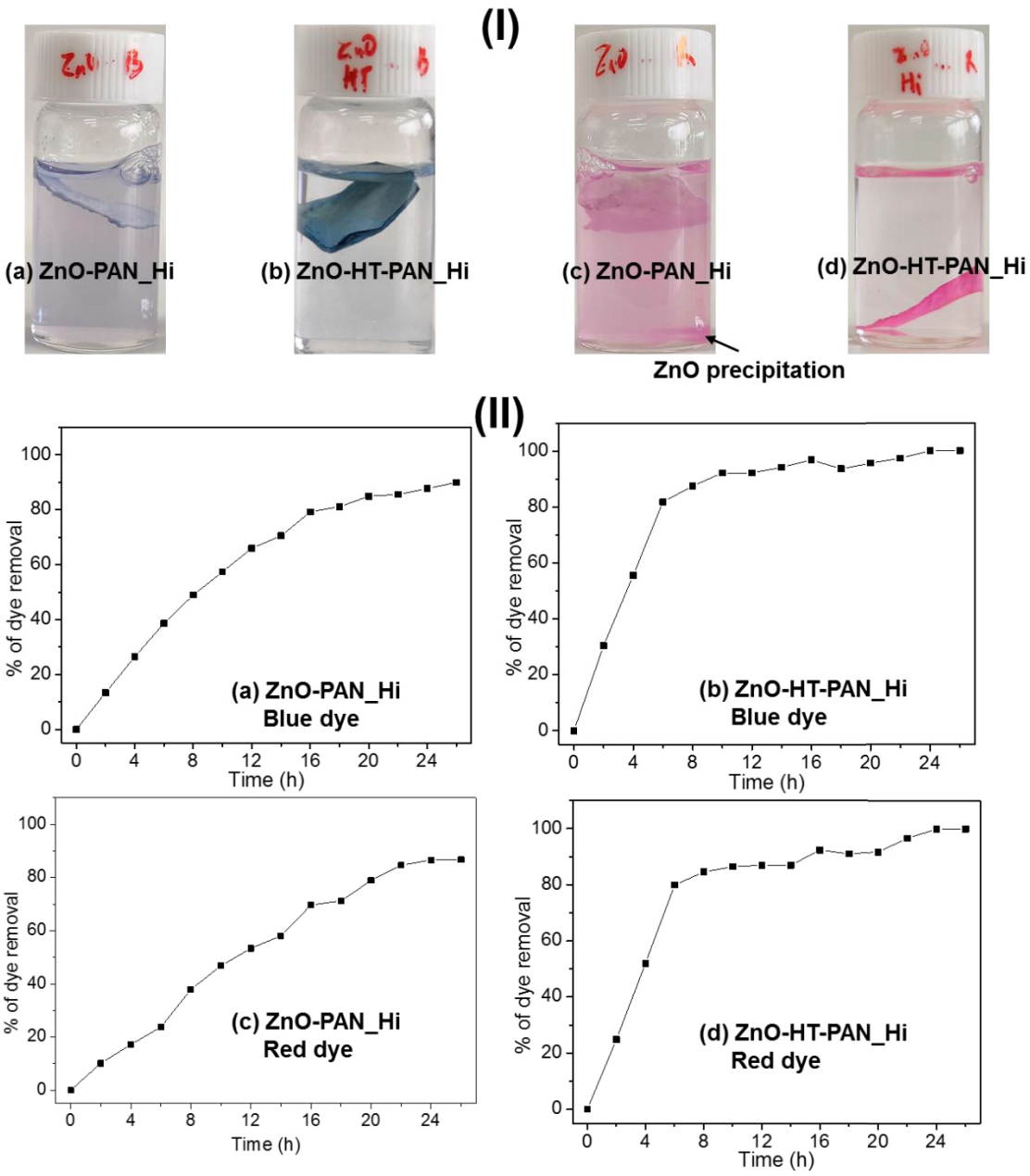

Figure 5. 9 - (I) The ZnO-leaching phenomena at the 8-h time point for ZnO-PAN_Hi samples in dye solutions (a) and (c), compared to ZnO-HT-PAN_Hi

samples with Hinokitiol coating (b) and (d). (II) The adsorption kinetics of ZnO-PAN_Hi and ZnO-HT-PAN_Hi toward blue and red dyes

5.4. Conclusion

We successfully synthesized PAN nanofibers containing ZnO nanoparticles with Hinokitiol acting as gluing agent, denoted as ZnO-HT-PAN, for the antibacterial and dye removing purposes. By adding Hinokitiol to the ZnO-PAN nanofibers, the composite samples exhibited synergistic antibacterial activities against *S. aureus*. ZnO and Hinokitiol are both hydrophobic agents, adding them to nanofibers thereby reduced the hydrophilicity of the resulted nanofibers, inadvertently, hindered the synergism toward gram-negative bacteria, *E. coli*. However, Hinokitiol demonstrated effective prevention of the leaching of ZnO nanoparticles to aqueous environments, hence improved the dye removal efficiency and potentially the recyclability.

References

[1] H. Mirzaei, M. Darroudi, Zinc oxide nanoparticles: Biological synthesis and biomedical applications, Ceramics International 43(1, Part B) (2017) 907-914.
[2] A. Abdal Dayem, M.K. Hossain, S.B. Lee, K. Kim, S.K. Saha, G.-M. Yang, H.Y. Choi, S.-G. Cho, The Role of Reactive Oxygen Species (ROS) in the Biological Activities of Metallic Nanoparticles, International Journal of Molecular Sciences 18(1) (2017) 120.
[3] J. Wang, W. Vermerris, Antimicrobial Nanomaterials Derived from Natural Products—A Review, Materials 9(4) (2016) 255.
[4] K.-C. Chang, D.-J. Lin, Y.-R. Wu, C.-W. Chang, C.-H. Chen, C.-L. Ko, W.-C. Chen, Characterization of genipin-crosslinked gelatin/hyaluronic acid-based hydrogel membranes and loaded with hinokitiol: In vitro evaluation of antibacterial activity and biocompatibility, Materials Science and Engineering: C 105 (2019) 110074.
[5] J. Zhang, W. Wei, L. Yang, Y. Pan, X. Wang, T. Wang, S. Tang, Y. Yao, H. Hong, J. Wei, Stimulation of cell responses and bone ingrowth into macro-microporous implants of nano-bioglass/polyetheretherketone composite and enhanced antibacterial activity by release of hinokitiol, Colloids and Surfaces B: Biointerfaces 164 (2018) 347-357.
[6] M.-H. Huang, Y.-F. Shen, T.-T. Hsu, T.-H. Huang, M.-Y. Shie, Physical characteristics, antimicrobial and odontogenesis potentials of calcium silicate cement containing hinokitiol, Materials Science and Engineering: C 65 (2016) 1-8.
[7] S. Sabir, A. Ahmad Anjum, T. Ijaz, M. Asad Ali, M. Ur Rehman Khan, M. Nawaz, Isolation and antibiotic susceptibility of E. coli from urinary tract infections in a tertiary care hospital, Pak J Med Sci 30(2) (2014) 389-392.

[8] C. Lei, M. Pi, C. Jiang, B. Cheng, J. Yu, Synthesis of hierarchical porous zinc oxide (ZnO) microspheres with highly efficient adsorption of Congo red, Journal of Colloid and Interface Science 490 (2017) 242-251.
[9] K. Nomiya, K. Onodera, K. Tsukagoshi, K. Shimada, A. Yoshizawa, T.-a. Itoyanagi, A. Sugie, S. Tsuruta, R. Sato, N.C. Kasuga, Syntheses, structures and antimicrobial activities of various metal complexes of hinokitiol, Inorganica Chimica Acta 362(1) (2009) 43-55.
[10] M.C. Barret, M.F. Mahon, K.C. Molloy, J.W. Steed, P. Wright, Synthesis and Structural Characterization of Tin(II) and Zinc(II) Derivatives of Cyclic α-Hydroxyketones, Including the Structures of Sn(maltol)2, Sn(tropolone)2, Zn(tropolone)2, and Zn(hinokitiol)2, Inorganic Chemistry 40(17) (2001) 4384-4388.
[11] D.-N. Phan, N. Dorjjugder, Y. Saito, G. Taguchi, H. Lee, J.S. Lee, I.-S. Kim, The mechanistic actions of different silver species at the surfaces of polyacrylonitrile nanofibers regarding antibacterial activities, Materials Today Communications (2019) 100622.
[12] K. Nomiya, A. Yoshizawa, K. Tsukagoshi, N.C. Kasuga, S. Hirakawa, J. Watanabe, Synthesis and structural characterization of silver(I), aluminium(III) and cobalt(II) complexes with 4-isopropyltropolone (hinokitiol) showing noteworthy biological activities. Action of silver(I)-oxygen bonding complexes on the antimicrobial activities, Journal of Inorganic Biochemistry 98(1) (2004) 46-60.
[13] Y. Morita, Y. Sakagami, T. Okabe, T. Ohe, Y. Inamori, N. Ishida, The Mechanism of the Bactericidal Activity of Hinokitiol, Biocontrol Science 12(3) (2007) 101-110.
[14] Y.-H. Shih, D.-J. Lin, K.-W. Chang, S.-M. Hsia, S.-Y. Ko, S.-Y. Lee, S.-S. Hsue, T.-H. Wang, Y.-L. Chen, T.-M. Shieh, Evaluation Physical Characteristics and Comparison Antimicrobial and Anti-Inflammation Potentials of Dental Root Canal Sealers Containing Hinokitiol In Vitro, PLOS ONE 9(6) (2014) e94941.
[15] T.-H. Wang, S.-M. Hsia, C.-H. Wu, S.-Y. Ko, M.Y. Chen, Y.-H. Shih, T.-M. Shieh, L.-C. Chuang, C.-Y. Wu, Evaluation of the Antibacterial Potential of Liquid and Vapor Phase Phenolic Essential Oil Compounds against Oral Microorganisms, PLOS ONE 11(9) (2016) e0163147.

CHAPTER 6 Conclusions

Nanotechnology is a hot pot for researcher to focus on with varied potentials. However, moving nanofibers from the current state to commercialization and implementation is still a big challenge for academia and industry. The dissertation illustrated several synthesizing methods for fabricating different composite nanofibers with or without additional substances and compounds to enhance the functionalities; these methods are straightforward and simple with the potential to be applied in industrial scale. Chapter 2, 3, and 4 presented composite nanofibers with single function of either heavy metal adsorption or antibacterial activities. In chapter 6, the PAN nanofibers containing Hinokitiol and ZnO were introduced with duo-function of antibacterial effects and dye removal.

Natural polymers are considered as one of the safest nanomaterials, in the form of nanofibers with long and highly porous features, they can serve as a promising platform for environment applications. For the application of heavy metal adsorption, in Chapter 2, the hybrid system of chitosan and cellulose overcame the drawbacks of each component, the instability of chitosan and the non-adsorptive property of cellulose. The resulted nanofibers showed good metal adsorption property with enhanced mechanical characteristics. With the nanofibrous structure, the material has significantly enhanced the adsorption capacity and efficiency. The adsorption capacities against As(V), Pb(II), and Cu(II) ions were 26.7, 39.7, and 81.51 mg/g. The adsorption data were fitted with Langmuir and Freundlich isotherm models with the calculated maximum capacities were 39.4, 57.4, and 112.6 mg/g for As(V), Pb(II), and Cu(II), respectively. The chitosan cellulose nanofibers possess great potential to be used as an adsorbent in wastewater effluents.

Silver contributes a promising approach for new antimicrobial development against the drug resistance. The mechanism of actions can be regarded as the dissolution via oxidation. In chapter 3, different silver species could exert various bactericidal mechanisms toward bacteria under the interference of halide salt in bacterial medium. Thus, investigation of various silver species integrated in nanofibrous scaffold regarding antibacterial properties is an interesting research. The silver salt - $AgNO_3$ unpredictably exhibited weakest bactericidal effects, due to the impediment of NaCl in the medium, resulted in the aggregation of Ag ions to form AgCl nanoparticles. Whereas, the passivation layer of AgCl instituting on Ag_2O or Ag nanoparticles presented a barrier to prevent the diffusion of silver ions to the environments. The AgCl layer can be demolished by the formation of poly-chloride complexes. Therefore, Ag_2O and Ag exhibited good antibacterial efficiency on the first cycle. The discharge rate of silver from Ag_2O was higher than Ag, which led to the better bactericidal actions. To release silver, zero-valent silver needs to follow the oxidation and dissolution, whereas the silver oxide can be released with single step.

In chapter 4, silver and copper could be base substances to build biological system. There are several scientific articles about physical and chemical synthesis of copper and silver based composite materials. Our synthetic strategy is to incorporate silver and copper to cellulosic nanofibers with easily scalable, simple, cost-effective, and environmentally friendly approach. Silver and copper nanoparticles were successfully decorated on cellulosic nanofibers to grant the polymeric fibers the antibiotic effects. The resulted composite nanofibers presented good antibacterial activities against both gram negative and gram positive bacteria. The metal release was observed over the course of 7 days and was proved to be direct proportional to the metal contents.

In the chapter 5, we successfully introduced PAN nanofibers encompassing ZnO nanoparticles with Hinokitiol, which added to the system synergistic antibacterial activities against gram positive bacteria – S. aureus. Moreover, Hinokitiol enhanced the adsorption of ZnO nanoparticles and kept the particles secured within the nanofibrous membrane. The resulted nanofibers exhibited duo functions, antibacterial activities and dye adsorption characteristic. This research showcased the potential of nanofibers to span over applications in the fields of water and environment, and healthcare.

The combination of different substances in electrospun mesh can provide strong base materials for the water filters or wound dressing of the future, although challenges are still there to be overcome. The water filters with the nanotechnology should be able to remove bacterial contamination and other inorganic or organic toxins, while still are mechanically or chemically stable for long-term uses. Innovative research involving varied bio-materials are helping scientific world to battle the antimicrobial resistance – a slowly emerging epidemic. The end of traditional antibiotics is coming, ushering the era of new advanced biomaterials. Electrospinning technique with new sets-up and innovative composite materials could possibly help humankind to a better life.

Accomplishments

List of papers published

1. Synthesis and attachment of silver and copper nanoparticles on cellulose nanofibers and comparative antibacterial study

Duy-Nam Phan, Nasanjargal Dorjjugder, Muhammad Qamar Khan, Yusuke Saito, Goro Taguchi, Hoik Lee, Yasuhito Mukai, and Ick-Soo Kim

Cellulose 26(11) (2019) 6629-6640

2. Fabrication of electrospun chitosan/cellulose nanofibers having adsorption property with enhanced mechanical property

Duy-Nam Phan, Hoik Lee, Bijun Huang, Yasuhito Mukai, and Ick-Soo Kim

Cellulose 26(3) (2019) 1781-1793

3. Fabrication of Two Polyester Nanofiber Types Containing the Biobased Monomer Isosorbide: Poly (Ethylene Glycol 1,4-Cyclohexane Dimethylene Isosorbide Terephthalate) and Poly (1,4-Cyclohexane Dimethylene Isosorbide Terephthalate)

Duy-Nam Phan, Hoik Lee, Dongeun Choi , Chang-Yong Kang , Seung Soon Im, and Ick Soo Kim

Nanomaterials 2018, 8, 56

4. The mechanistic actions of different silver species at the surfaces of polyacrylonitrile nanofibers regarding antibacterial activities.

Duy-Nam Phan, Nasanjargal Dorjjugder, Yusuke Saito, Goro Taguchi, Hoik Lee, Jung Soon Lee, and Ick-Soo Kim

Materials Today Communications 2019, 100622,

https://doi.org/10.1016/j.mtcomm.2019.100622

5. The synthesis of silver-nanoparticle-anchored electrospun polyacrylonitrile nanofibers and a comparison with as-spun silver/polyacrylonitrile nanocomposite membranes upon antibacterial activity

Duy-Nam Phan, Nasanjargal Dorjjugder, Yusuke Saito, Goro Taguchi, Azeem Ullah, Davood Kharaghani, Ick-Soo Kim

Polymer Bulletin 2019, https://doi.org/10.1007/s00289-019-02969-8

6. Zinc oxide nanoparticles attached to polyacrylonitrile nanofibers with hinokitiol as gluing agent for synergistic antibacterial activities and effective dye removal

Duy-Nam Phan, Rina Afiani Rebia, Yusuke Saito, Davood Kharaghani, Muzamil Khatri, Toshihisa Tanaka, Hoik Lee, Ick-Soo Kim

Journal of Industrial and Engineering Chemistry, 2020, https://doi.org/10.1016/j.jiec.2020.02.008

7. Composite Nanofibers: Recent Progress in Adsorptive Removal and Photocatalytic Degradation of Dyes

Duy-Nam Phan and Ick-Soo Kim

IntechOpen, DOI: 10.5772/intechopen.91201

8. The Chemical Deposition Method for the Decoration of Palladium Particles on Carbon Nanofibers with Rapid Conductivity Changes

Hoik Lee, **Duy-Nam Phan**, Myungwoong Kim, Daewon Sohn, Seong-Geun Oh, Seong Hun Kim and Ick Soo Kim

Nanomaterials. 2016; 6(12):226

9. Effect of graphene incorporation in carbon nanofiber decorated with TiO2 for photoanode applications

Hoik Lee, Tomoki Nagaishi, **Duy-Nam Phan**, Myungwoong Kim, Ke-Qin Zhang, Kai Wei and Ick Soo Kim

RSC Adv. (2017) 7, 6574-6582

10. Dyeing and characterization of regenerated cellulose nanofibers with vat dyes

Muzamil Khatri, Farooq Ahmed, Irfan Shaikh, **Duy-Nam Phan**, Qamar Khan, Zeeshan Khatri, Hoik Lee, Ick Soo Kim

Carbohydrate Polymers, 2017, 174, 443-449

11. Fabrication of silk fibroin/eggshell nanofiber membranes for facemasks

Jatoi Abdul Wahab, Gang Xu, Hoik Lee, **Phan Duy Nam**, Kai Wei, Seong Hun Kim, Ick Soo Kim

Fibers Polym (2016) 17: 1776

12. Development of antibacterial contact lenses containing metallic nanoparticles

Davood Kharaghani, Debarun Dutta, Parastoo Gitigard, Yasushi Tamada, Anna Katagiri, **Duy-Nam Phan**, Mark D.P. Willcox, Ick Soo Kim

Polymer Testing (2019), 79, 106034

13. Development of VOCs gas sensor with high sensitivity using colorimetric polymer nanofiber: a unique sensing method

Myoung Ok Kim, Muhammad Qamar Khan, Azeem Ullah, **Nam Phan Duy**, Chunhong Zhu, Jung-Soon Lee, and Ick Soo Kim

Materials Research Express (2019), 6, 10

14. Fabrication of Antibacterial Nanofibers Composites by Functionalizing the Surface of Cellulose Acetate Nanofibers

Muhammad Qamar Khan, Davood Kharaghani, Sanaullah, Amir Shahzad, **Nam Phan Duy,** Yohei Hasegawa, Azeemullah, Jungsoon Lee, Ick Soo Kim

ChemistrySelect 2020, 5, 1315

15. Application of Nanowires for Retinal Regeneration

Davood Kharaghani, Zahra Tajbakhsh, **Phan Duy Nam** and Ick Soo Kim

IntechOpen, DOI: 10.5772/intechopen.90149

Oral Presentations at conferences

1. Fabrication and characterization of high thermal stability and high-tensile strength biodegradable nanofibers

Duy-Nam Phan, Ick-Soo Kim

The 70th Annual Meeting of The Textile Machinery Society of Japan, Osaka, Japan, from June 1st to 3rd, 2017. http://tmsj.or.jp/annual/70/index.html

2. Fabrication of electrospun chitosan/cellulose nanofibers having adsorption property with enhanced mechanical property

Duy-Nam Phan, Ick-Soo Kim

10th International Symposium on High-Tech Fiber Engineering for Young Researcher at Soochow University, China, From August 24th to 31st, 2018.

3. Fabrication of hybrid electrospun chitosan/cellulose nanofibers for Cu adsorption

Duy-Nam Phan, Ick-Soo Kim

The Society of fiber Science and Technology, Japan (Tokyo), From June 13th and 14th. http://www.fiber.or.jp/jpn/events/2018/year/index.html

4. Fabrication of chitosan/cellulose nanofibers with adsorption characteristics and enhanced mechanical properties

Duy-Nam Phan, Ick-Soo Kim

The Korean Fiber Society, EXCO, South Korea, Daegu, Buk-gu, Sangyeok 2(i)-dong, from April 17th to 20th, 2019

5. Investigation upon the nature of silver species composited with polyacrylonitrile nanofibers and antibacterial activities

Duy-Nam Phan, Ick-Soo Kim

The 72nd Annual Meeting of The Textile Machinery Society of Japan, Osaka, Japan, from May 29th to 31st, 2019. http://tmsj.or.jp/annual/72/index.html